SUPERCONDUCTIVITY AND ANTI FERROMAGNETIC SPIN DENSITY WAVE IN IRON BASED SUPERCONDUCTORS

A Dissertation Submitted for the

Degree of Doctor of Philosophy in the Field of Physics

BY

GIRMA KITACHEW JENBERIE

Graduate School of natural Sciences of

Addis Ababa University

Department of Physics

JANUARY, 2015

SUPERCONDUCTIVITY AND ANTIFERROMAGNETIC SPIN DENSITY WAVE IN IRON BASED SUPERCONDUCTORS

By

Girma Kitachew Jenberie

Supervisor: Prof P. Singh

A dissertation submitted for the degree of Doctor of Philosophy in the field of Physics

Graduate School of natural Sciences of

Addis Ababa University

January, 2015

ACKNOWLEDGMENTS

Undertaking real research as a PhD student could have never been so fertile and pleasant with out an eminent and charismatic supervisor like Professor P. Singh. I would like to verbalize my sincere and warm gratitude to him for his faith and inspiration, and for guiding me to work in a highly interactive research environment.

I would like to acknowledge the Dilla University for sponsoring the PhD program. I wont to acknowledge Addis Ababa university Department of Physics for the unlimited facilities provided and the staff members kindness from the head of the department of Physics (Dr. Belayneh Mesfin) to the secretory (Tsilat Adinew). Great thanks to College of Development Studies of Addis Ababa university for providing me full accommodation and facilities.

I would like to deem my deepest and keenest affection to all my friends for being my friend and helping me adorn and improve every aspect of my life academically, personally, and professionally. I want to thank them both for being with me in every happy and difficult time and sharing innumerable scholarly and charming moments of their lives. Finally, I would like to inscribe my candid regard and gratitude to my parents, bathers and sisters for loving me and supporting me to their fullest. In their nourishment and guidance, I have enjoyed the ultimate freedom both academically and personally.

To my lovely Grandparents.....

LIST OF FIGURES

CONTENTS

CONTENTS

CONTENTS

CONTENTS

CONTENTS

CONTENTS

CONTENTS

CONTENTS

CONTENTS

CONTENT

ABSTRACT

ABSTRACT

ABSTRACT

ABSTRACT

ABSTRACT

The interplay between magnetism and superconductivity had attracted immence interest and effort following the discovery of magnetic superconductors like heavy fermion, cuprate and recent iron based superconductors (FebSC). The study of their interplay between has also been fascinating area of study due to complex magnetic interactions in the systems. In the latest, FebSCs the competition between antiferromagnetic (AFM) spin density wave (SDW) and superconductivity (SC) has attracted considerable attention in the current research in the field of superconductivity. The magnetic order in most FebSCs is the result of nesting between hole and electron pockets found at the the center and corners of the unfolded Brillouin zones. The interaction between fermions forming these pockets is important to study the low temperature physics of FebSCs. The model Hamiltonian consisting of these fermions responsible for magnetic and superconducting pairing interactions is developed to study their interplay. Using either Green function or Bogoligiv transformation method gap equations for SDW and s- wave superconductivity order parameters have been established for pure systems and for interacting ones. The gap equations have been studied in detail as physically accepted choice of parameters. We have established experimentally accepted Electronic Phase diagrams for some FebSCs. First we study the interplay between sign reversal s-wave symmetry superconductivity (SC_{+-}) and SDW order parameters and found their homogeneous microscopic coexistence in under doped region. On the other hand the competition between sign preserving s-wave superconductivity (SC_{++}) and SDW order parameters produce their homogeneous overlap near quantum critical point which is

ABSTRACT

consistent with the phase diagram of electron doped $LaFeAsF$ compounds. When the magnetic order is commensurate SDW (SDW_c) the interplay calculation presents the first order transition from SDW to SC_{++} which is consistent with the phase separated doped FebSCs compounds like doped $Li\,Fe\,As$ compounds. The first model calculation results can be compared with the experimental report of doped $Ba\,Fe_2\,As_2$ iron based families, doped $Sm\,Fe\,As\,O$ and electron doped $La\,Fe\,As$ compounds. Even more interestingly, the result of our study showed first order transition from SDW_c to incommensurate SDW (SDW_δ) which is directly related to the observed magnetic orders near optimal doped region of $Ba\,Fe_2\,As_2$. The strong suppression of SDW order parameter in the SC phases and the suppression of superconductivity in both under doped and over doped regions are some of the interesting results.

ABSTRACT

CHAPTER 1: INTRODUCTION

CHAPTER 1

INTRODUCTION

1.1 Superconductivity

Superconductivity is the most remarkable phenomenon that has been puzzling scientists ever since it was discovered by Kamerlingh Onnes in 1911 [1]. In the following years of discovery it was established that superconductivity is a very common feature at low temperatures. In otherworld superconductivity is one area of science that is full of surprises. For example in the past three decades, intensive research has exposed a rich variety of extraordinary superconducting and magnetic states in novel materials arising out of the cooperative interaction between the magnetic and superconducting states.

Most superconducting elements have been found to become superconducting at low temperatures. However, frequently it is necessary to apply pressure. Superconductors are characterized not only by the absence of electrical resistance. They were furthermore found to exhibit certain unusual properties [2]. Most notably among those is the Meissner effect (exclusion of magnetic field) [3]. A superconductor is a perfect diamagnet (a magnetic field is completely expelled from its bulk. However, for one kind of superconductors,usually called type-I superconductors, there is a critical field H_c above which the superconductivity is destroyed and the magnetic field can penetrate the material. There are also type-II superconductors on which there exists a lower critical field H_{c1} above which the magnetic flux lines can penetrate the bulk of the superconductor with out destroying the superconductivity and an upper critical field H_{c2} above which the superconductivity is destroyed [4]. Another striking property of superconductors

is the opening of an energy gap of size 2Δ in the elementary excitation spectrum which can be observed directly and indirectly [5]. Furthermore, the SC transition temperature T_c was found to depend on the isotope and thus the mass of the superconducting element [6]. Though later superconductors showing weak to no isotope effect were found [7].

From the beginning superconductivity attracted large efforts from theoretical physicists. But the first successful step on the way to a microscopic understanding of superconductivity was not made before 1950 when quantized lattice vibrations (phonons) are realized [8], phonons, can lead to an attractive effective interaction between electrons in a metal. Bardeen, Cooper and Schrieffer developed (BCS) theory of superconductivity in 1957 [9] which could describe all superconductors known at that time. The BCS theory is based on the idea that electrons in a shell of width of the Debye frequency around the Fermi surface can overcome the Coulomb repulsion via the exchange of virtual phonons leading to an effective attractive interaction. Due to this interaction two electrons with opposite spin and momentum form bound (usually called Cooper pairs) which then build up a superconducting phase coherent condensate. This new state of matter is characterized by the gap function or order parameter. The gap function is non zero in the vicinity of the Fermi surface only, where, with in the original BCS theory, it is isotropic and finite.

1.2 Magnetic superconductors

Interaction between superconductivity and magnetism has always been an area of interest in condensed matter physics, especially because of the antagonistic nature of these two phenomena. It was proposed [9] magnetically mediated pair breaking mechanism in superconductors. In a superconductor, the electron pairs, called Cooper pairs, are formed by electrons of opposite spin, which cancels the pair’s

magnetic moment. However, when the material is placed in a strong magnetic field, the spins are forced to orient themselves along the field. Usually, this breaks the pairs and destroys superconductivity. The magnetic fields inside a magnetically ordered material tend to act in the same manner, and thus superconductivity and magnetism tend to avoid each other. This mechanism is in agreement with the suppression of superconductivity due to exchange scattering between the superconducting electron and the local moments [10]. It has generally been believed that, within the context of the BCS theory of superconductivity, the conduction electrons in a metal can not be both ferromagnetically ordered and superconducting [11]. It was estimated [11] that coexistence of superconductivity and ferromagnetism might be possible if the induction created by the magnetization did not exceed the critical field for superconductivity.

A doped superconductor with a magnetic rare earth element in order to study the interaction between superconductivity and magnetism, and predicted a region of coexistence of the two phenomena at very low temperatures [9]. Two systems of ternary rare earth compounds [12-14], the rare earth molybdenum chalcogenides, RMo_6X_8 (R= rare earth element and X = S, Se) and the rare earth rhodium borides Rrh_4B_4, are also magnetic. These compounds undergo ferromagnetic or antiferromagnetic (AFM) transitions depending on the strength of the exchange interactions of the rare earth elements at temperatures far below the superconducting transition temperature. In these materials, the long range ordering occurs due to the localized moments of rare earth element with partially filled 4f orbital, where as superconductivity occurs due to the conduction electrons, which are built up from outer 5d and 6s orbitals. These conduction electrons interact magnetically with 4f local moments [15]. The coexistence of superconductivity and magnetism in the RMo_6X_8 and RRh_4B_4 systems is possible

due to the weak over lapping of the conduction and magnetic orbitals.

Heavy fermion systems are another magnetic class of superconductors, which consist of metallic compounds that contain rare earth elements, such as Ce or Yb, or actinide elements such as U with partially filled 5f shells. The name comes because the effective mass of electrons in these systems is in the order of a hundred times larger than the mass of normal electrons at low temperatures [16]. In 1979, the discovery of superconductivity in the heavy fermion compound, $CeCu_2 Si_2$ [17] came as a surprise, because the pairing of heavy fermions through electron phonon interaction, as postulated by BCS theory [8], is highly unlikely. Also, Ce ions have local magnetic moment due to partially filled 4f orbitals.

The substitution of a non magnetic impurity at Ce sites destroys the superconductivity in this material, in contrast to what occurs in conventional superconductors. The interaction between local moments and the conduction electrons in heavy fermion systems involves various types of interplay between superconductivity and magnetism. In URu_2Si_2, $UPd_2 Al_3$ and $UNi_2 Al_3$ [18-20], magnetic order coexists with superconductivity on the microscopic scale without any strong mutual interaction. The other compound UPt_3 [21] undergoes an AFM transition below Neal temperature of 5K, and it exhibits multiple superconducting phases, which is attributed to the coupling between SC and AFM order parameters [21,22].

Heavy fermions like $CePd_2Si_2$ and $CeIn_3$ [23], in which superconductivity appears under pressure. These compounds are AFM at ambient pressure. Under high pressure, AFM order abruptly disappears, accompanied by a superconducting transition. It has been suggested that in these compounds, the superconducting charge carriers are bound together in pairs by magnetic spin spin interactions, showing that spin fluctuations (electron-electron interaction) mediate the electron

pairing that lead to superconductivity in heavy fermion compounds.

Cuprates are another class of magnetic superconductor. The discovery of SC in cuprates at temperatures as high as 30K in LaBaCuO [24] revealed a brand new field of high temperature superconductors. Later, the observation of a superconducting transition at 92K by substituting yttrium in place of La intensified the research on the high temperature cuprate superconductors. Similar to the case of the former two magnetic superconductors and heavy fermion superconductors, high temperature cuprate superconductors also exhibit a delicate balance between superconductivity and magnetism. In order to understand the interplay of superconductivity and magnetism in cuprate, it is important to understand the layered perovskite like crystal structure of these compounds. The layered structure [25, 26] consists of CuO_2 planes. This layer acts as a charge reservoir and is responsible for doping electrons or holes into the CuO_2 planes. The movement of holes and in some cases electrons in the CuO_2 planes gives rise to superconductivity. The parent compound of cuprate is a Mott insulator, which should be metal according to band theory, but is insulating, due to electron electron interactions. Substitution of divalent Sr for trivalent La in the AFM insulator La_2CuO_4 dopes the CuO_2 plane with holes and produces superconductivity [27]. For different concentrations of the dopant Sr, the system is either superconducting, normal, or antiferromagnetic, a region of coexistence of superconductivity and AFM order.

From a generic temperature versus dopant concentration [28] phase diagram for cuprate at very low doping concentration, AFM order exists in the cuprate system and the temperature dependence of the resistivity exhibits an insulating behavior. Upon increasing the doping, AFM order is destroyed rapidly and vanishes at about some doping, and the superconducting order develops. As the

doping increases, SC T_c increases. At an optimum value of doping, T_c reaches a maximum and the system behave as a non Fermi liquid. On further increasing the doping, T_c decreases and finally drops to zero. The phase diagram suggests that AFM order does not play a decisive role in the suppression of superconductivity, because superconductivity does not appear as soon as AFM order is destroyed, rather, it appears gradually with increasing doping concentration.

The recent observation of superconductivity at 56K in rare earth system, $FeAsO_{1-x}F_x$ [28-33] has marked the discovery of the first non copper oxide based high temperature magnetic superconductor [34]. Similar to cuprate superconductors, high temperature superconductivity in these iron based superconductors (FebSC) systems is also derived from either electron or hole [35-40] doping of their parent compounds, which exhibit long range AFM static order, which is suppressed on electron/hole doping to induce superconductivity [39]. For FebSCs magnetism arising from a nesting induced spin density wave, unlike to the cuprates where the parent compounds are Mott insulators, where strongly repulsive electronic correlations yield an insulating and ground state despite a half filled conduction band.

The discovery of this new magnetically active superconductivity has renewed interest in the interrelationship between magnetism and superconductivity. Similar to cuprates and several heavy fermion superconductors, superconductivity emerges here in close proximity to AFM state. In the itinerant electron systems, the interactions that lead to the formation of superconducting and orders pull and push the same particles, and as a result, influence each other. In particular, two orders may support each other and lead to the homogeneous coexistence of superconducting and magnetic states; or one of them may completely suppress the other order, resulting in state with spatially separated regions of pure magnetic or

superconducting orders.

These multi band superconducting materials consist hole and electron pockets in their fermilogy. Hole pockets are near circular, but different hole pockets in the same material usually have different sizes, electron pockets are nearly elliptic. The transitions between various states (like magnetic and superconducting) may also be either second order or first order. The outcome of the interplay depends critically on a number of parameters: *properties of the interactions, such as symmetry of superconducting pairing, their relative strengths, and on properties that Fermi surface, such as the shape or the density of electronic states*.

Multiple Fermi surfaces may also create a number of different possibilities for electron ordering in the form of spin density wave, charge density wave states, and various superconducting states. Because of this complex (multi band) environment, the interplay of magnetic and superconducting orders also shows some degree of variations. Upon doping, magnetism eventually yields to superconductivity [39] but how this transformation occurs varies significantly between different FebSCs [38,40]. The early experimental probe did show the homogeneous coexistence and transitions from magnetic to superconducting phase due to different reasons like sample quality, however the last two year evidences have been solving the problems of homogeneity in most FebSCs compounds [36, 40]. There fore the competition between the AFM and SC in FebSCs compound results the currently observed phase coexistence and phase separation.

At the end the phenomenon arising due to magnetic and superconductivity are one of the intensively studied and fascinating fields of research due to its relevance to superconducting and spin electronics and mechanism of superconductivity. This drives the current interest in this recently synthesized magnetic superconducting materials combining magnetic ordering properties with

superconducting properties. These compounds exhibit an interesting interplay of superconductivity and magnetism. As experimental investigations, show the superconductivity in FebSC compounds is not destroyed by the presence of magnetic correlations, which contradicts the antagonistic nature of these two phenomena. In order to understand how the mutually exclusive phenomena (superconductivity and magnetism) coexist within a unit volume in FebSCs, it is important to understand their magnetic behavior as well as the result of competition between the two orders theoretically.

It has been over three years that efforts have been devoted to understand the nature of magnetic ordering and the interaction between magnetism and superconductivity in these new FebSCs compounds. However, up to date consensus has not been reached on the microscopic coexistence of magnetic spin density wave and superconductivity for some compounds. The main intent of this thesis is to develop a compressive model and driving generic equations for the magnetic and superconducting order parameters. Then we apply the model to understand the magnetic spin density wave ordering and superconducting order, and then to study their interplay, microscopic coexistence between antiferromagnetic SDW and superconductivity in different FebSCs families

1.3 Organization of the thesis

This thesis consists of the following chapters: In the second chapter we will review the physics of FebSCs based on the experimental and theoretical investigations. In the third chapter, we introduce the model for SDW-SC interplay and apply the model to the electron and hole doped FebSC systems and then drive the gap equations. In chapter four we study the electronic structure of different state (normal, magnetic and superconducting) for different orbitals and gap symmetries based on our model calculations. In chapter five the the result of the

interplay such as the microscopic coexistence of both commensurate and incommensurate SDW order with s-wave (both conventional s-wave and unconventional one) superconductivity and phase separation are discussed. Here we present the results of our numerical calculations in the form of phase diagrams and we discuss their properties. First we address the SDW and superconductivity separately, and then discuss the properties of the combined state. We find that the two orders generally tend to suppress each other; however, regions in the parameter space exist, where the microscopic coexistence or separation occurs. Finally summery and conclusion are given in the last chapter.

CHAPTER 2: IRON-BASED SUPERCONDUCTORS

CHAPTER 2

IRON-BASED SUPERCONDUCTORS

2.1 Iron based Superconductors

The first material of iron based superconductors (FebSC) to show superconductivity are LaOFeP reported in 2006, whose superconducting transition temperature T_c is 7K [41] but it did not attract wide spread attentions at that time because of its low SC transition temperature. After two years, the discovery of T_c=26K superconductivity in fluorine doped LaFeAsO [39] and consequently the findings of other FebSCs with an even higher transition temperatures which suggest that the FebSCs are high temperature superconducting materials, mark the beginning of world wide efforts to investigate this new iron family of superconductors. So far, the FebSCs have been extended to include a large variety of materials, and the family still keeps growing. According to their formulas, they are often classified as 1111, 122, 111, 11, and 245 families of FebSC. To date, all family exhibit a clear evidence of superconductivity, with the highest transition temperatures up to 55K–56K in the 1111 family, [37]. There fore FebSC is the second family of high temperature superconductors.

All FebSC compounds share similar electronic band structure in which the electronic states at the Fermi level are occupied predominantly by the Fe 3d electrons. The structure itself is quite complex and, in most cases, consist of five conduction bands that result in rather complex fermiology that changes rapidly with doping and, consequently, leads to many unusual superconducting and normal state properties. The FebSC phase diagrams with distinct areas of the AFM ordered spin density wave and superconductivity phases. In the following sessions we try to review their electronic, magnetic and superconductivity properties.

2.1.1 1111 Iron Based Superconductors Family

This family general form is $RFeAsO_{1-x}F_x$ where R= La, Nd, Sm Gd and Pr [41-51] called the 1111 FebSC family with maximum superconducting T_c=56K for R=Sm, but the material is hard to study by two reasons. First, the available single crystals are too small for all members of the family, second, the termination of the crystal reveals a polar surface with distinct surface states that are markedly different from the bulk electronic structure [42] and highly complicate the use of any surface sensitive experimental probe [43]. The crystal structure is shown in Fig. 2.1.

With the exception of $SmFeAsO_{1-x}F_x$, both structural and magnetic transitions temperatures are suppressed by doping in 1111 family before superconductivity appears. There are only a few examples of hole doping caused superconductivity in this family, primarily in $R_{1-x}Sr_xFeAsO$ [50] arguing for oxygen deficiency and thus effective electron doping in the R=La case. There is one example of iso electronic doped $CeFeAs_{1-x}P_xO$, where T_c remains zero [43] for $0 \le x \le 1$. Other wise, the doping in 1111's has been electron doping, with T_c's found above 50K.

2.1.2 122 Iron Based Superconductors Family

This 122 FebSC family has a general form AFe_2An_2 where A=Ca, Ba, and An= As, P, Se. The 122 FebSC family consists of a variety of different compounds with wide ranges of doping in both hole and electron sides [52-109] that form a rich phase diagram where the superconductivity and magnetism compete or coexist. The most studied compounds are the hole doped $Ba_{1-x}K_xFe_2As_2$ (K-Ba122) with T_c=38K [53] and the electron doped $Ba(Fe_{1-x}Co_x)_2As_2$ (Co-Ba122) of 24K T_c[54, 55]. Both share the same parent compound, $BaFe_2As_2$ (Ba122), which is a compensated metal, that is the total volume of its three hole Fermi surfaces is equal to the total volume of two electron Fermi surface [56, 57]. The parent

Ba122 goes into magnetically ordered phase below 140K [58] and never superconduc. An extremely over doped Ba122 is a stoichiometric KFe_2As_2 [59], which is non-magnetic, with T_c= 3K.

There is also an interesting case of isovalent doping, $BaFe_2(As_{1-x}P_x)_2$ with T_c= 30K [52] with similar phase diagram of other doped Ba122 compounds. To this, one can add a number of similar compounds like $Ba_{1-x}Na_xFe_2As_2$ with T_c=34K [60,61], $Ca_{1-x}Na_xFe_2As_2$ of T_c=20 K [62], $CaFe_2As_2$ of T_m=170K and T_c greater than 10K under pressure [63], $EuFe_2(As_{1-x}P_x)_2$ with T_c=26 K [64]. The ARPES spectra well represent the bulk electronic structure of this family, at least, for the hole doped 122 systems, where the superconducting gap is routinely observed [39, 41, 59] and is in a good agreement with the bulk probes [71,72]. This poses the 122 family as most familiar to study the rich physics of FebSCs superconductors.

2.1.3 111 Iron Based Superconductors Family

This iron family superconductors, RFeAs where R=Li, Na, La, Ce have variety of magnetic and superconducting properties [110-123]. They are being highly reactive with air and, consequently, more challenging to study. The 111 FebSC family has given many interesting results that keep growing. The main representative of the family, LiFeAs [110-113], is the most familiar compound. It grows in good quality single crystals [112] that cleave between the two Li layers as shown in Fig. 2.2, thus showing a non-polar surface with protected top most FeAs layer; it is stoichiometric, that is impurity clean; it has the SC transition temperature about 18K. It is non-magnetic and, consequently, the observed band structure is free of SDW replicas; and, finally, its electronic bands are the most separated from each other that allows one to disentangle them most easily and analyze their fine structure [113]. In Fig. 2.2 the crystal structure is shown.

The other 111 FebSC compound, NaFeAs, shows three successive phase transitions at around 52, 41, and 22K, which correspond to structural, magnetic, and SC transitions, respectively [114,115]. The compound is less reactive with the environment than the former LiFeAs but the exposure to air strongly affects SC transition temperature [116]. Replacing iron by either Cobalt or Nickel suppresses the magnetism and enhances superconductivity and coexistence between the two is also observed [117,118,119].

2.1.4 11 Iron Based Superconductors Family

Like previous three FebSCs this family consists variety of compounds [124-138] In Fig. 2.2 the crystal structure of 11 family is shown. The binary FeAs does not crystallize in the FeAs layered structure (it adopts an orthorhombic structure consisting of distorted $FeAs_6$ octahedra unlike the superconducting ferropnictides in which $FeAs_4$ tetrahedra form square lattices of iron atoms [124], but the FeSe does. So, the 11 FebSC family is presented by simplest ferro chalcogenides FeSe and FeTe, and their ternary combination $FeSe_xTe_{1-x}$ [73]. The FeSe has been found to superconduct at T_c=8K [126]), and up to 37K under pressure [127]. $Fe_{1+y}Se_xTe_{1-x}$ shows maximum T_c about 14K at x=0.5 [125, 126]. The crystals grow with excess dopant of iron Fe atoms that present beyond those needed to fill the Fe square lattice layers and go into interstitial positions within the Te layers [129-132].

2.1.5 245 Iron Based Superconductors Family

The attempts to intercalate the 11 family FeSe, the simplest FebSC, resulted in discovery of a new family $A_xFe_{2-y}Se_2$ (A stands for alkali metal like K, Rb, Cs, Tl) [139-148] with T_c up to 30K and with exceptionally magnetic transition temperature greater than 500K and magnetic moment greater than 3μB. This family called most often 245 because of its parent compound

$A_{0.8}Fe_{1.6}Se_2 \equiv A_2Fe_4Se_5$. It is interesting that their resistivity shows insulating behavior down to 100K and superconductivity seems to occur from an AFM semiconductor [142]. This, however, is not consistent with some experimental results which show the presence of a Fermi surface [143-146]. It is even more interesting that the observed Fermi surface is completely electron like that, seemingly, contradicts to the most popular s^{+-} scenario for superconducting pairing [101]. Recently, it has been shown [146], that the puzzling behavior of these materials is the result of separation into metallic and AFM insulating phases, from which only the former becomes superconducting, while the later has hardly any relation to superconductivity.

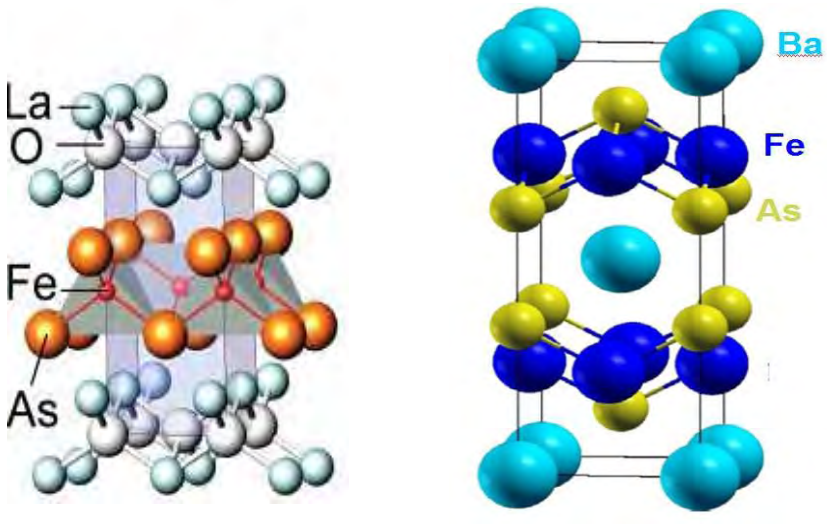

Figure 2.1:From , the lattice structure of 1111 LaFeAsO [52] (left panel) and lattice structure of 122 BaFe2As2. [52] (right panel)

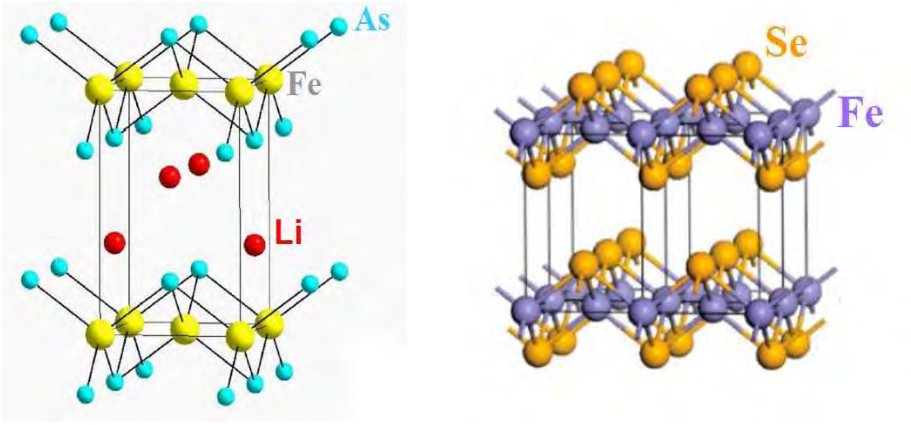

Figure 2.2: Crystal structure of 111 FebSC LiFeAs (left panel) and crystal structure of 11 FebSC FeSe [101] (right panel)

2.2 Electronic Structure of Iron Based Superconductors

After the discovery of the first FebSCs, different theories were applied to calculate the band structure and density of state [37]. They found that the parent compounds are semi metallic and the density of state near Fermi surface is mainly contributed by the iron 3d electrons and all five of the 3d electrons crosses Fermi surface. The shape of the structure depends on the doping level. The electronic structure of FebSCs at low energies is rather well established by different experiments like ARPES and quantum oscillation measurements [101,149]. In weakly and moderately electron doped materials, such as 122 FebSC compounds, the Fermi surface contains several quasi 2D warped cylinders centered at (0,0) and (π,π) in a 2D cross section, and may also contain a quasi 3D pocket near $K_z=\pi$ shown in figure 2.3. The fermionic dispersion is electron like near the Fermi surfaces at (π, π) and hole like near the Fermi surfaces centered at (0,0). In

heavily electron doped 245 FebSCs, only electron pockets remain [52].

In weakly and moderately hole doped FebSCs, such as K-Ba122, the electronic structure is similar to that at moderate electron doping, however the spherical Fermi-surface becomes the third quasi 2D hole Fermi-surface centered at (2π, 0) and (0,0). In addition, new low energy hole states likely appear around (π, π) and squeeze electron pockets [40]. At strong hole doping, electron Fermi-surfaces disappear and only hole Fermi-surfaces are present [40]. These electronic structures agree well with theoretical calculations [71,72], which is another argument to treat FebSCs as itinerant fermionic systems. The measured Fermi-surface reflects the actual crystal structure of FebSCs in which there are two non equivalent positions of a FebSCs above and below an iron plane, and, as a result, there are two Fe atoms (called folded BZ) in the unit cell. From a theoretical perspective, it would be easier to work in the BZ that contains only one Fe atom in the unit cell. In general both only a folded and unfolded BZs are physically meaningful and essential.

Most of the existing theoretical works [40, 52]on the pairing mechanism and the structure of the SC gap analyze the pairing problem in the unfolded BZ, in which two hole pockets are centered at (0,0) and at (π, π), and the two electron pockets are at (0, π) and (π, 0). It became increasingly clear recently that the interaction via a pnictogen or chalcogen and also 3D effects do play some role in the pairing, particularly in strongly electron doped systems [33]. However, it is still very likely that the key aspects of the pairing in FebSCs can be understood by analyzing a pure 2D electronic structure with only Fe states involved. It is recommended to consider a 2D model in the unfolded BZ with hole Fermi surfaces near (0,0) and (π, π) and electron Fermi-surfaces at (0, ±π) and (±π, 0).

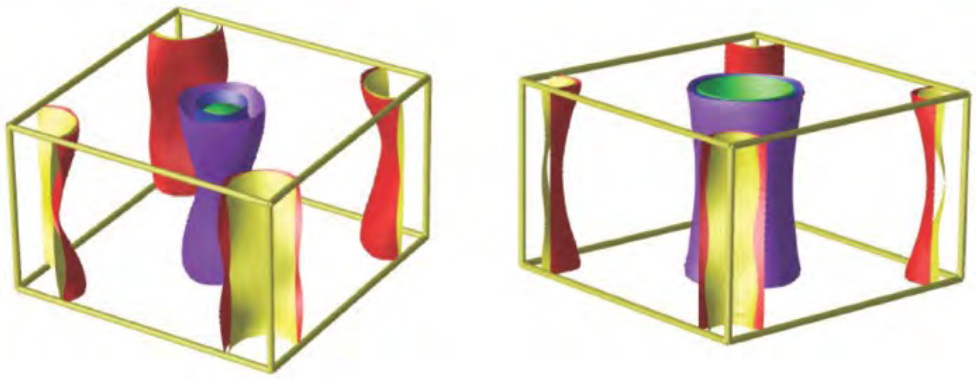

Figure 2.3: The electronic structure of FebSCs. In weakly and moderately electron doped (left panel) the Fermi-surface (FS) consists of quasi-2D warped cylinders centered at (0,0) and (π, π) in a 2D cross section. The ones near (0,0) are hole pockets (filled states are outside cylinders); the ones near (π, π) are electron pockets (filled states are inside cylinders). There also exists a quasi-3D hole pocket near $k_z = \pi$. In hole doped FebSCs (right panel) the electronic structure is very similar, but the 3D hole pocket becomes a quasi-2D warped hole cylinder. [33]

The quasi 2D feature in the electronic structure typically supports large fluctuation effect [40] when the system has the tendency to develop long range order. Another important feature associated with the two well separated sets of hole and electron pockets stems from fermiology: the nesting between matching hole and electron Fermi-surface pieces, which can drive the system into certain particle-hole instabilities. The nesting between hole and electron pockets in doped 122 FebSC family is observed by ARPES in a systematic study [40]. No doubt that there appear three- dimensional pockets in the complicated band structure of the materials, which affect the physical properties and necessarily need to be taken into account to understand some experimental data. But the existence of

quasi-2D structure may play a crucial role in the magnetic and superconducting phenomena.

2.3 Magnetic Order in Iron Based Superconductors

The nature of magnetism in FebSC compound is an intensively studied topic, due to its interplay with superconductivity and the possible relation with the pairing mechanism. As Neutron scattering experiments [36] illustrated most FebSC materials share an AFM long range order in the parent compounds with two inter penetrated Neel spin lattices such that AFM stripes form along one direction with ferromagnetic stripes along the perpendicular direction as shown in Fig. 2.4 (a). This type of magnetic order has an ordering wave vector at (π, 0) that matches the nesting wave vector. Therefore it is a major opinion that this magnetic state is a SDW state arising from the particle hole instability due to nesting, which is itinerant in nature. An interesting exception is the 11 FebSC family, in which the nesting is still at (π, π) but the static magnetic ordering vector is rotated by $\pi/4$, which is different from the nesting vector [40]. However, the observation of magnetic resonance mode corresponds to the nesting wave vector instead of the long-range magnetic ordering vector [101]. This interesting discrepancy indicates that nesting might be directly related to superconductivity through dynamical magnetism (spin fluctuations) while there is other stronger source to dominate static magnetism.

2.4 The Effect of Doping on Magnetic Order

One of the ways of achieving superconductivity in FebSC materials is via electron/hole doping. In the undoped state, the 122 compound exhibits simultaneous structural and magnetic phase transitions below 140K, changing from the high temperature paramagnetic tetragonal phase to the low temperature orthorhombic phase with the collinear AFM structure. On electron doping on 122

FebSC family the static AFM order is suppressed and superconductivity emerges [39]. From magnetic measurements of single crystals [86, 87], the phase diagram for Co-Ba122 was established, where the single structural/magnetic phase transition in Ba122 splits with increasing Co doping. Neutron diffraction experiments on Co-Ba122 [88] confirm that the commensurate AFM order appears below the structural transition temperature and superconductivity coexists with AFM order for $0.06 \leq x \leq 0.102$.

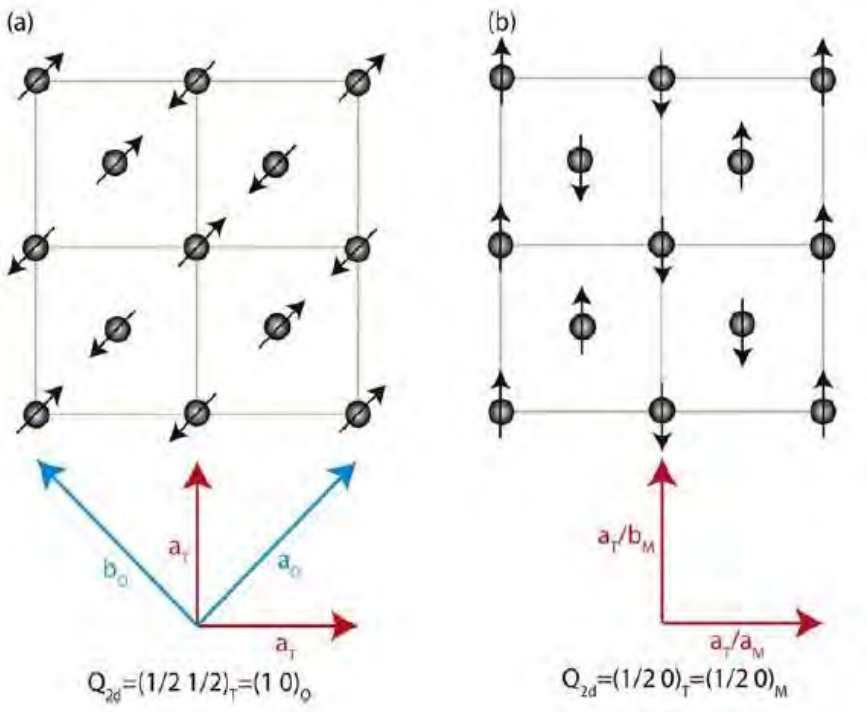

Figure 2.4: (color on line) In plane magnetic spin arrangement for undoped 1111 and 122 materials, part (a) and for 11 materials, part (b). The colored vectors denote the tetragonal ('T'), orthorhombic ('O') and monoclinic ('M') structures. [101].

Neutron scattering and other experiments on electron doped 122 FebSCs [89-92] confirmed that commensurate long range AFM coexist with SC in underdoped region. In addition, for electron doped Ba122 samples near optimal SC, it has been shown that the commensurate static AFM order changes into transversely incommensurate short range AFM order that coexists and competes with superconductivity [93,94]. For the underdoped regime commensurate AFM order seems to microscopically coexist with superconductivity in hole doped 122 compound short range incommensurate AFM order in K-Ba122 near optimal superconductivity [98].

2.5 Superconducting Gap Structure and Symmetry

As discussed, in FebSCs, superconductivity can be induced either by chemical doping or by external pressure [89]. Although chemical doping is more convenient, the pressure induced method is also appealing as it allows to study different phases in the same sample without comparing differently fabricated crystals. Similar to chemical doping, the external pressure then suppresses the magnetic ordering and superconductivity emerges. The vicinity of magnetic next to superconducting order appears in most families of FebSCs and possibly suggests a common spin fluctuation based pairing mechanism. Here, the rigid magnetic order is destabilized and provides a polarizable background which allows to mediate pairing. Additionally, the pairing mechanism also affects the symmetry of the superconducting gap (pair wave function), as the spin fluctuations (repulsive interaction) of ordering momentum **Q** only lead to pairing if the gap changes sign between connected portions of the Fermi-surface. In the FebSCs, this then implies a sign change in the superconducting gap between hole and electron pockets [37]. The corresponding pairing symmetry is commonly denoted as s^{+-} wave, since the superconducting gap reveals a sign change but

breaks no additional point group symmetries.

As mostly accepted the spin fluctuation mediated pairing is proposed as the common link in a broad class of SC materials [37]. Other pairing mechanisms based on the polarizability of the pnictogen or chalcogen ions [102], orbital fluctuations [104], or the Hund's coupling [46,105] were also proposed in the beginning, but mostly turned out to be inconsistent with certain experiments. In particular, conventional phonon based pairing was ruled out right from the beginning, as the calculated electron phonon coupling turned out to be too small [47] to account for the high T_c in FebSCs. Nevertheless, it was pointed out [39] that phonons could provide an indirect contribution to superconductivity via spin lattice coupling.

The pairing symmetry and pairing mechanism of FebSCs have also been the focus of numerous experimental works. Several important indications could be obtained. For example NMR measurements [48] reported spin singlet pairing in all crystallographic directions. Others like neutron scattering [101] and scanning tunneling experiments [139] suggest a sign changing pair wave function that is not inconsistent with an s^{+-} wave gap. In addition, certain Josephson interference experiments make the d wave pairing unlikely [108], and rather support an s^{+-} wave scenario.

Usually, the s^{+-} wave gap was assumed to be fully gapped and a number of experiments reporting gap nodes seemed to be at odds with such an s^{+-} wave pairing state. However, it is now understood that the existence of nodes in an s^{+-} wave gap depends on details of the multi orbital band structure and may vary between different FebSC compounds. Experiements consistently reported a full gap [78,99,100] and never revealed significant gap anisotropies or gap nodes which are, one the other hand, clearly seen in the cuprate d wave gap. A possible

explanation for this disagreement between bulk and surface probes was provided in [101] who pointed out the existence of an additional pocket in the surface band structure stabilizing a full gap.

2.6 Spin density wave and Superconductivity in Iron Based Superconductors

The evolution between the SDW and SC phases in the underdoped regime of the FebSCs has been extensively investigated, though consistent result is still lacking. Different experimental probes on various iron pnictide compounds have revealed different categories of behavior. Evidences on first family $LaFeAsO_{1-x}F_x$ (La111) [48] suggests that the abrupt transition from SDW to SC is first order like with out coexistence of the two phases. On the other 1111 compound, $SmFeAsO_{1-x}F_x$ [40] reveal second order transition from SDW to SC states. The electron doped 1111 family such as Co/Ni/Ru-Ca1111 the second order phase transition [39]. In an intermediate case, neutron scattering in $CeFeAsO_{1-x}F_x$ reveals a continuous transition, but the SDW and SC regimes only touches at a quantum critical point. Even recent nuclear magnetic resonance measurements for the La1111 series suggest that the AFM and SC phases are segregated on the electronic phase diagram [147]. Although the coexistence of these phases has been suggested in the Ca1111 series, it is not certain whether the AFM ordering in the crossover regime is of the same nature as that of the underdoped regime.

In the third family, 111 FebSC system the electron doped Co/Ni/Ru-Na111 the overlap region between the two states has been shown according to the experimental evidences [147], the other compounds of this group transition from SDW to SC is first order [38]. There is also strong evidence for microscopic coexistence coming from the same Fe 3d electrons in 122 family like Co-Ba122 which has excellent sample homogeneity. Other studies in underdoped region of

doped 122 FebSCs compounds like $BaFe_2(As_{1-x}Px)_2$, $Ba(Fe_{1-x}Ru_x)_2As_2$ and K-Ba122 [150-151] the microscopic coexistence between SDW and superconductivity had been shown.

Homogeneous coexistence of the SDW and SC states has been suggested on oxygen free electron-doped 1111 family $CaFe_{1-x}Co_xAsF$ (Co-Ca1111) [147]. An overlap between the SDW and SC domes decreases with increasing interlayer distance of FeAs planes; therefore, the Ba122 series has a large overlap, the Ca1111 series has a smaller one, and the La1111 series has no overlap.

When we come to the width of the coexistence for the Ba122 series, the phase overlap is large because the optimal doping level for superconductivity is located at the phase boundary between the AFM and SC phases. However, for the Co/Ni-Ca1111 series, the phase overlap is smaller than that of the Ba122 series because the optimal doping level is away from the phase boundary [147]. The homogeneous coexistence of the incommensurate SDW and SC states occurs only in a narrow doping region around the crossover regime, which supports s^{+-} wave symmetry.

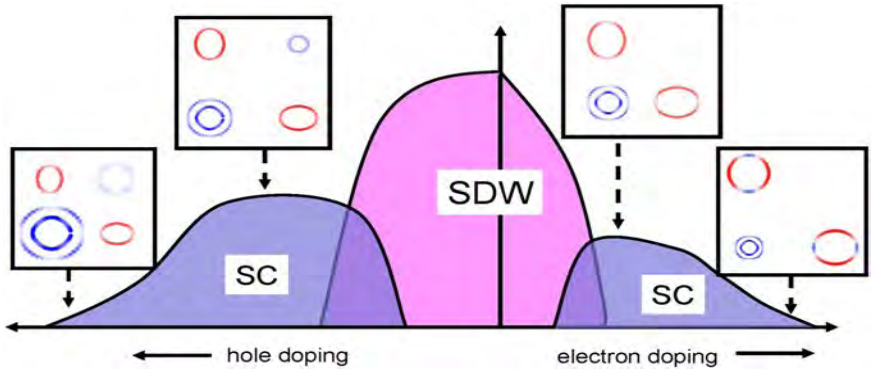

Figure 2.5:.Schematic phase diagram of FebSC versus doping, with the order parameter expected from 2D spin fluctuation theory [101]

The general phase diagram showing the magnetic spin density wave and superconductivity states for the two (hole and electron doped) FebSCs are shown in Fig. 2.5. Now in both electron doped and hole doped FebSCs systems the microscopic coexistence of the two order parameters is being accepted even though there are few conflicting early reports. Therefor the microscopic coexistence of magnetism and superconductivity has attracted wide attention for its possible implication on pairing symmetry and mechanism of superconductivity.

CHAPTER 3: A MODEL FORMULATION FOR SDW-SC INTERPLAY

CHAPTER 3

A MODEL FORMULATION FOR SDW-SC INTERPLAY

3.1 Model Hamiltonian

In developing the Hamiltonian we consider a multiband model nature of FebSC compounds as an itinerant metal containing electron bands and hole bands at the center of unfolded Brillouin zones and at the corners of each Brillouin zone respectively. On other word, the Fermi surface for the hole band is centered at the point center of BZ of the unfolded Brillouin zone defined by **Q**=(0,0) and the Fermi surface of the electron bands are centered at the corner points, defined by vectors $\mathbf{Q}_1$ = (±π, 0) and $\mathbf{Q}_2$ = (0, ±π). As explained in previous chapter the inter pocket [37] interaction is important to study the low energy physics particularly the interplay between SDW and SC of most FebSCs. This is where we emphasize in developing the Hamiltonian.

$$\begin{aligned} \boldsymbol{H} &= \sum_{\boldsymbol{k}\sigma} \xi_a(\boldsymbol{k}) a^{\dagger}_{\boldsymbol{k}\sigma} a_{\boldsymbol{k}\sigma} + \sum_{\boldsymbol{k}\sigma} \xi_d(\boldsymbol{k}) d^{\dagger}_{\boldsymbol{k}\sigma} d_{\boldsymbol{k}\sigma} \\ &+ \sum_{\boldsymbol{k}\boldsymbol{k}'} V^{s}_{\boldsymbol{k}\boldsymbol{k}'} \left(a^{\dagger}_{\boldsymbol{k}\uparrow} a^{\dagger}_{-\boldsymbol{k}\downarrow} d_{-\boldsymbol{k}'\uparrow} d_{\boldsymbol{k}'\downarrow} + d^{\dagger}_{\boldsymbol{k}\uparrow} d^{\dagger}_{-\boldsymbol{k}\downarrow} a_{-\boldsymbol{k}'\uparrow} a_{\boldsymbol{k}'\downarrow} \right) \\ &+ \sum_{\boldsymbol{k}\boldsymbol{k}'\sigma} V^{m}_{\boldsymbol{k}\boldsymbol{k}'\sigma} \sigma a^{\dagger}_{\boldsymbol{k}\sigma} d_{\boldsymbol{k}'\sigma} a_{\boldsymbol{k}'\sigma'} d^{\dagger}_{\boldsymbol{k}\sigma'} \end{aligned} \tag{3.1}$$

In the model Hamiltonian, the first two terms describe the itinerant electrons forming the hole and electron Fermi pockets near the Fermi energy. Moreover, these electrons are responsible for the third pair interaction (singlet superconducting channel) and the fourth magnetic interactions. The operates $a_k \; and \; d_k$ are the operators for hole and electron bands respectively, and the respective dispersions near the two pockets are $\xi_a(\boldsymbol{k}) \; and \; \xi_d(\boldsymbol{k})$.

3.2 Superconducting State

In most FebSC systems, superconductivity emerges upon electron or hole doping, or can be induced by pressure or by isovalent doping. In some FebSCs like electron doped Ca111 compound, superconductivity emerges already at zero doping. Therefor it is necessarily to study superconducting state when the magnetic interaction is neglected so that the Hamiltonian could be

$$\begin{aligned} \boldsymbol{H}_S &= \sum_{k\sigma} \xi_a(\boldsymbol{k})\, a^{\dagger}_{k\sigma} a_{k\sigma} + \sum_{k\sigma} \xi_d(\boldsymbol{k})\, d^{\dagger}_{k\sigma} d_{k\sigma} \\ &+ \sum_{kk'} V^{s}_{kk'} \left(a^{\dagger}_{k\uparrow} a^{\dagger}_{-k\downarrow} d_{-k'\uparrow} d_{k'\downarrow} + d^{\dagger}_{k\uparrow} d^{\dagger}_{-k\downarrow} a_{-k'\uparrow} a_{k'\downarrow} \right). \end{aligned} \tag{3.2}$$

To decouple the Hamiltonian we use the mean field approximation, and thus the mean field Hamiltonian of SC state, expressed as

$$\begin{aligned} \boldsymbol{H}_{Sf} &\approx \sum_{k\sigma} \xi_a(\boldsymbol{k})\, a^{\dagger}_{k\sigma} a_{k\sigma} + \sum_{k\sigma} \xi_d(\boldsymbol{k}) d^{\dagger}_{k\sigma} d_{k\sigma} \\ &+ \sum_{k} \Delta_a(\boldsymbol{k}) \left(a^{\dagger}_{k\uparrow} a^{\dagger}_{-k\downarrow} + h.c \right) + \sum_{k'} \Delta_d(\boldsymbol{k}) \left(d^{\dagger}_{k\uparrow} d^{\dagger}_{k\downarrow} + h.c \right) \end{aligned} \tag{3.3}$$

where the mean fields are

$$\begin{aligned} \Delta_a(\boldsymbol{k}) &= \sum_{k\sigma} V^{s}_{kk'} \langle a^{\dagger}_{k\uparrow} a^{\dagger}_{-k\downarrow} \rangle \\ \Delta_a(\boldsymbol{k}) &= \sum_{k'} v^{S}_{kk'} \langle d^{\dagger}_{k\uparrow} d^{\dagger}_{-k\downarrow} \rangle . \end{aligned} \tag{3.4}$$

3.2.1 Green function theory and Superconductivity

Here we present the method of Green functions and see how gap functions are calculated. The Green function method, in contrast to other diagonalization methods like Bogoljubov transformation requires a matrix inversion and application of basic complex analysis. In order to drive the gap equation one of the formalism is the Green function method. To do this we must express the Hamiltonian using Nambu operators like

$$\boldsymbol{H}_S \approx \sum_{k\sigma} \hat{\phi}^{\dagger}_k \hat{H}_{sk} \phi_k \tag{3.5}$$

where the Nambu spinors are

$$\hat{\phi}_{\boldsymbol{k}}^{\dagger} = \begin{pmatrix} \hat{\eta}_{a\boldsymbol{k}} & \hat{\eta}_{d\boldsymbol{k}} \end{pmatrix} \tag{3.6}$$

with

$$\begin{aligned} \hat{\eta}_{a\boldsymbol{k}} &= \begin{pmatrix} a_{\boldsymbol{k}\uparrow}^{\dagger} & a_{-\boldsymbol{k}\downarrow} \end{pmatrix} \\ \hat{\eta}_{d\boldsymbol{k}} &= \begin{pmatrix} d_{\boldsymbol{k}'\uparrow}^{\dagger} & d_{-\boldsymbol{k}'\downarrow} \end{pmatrix}. \end{aligned} \tag{3.7}$$

The energy matrix

$$\hat{H}_{S\boldsymbol{k}} = \begin{pmatrix} \hat{H}_{a\boldsymbol{k}} & 0 \\ 0 & \hat{H}_{d\boldsymbol{k}} \end{pmatrix} \tag{3.8}$$

with

$$\begin{aligned} \hat{H}_{a\boldsymbol{k}} &= \begin{pmatrix} \xi_a(\boldsymbol{k}) & \Delta_a(\boldsymbol{k}) \\ \Delta_a(\boldsymbol{k}) & -\xi_a(\boldsymbol{k}) \end{pmatrix} \\ \hat{H}_{d\boldsymbol{k}} &= \begin{pmatrix} \xi_d(\boldsymbol{k}) & \Delta_d(\boldsymbol{k}) \\ \Delta_d(\boldsymbol{k}) & -\xi_d(\boldsymbol{k}) \end{pmatrix}. \end{aligned} \tag{3.9}$$

The Green function matrix is defined as

$$\hat{\boldsymbol{G}}(\boldsymbol{k}) = \begin{pmatrix} \hat{G}_{a\boldsymbol{k}} & 0 \\ 0 & \hat{G}_{d\boldsymbol{k}} \end{pmatrix} \tag{3.10}$$

where

$$\begin{aligned} \hat{\boldsymbol{G}}_a(\boldsymbol{k}) &= \begin{pmatrix} G_a^{\uparrow}(\boldsymbol{k}) & G_a^{\uparrow\downarrow}(\boldsymbol{k}) \\ G_a^{\downarrow\uparrow}(\boldsymbol{k}) & G_a^{\downarrow}(\boldsymbol{k}) \end{pmatrix} \\ \hat{\boldsymbol{G}}_d(\boldsymbol{k}) &= \begin{pmatrix} G_d^{\uparrow}(\boldsymbol{k}) & G_d^{\uparrow\downarrow}(\boldsymbol{k}) \\ G_d^{\downarrow\uparrow}(\boldsymbol{k}) & G_d^{\downarrow}(\boldsymbol{k}) \end{pmatrix}. \end{aligned} \tag{3.11}$$

From the Hamiltonian in equation (3.5) the inverse Greens function can be calculated easily using

$$\hat{\boldsymbol{G}}(i\omega,\boldsymbol{k}) = \left(i\omega.\hat{I} - \hat{\boldsymbol{H}}_{\boldsymbol{k}}\right)^{-1} = \begin{pmatrix} \hat{\boldsymbol{G}}_a(i\omega,\boldsymbol{k}) & 0 \\ 0 & \hat{\boldsymbol{G}}_d(i\omega,\boldsymbol{k}) \end{pmatrix} \tag{3.12}$$

where

$$\hat{G}_a(i\omega,\boldsymbol{k}) = \begin{pmatrix} G_a^{\uparrow}(i\omega,\boldsymbol{k}) & G_a^{\uparrow\downarrow}(i\omega,\boldsymbol{k}) \\ G_a^{\downarrow\uparrow}(i\omega,\boldsymbol{k}) & G_a^{\downarrow}(i\omega,\boldsymbol{k}) \end{pmatrix}$$
$$\hat{G}_d(i\omega,\boldsymbol{k}) = \begin{pmatrix} G_d^{\uparrow}(i\omega,\boldsymbol{k}) & G_d^{\uparrow\downarrow}(i\omega,\boldsymbol{k}) \\ G_d^{\downarrow\uparrow}(i\omega,\boldsymbol{k}) & G_d^{\downarrow}(i\omega,\boldsymbol{k}) \end{pmatrix}. \quad (3.13)$$

The equations of the components of the matrix (3.12) can be easily found from the inverse matrix of (3.12)

$$G_a^{\uparrow\downarrow}(i\omega,\boldsymbol{k}) = \langle\langle a_{\boldsymbol{k}\uparrow}^{\dagger}; a_{-\boldsymbol{k}\downarrow}^{\dagger}\rangle\rangle_{\omega}$$
$$= \frac{\Delta_a(\boldsymbol{k})\left((i\omega)^2+\xi_a^2(\boldsymbol{k})\Delta_d^2(\boldsymbol{k})\right)}{\left(i\omega-E_a(\boldsymbol{k})\right)\left(i\omega+E_a(\boldsymbol{k})\right)\left(i\omega-E_d(\boldsymbol{k})\right)\left(i\omega+E_d(\boldsymbol{k})\right)} \quad (3.14)$$

and

$$G_d^{\uparrow\downarrow}(i\omega,\boldsymbol{k}) = \langle\langle d_{\boldsymbol{k}+\boldsymbol{Q}\uparrow}^{\dagger}; d_{-\boldsymbol{k}-\boldsymbol{Q}\downarrow}^{\dagger}\rangle\rangle_{\omega}$$
$$= \frac{\Delta_d(\boldsymbol{k})\left((i\omega)^2+\xi_d^2(\boldsymbol{k})\Delta_a^2(\boldsymbol{k})\right)}{\left(i\omega-E_a(\boldsymbol{k})\right)\left(i\omega+E_a(\boldsymbol{k})\right)\left(i\omega-E_d(\boldsymbol{k})\right)\left(i\omega+E_d(\boldsymbol{k})\right)} \quad (3.15)$$

where $E_{a/d}$ (k) are the eigenvalue expressed as

$$E_{a/d}^2(\boldsymbol{k}) = \xi_{a/d}^2(\boldsymbol{k})+\Delta_{a/d}^2(\boldsymbol{k}). \quad (3.16)$$

The superconducting gap equations: The mean value of the right side of the gap equation (3.4) are expressed as a sum over the discreet Matsubara frequencies:

$$\langle a_{\boldsymbol{k}\uparrow}^{\dagger} a_{-\boldsymbol{k}\downarrow}^{\dagger}\rangle = \frac{1}{\beta}\sum_{i\omega} e^{i\omega} G_a^{\uparrow\downarrow}(\boldsymbol{k},i\omega). \quad (3.17)$$

Substituting the Green function (3.14) to (3.15) and summing over Matsubara frequencies results using [154]

$$\langle a_{\boldsymbol{k}\uparrow}^{\dagger} a_{-\boldsymbol{k}\downarrow}^{\dagger}\rangle = \Delta_a\left(\frac{f(E_a(\boldsymbol{k}))}{2E_a(\boldsymbol{k})} - \frac{f(-E_a(\boldsymbol{k}))}{2E_a(\boldsymbol{k})}\right)$$
$$= \frac{\Delta_a(\boldsymbol{k})}{2E_a(\boldsymbol{k})}\tanh\left(\frac{E_a(\boldsymbol{k})}{2T}\right). \quad (3.18)$$

Similarly

$$\begin{aligned}\langle d^{\dagger}_{\boldsymbol{k}+\boldsymbol{Q}\uparrow} d^{\dagger}_{-\boldsymbol{k}+\boldsymbol{Q}\downarrow}\rangle &= \Delta_d\left(\frac{f(E_d(\boldsymbol{k}))}{2E_d(\boldsymbol{k})} - \frac{f(-E_d(\boldsymbol{k}))}{2E_d(\boldsymbol{k})}\right) \\ &= \frac{\Delta_d(\boldsymbol{k})}{2E_d(\boldsymbol{k})}\tanh\left(\frac{E_d(\boldsymbol{k})}{2T}\right).\end{aligned} \tag{3.19}$$

Hence the two gap equations are calculated to be

$$\begin{aligned}\Delta_a(\boldsymbol{k}) &= \sum_{\boldsymbol{k}} V^{S}_{\boldsymbol{k}\boldsymbol{k}'}\frac{\Delta_d(\boldsymbol{k})}{2E_d(\boldsymbol{k})}\tanh\left(\frac{E_d(\boldsymbol{k})}{2T}\right) \\ \Delta_d(\boldsymbol{k}) &= \sum_{\boldsymbol{k}} V^{S}_{\boldsymbol{k}\boldsymbol{k}'}\frac{\Delta_a(\boldsymbol{k})}{2E_a(\boldsymbol{k})}\tanh\left(\frac{E_a(\boldsymbol{k})}{2T}\right).\end{aligned} \tag{3.20}$$

3.2.2 Bogoliubov Transformation in Superconductivity

A Bogoliubov transformation can also be used to diagonalize the Hamiltonian and to drive gap equations. That is a simple two-dimensional rotation can diagonalize the mean-field Hamiltonian. Such a rotation is equivalent to introducing new operators, called Bogoliubov operators, which are certain linear combinations of the old ones, where the fermionic anti-commutation relations remain valid. This kind of rotation is known as canonical or Bogoliubov transformation [XX]. The mean-field Hamiltonian (3.3) can be written as

$$\begin{aligned}\boldsymbol{H}_{Sf} &\approx \sum_{\boldsymbol{k}\sigma}\hat{\phi}^{\dagger}_{a\boldsymbol{k}}\hat{\boldsymbol{H}}_{a\boldsymbol{k}}\hat{\phi}_{a\boldsymbol{k}} + \sum_{\boldsymbol{k}}\hat{\phi}^{\dagger}_{d\boldsymbol{k}}\hat{\boldsymbol{H}}_{d\boldsymbol{k}}\hat{\phi}_{d\boldsymbol{k}} \\ &= \sum_{\boldsymbol{k}}\hat{X}^{\dagger}_{a\boldsymbol{k}}\hat{\boldsymbol{H}}^{D}_{a\boldsymbol{k}}\hat{X}_{a\boldsymbol{k}} + \sum_{\boldsymbol{k}}\hat{X}^{\dagger}_{d\boldsymbol{k}}\hat{\boldsymbol{H}}^{D}_{d\boldsymbol{k}}\hat{X}_{d\boldsymbol{k}}.\end{aligned} \tag{3.21}$$

The Bogoliubov quasi particle matrix for this transformation is defined as

$$\begin{aligned}\hat{X}^{\dagger}_{a\boldsymbol{k}} &= \begin{pmatrix} f^{\dagger}_{\boldsymbol{k}} & f_{-\boldsymbol{k}}\end{pmatrix} \\ \hat{X}^{\dagger}_{d\boldsymbol{k}} &= \begin{pmatrix} b^{\dagger}_{\boldsymbol{k}} & b_{-\boldsymbol{k}}\end{pmatrix}.\end{aligned} \tag{3.22}$$

Their relation with old fermion operators is defined as

$$\begin{aligned}a^{\dagger}_{\boldsymbol{k}\uparrow} &= u_{\boldsymbol{k}}f^{\dagger}_{\boldsymbol{k}\uparrow} + v_{\boldsymbol{k}}f_{-\boldsymbol{k}\downarrow} \\ d^{\dagger}_{\boldsymbol{k}\uparrow} &= x_{\boldsymbol{k}}b^{\dagger}_{\boldsymbol{k}} + y_{\boldsymbol{k}}b_{-\boldsymbol{k}\downarrow}.\end{aligned} \tag{3.23}$$

The coherence factors satisfy the following relation

$$\begin{aligned} u_k^2, v_k^2 &= \frac{1}{2}\left(1 \pm \frac{\xi_a(\boldsymbol{k})}{\sqrt{\xi_a^2(\boldsymbol{k}) + \Delta_a^2(\boldsymbol{k})}}\right) \\ u_k v_k &= -\frac{\Delta_a(\boldsymbol{k})}{2E_a(\boldsymbol{k})} \end{aligned} \tag{3.24}$$

and

$$\begin{aligned} x_k^2, y_k^2 &= \frac{1}{2}\left(1 \pm \frac{\xi_d(\boldsymbol{k})}{\sqrt{\xi_d^2(\boldsymbol{k}) + \Delta_d^2(\boldsymbol{k})}}\right) \\ x_k y_k &= -\frac{\Delta_d(\boldsymbol{k})}{2E_d(\boldsymbol{k})} \quad . \end{aligned} \tag{3.25}$$

Applying the stated transformations diagonalizes the Hamiltonian in the following form

$$\boldsymbol{H}_{sf} \approx \sum_{k\sigma} E_f(\boldsymbol{k}) f_{k\sigma}^{\dagger} f_{k\sigma} + \sum_{k\sigma} E_b(\boldsymbol{k}) b_{k\sigma}^{\dagger} b_{k\sigma}. \tag{3.26}$$

The eigenvalues $E_{f/b}(k)$ are the same as that of the section 3.2.1

The SC gap equations: To calculate the gap equations, the expectation value of (3.4) is computed using the mean-field Hamiltonian which is diagonal in the BG quasi particle. Thefor the electron operators are expressed in terms of the quasi particle operators and then we apply Fermi statistics.

$$\begin{aligned} \langle a_{k\uparrow}^{\dagger} a_{-k\downarrow}^{\dagger} \rangle &= \langle (u_k f_k^{\dagger} + v_k f_{-k})(-v_k f_k + u_k f_{-k}^{\dagger}) \rangle \\ &\approx u_k v_k \left(\langle f_k^{\dagger} f_k \rangle - \langle f_{-k}^{\dagger} f_{-k} \rangle \right) \\ &= u_k v_k \left(1 - 2 f(E_f(\boldsymbol{k}))\right) \\ &= \frac{\Delta_a(\boldsymbol{k})}{2E_f(\boldsymbol{k})} \tanh\left(\frac{E_f(\boldsymbol{k})}{2T}\right). \end{aligned} \tag{3.27}$$

The other band mean value

$$\begin{aligned} \langle d_{k\uparrow}^{\dagger} d_{-k\downarrow}^{\dagger} \rangle &= \langle (x_k b_k^{\dagger} + y_k b_{-k})(-y_k b_k + x_k b_{-k}^{\dagger}) \rangle \\ &\approx x_k y_k \left(\langle b_k^{\dagger} b_k \rangle - \langle b_{-k}^{\dagger} b_{-k} \rangle \right) \\ &= x_k y_k \left(1 - 2 f(E_b(\boldsymbol{k}))\right) \\ &= \frac{\Delta_a(\boldsymbol{k})}{2E_b(\boldsymbol{k})} \tanh\left(\frac{E_b(\boldsymbol{k})}{2T}\right) \quad . \end{aligned} \tag{3.28}$$

The gap equation therefore becomes

$$\begin{aligned}\Delta_a(\boldsymbol{k}) &= \sum_{\boldsymbol{k}} V^S_{\boldsymbol{k}\boldsymbol{k}'}\frac{\Delta_d(\boldsymbol{k})}{2E_d(\boldsymbol{k})}\tanh\left(\frac{E_d(\boldsymbol{k})}{2T}\right)\\ \Delta_d(\boldsymbol{k}) &= \sum_{\boldsymbol{k}} V^S_{\boldsymbol{k}\boldsymbol{k}'}\frac{\Delta_a(\boldsymbol{k})}{2E_a(\boldsymbol{k})}\tanh\left(\frac{E_a(\boldsymbol{k})}{2T}\right).\end{aligned} \tag{3.29}$$

3.2.3 Free Energy in Superconductivity

Free energy of a certain thermodynamic system is a function from which other thermodynamic quantities like entropy, energy gap functions, etc can be derived. Furthermore the minimum of the Free energy corresponds to the equilibrium state of the thermodynamic system. For example in superconducting state the minimum of the Free energy defined as $\partial \boldsymbol{F}/\partial\Delta=0$, has free energy and SC order parameter. From which we can compute the equation for SC order parameter. For our superconducting system the diagonal form of the mean-field Hamiltonian with inclusion of the interaction part is

$$\boldsymbol{H}_{sf} = \sum_{\boldsymbol{k}\sigma} E_f(\boldsymbol{k}) f^{\dagger}_{\boldsymbol{k}\sigma} f_{\boldsymbol{k}\sigma} + \sum_{\boldsymbol{k}\sigma} E_b(\boldsymbol{k}) b^{\dagger}_{\boldsymbol{k}\sigma} b_{\boldsymbol{k}\sigma} - 2\frac{\Delta_a(\boldsymbol{k})\Delta_d \boldsymbol{k}}{V^S_{\boldsymbol{k}\boldsymbol{k}'}}. \tag{3.30}$$

Recalling that the Free energy of the non interacting quasi-particles is defined as

$$\boldsymbol{F} = -T\ln(Z). \tag{3.31}$$

From (3.30) the Free energy is calculated to

$$F_S = -2T\sum_{\boldsymbol{k},\nu=f,b}\ln\left(\cosh\left(\frac{E_\nu(\boldsymbol{k})}{2T}\right)\right) - 2\frac{\Delta_a(\boldsymbol{k})\Delta_d(\boldsymbol{k})}{V^S_{\boldsymbol{k}\boldsymbol{k}'}}. \tag{3.32}$$

In (3.32) $E_f(\boldsymbol{k})\ and\ E_b(\boldsymbol{k})$ are the quasi particle energies. Now minimization of the Free energy (3.32) with respect to $\Delta_{a/d}$, $\partial F/\partial\Delta_{a/d}(k)=0$ and solving for the two gap parameter yields the following SC gap equations which are similar to the previous ones.

$$\begin{aligned}\Delta_a(\boldsymbol{k}) &= \sum_{\boldsymbol{k}} V^S_{\boldsymbol{k}\boldsymbol{k}'}\frac{\Delta_d(\boldsymbol{k})}{2E_d(\boldsymbol{k})}\tanh\left(\frac{E_d(\boldsymbol{k})}{2T}\right)\\ \Delta_d(\boldsymbol{k}) &= \sum_{\boldsymbol{k}} V^S_{\boldsymbol{k}\boldsymbol{k}'}\frac{\Delta_a(\boldsymbol{k})}{2E_a(\boldsymbol{k})}\tanh\left(\frac{E_a(\boldsymbol{k})}{2T}\right).\end{aligned} \tag{3.33}$$

3.3 Spin Density Wave State

The model Hamiltonian equation (3.1) can yield a Spin density wave phase for zero superconducting interaction. In order to induce Spin density wave order with ordering momentum at the corners of the Brillouin zone ,**Q** = (0, ±π) the interaction $V^{m}_{\boldsymbol{k}\boldsymbol{k}'\sigma}=V^{m}_{\boldsymbol{k}\boldsymbol{k}'}$ and then the mean-field Hamiltonian is

$$\begin{aligned}\boldsymbol{H}_{\boldsymbol{mf}} \approx & \sum_{\boldsymbol{k}\sigma}\xi_{a}(\boldsymbol{k})a^{\dagger}_{\boldsymbol{k}\sigma}a_{\boldsymbol{k}\sigma}+\sum_{\boldsymbol{k}\sigma}\xi_{d}(\boldsymbol{k})d^{\dagger}_{\boldsymbol{k}\sigma}d_{\boldsymbol{k}\sigma} \\ & +\sum_{\boldsymbol{k}\sigma}\Delta_{m}(\boldsymbol{k})\left(\sigma a^{\dagger}_{\boldsymbol{k}\sigma}d_{\boldsymbol{k}+\boldsymbol{Q}\sigma}+h.c\right).\end{aligned} \tag{3.34}$$

We note that (3.34) is obtained after introducing the mean field

$$\Delta_{m}(\boldsymbol{k}) = \sum_{\boldsymbol{k}\sigma}V^{m}_{\boldsymbol{k}\boldsymbol{k}'\sigma}\langle a^{\dagger}_{\boldsymbol{k}\sigma}d_{\boldsymbol{k}+\boldsymbol{Q}\sigma}\rangle. \tag{3.35}$$

3.3.1 Green Function Theory in Spin Density Wave State

The mean-field Hamiltonian of spin density wave phase in Nambu representation may be written as

$$\boldsymbol{H}_{\boldsymbol{mf}} \approx \sum_{\boldsymbol{k}\sigma}\hat{\phi}^{\dagger}_{m\boldsymbol{k}}\hat{\boldsymbol{H}}_{m\boldsymbol{k}}\hat{\phi}_{m\boldsymbol{k}} \tag{3.36}$$

where the Nambu operators

$$\begin{aligned}\hat{\phi}^{\dagger}_{m\boldsymbol{k}} &= \begin{pmatrix}a^{\dagger}_{\boldsymbol{k}\sigma} & d^{\dagger}_{\boldsymbol{k}+\boldsymbol{Q}\sigma}\end{pmatrix} \\ \hat{\boldsymbol{H}}_{m\boldsymbol{k}} &= \begin{pmatrix}\xi_{a}(\boldsymbol{k}) & \sigma\Delta_{m}(\boldsymbol{k}) \\ \sigma\Delta_{m}(\boldsymbol{k}) & \xi_{d}(\boldsymbol{k})\end{pmatrix}.\end{aligned} \tag{3.37}$$

The matrix (3.37) eigenvalue is

$$\Xi_{d/a}(\boldsymbol{k}) = \frac{1}{2}\left[\xi_{a}(\boldsymbol{k})+\xi_{d}(\boldsymbol{k}) \pm\sqrt{\left(\xi_{a}(\boldsymbol{k})-\xi_{d}(\boldsymbol{k})\right)^{2}+4\Delta^{2}_{m}(\boldsymbol{k})}\right]. \tag{3.38}$$

The Green function matrix for spin density wave state is defined as

$$\hat{\boldsymbol{G}}_m(\boldsymbol{k}) = \begin{pmatrix} G_{a\,\boldsymbol{k}} & G_{ad}(\boldsymbol{k}) \\ G_{ad}(\boldsymbol{k}) & \hat{G}_{d\,\boldsymbol{k}} \end{pmatrix}. \tag{3.39}$$

From the Hamiltonian in equation (3.36) the inverse Greens function can be calculated easily using

$$\hat{\boldsymbol{G}}_m(i\omega,\boldsymbol{k}) = \left(i\omega.\hat{I} - \hat{\boldsymbol{H}}_{\boldsymbol{k}}\right)^{-1} = \begin{pmatrix} G_a(i\omega,\boldsymbol{k}) & G_{ad}(i\omega,\boldsymbol{k}) \\ G_{ad}(i\omega,\boldsymbol{k}) & \hat{G}_d(i\omega,\boldsymbol{k}) \end{pmatrix}. \tag{3.40}$$

The equations of the components of the matrix (3.40) can easily be found from the inverse matrix.

$$\begin{aligned} G_{ad}(i\omega,\boldsymbol{k}) &= \langle\langle a^{\dagger}_{\boldsymbol{k}\sigma}; d_{\boldsymbol{k}+\boldsymbol{Q}\sigma}\rangle\rangle_{\omega} \\ &= \frac{\Delta_m(\boldsymbol{k})}{\left(i\omega-\Xi_a(\boldsymbol{k})\right)\left(i\omega+\Xi_d(\boldsymbol{k})\right)}. \end{aligned} \tag{3.41}$$

Like SC gap equation the spin density wave gap equation can be obtained starting from the expectation value

$$\langle a^{\dagger}_{\boldsymbol{k}\sigma} d_{\boldsymbol{k}+\boldsymbol{Q}\sigma}\rangle = \sum_{i\omega} \frac{\Delta_m(\boldsymbol{k})}{\left(i\omega-\Xi_a(\boldsymbol{k})\right)\left(i\omega+\Xi_d(\boldsymbol{k})\right)}. \tag{3.42}$$

There fore the SDW gap equation from this method is

$$\Delta_m(\boldsymbol{k}) = \sum_{\boldsymbol{k}} V^{m}_{\boldsymbol{k}\boldsymbol{k}'} \frac{\Delta_m(\boldsymbol{k})}{2\Xi(\boldsymbol{k})}\left[\tanh\left(\frac{\Xi_d(\boldsymbol{k})}{2T}\right) - \tanh\left(\frac{\Xi_a(\boldsymbol{k})}{2T}\right)\right] \tag{3.43}$$

where $\Xi(\boldsymbol{k}) = \Xi_a(\boldsymbol{k}) - \Xi_d(\boldsymbol{k})$. .

3.3.2 Bogoliubov Transformation in Spin Density Wave State

To apply the Bogoliubov transformation to SDW state, the mean-field Hamiltonian (3.36) can be diagonalized using the relevant quasi particle transformation, and its diagonalized form is

$$\boldsymbol{H}_{\boldsymbol{mf}} \approx \sum_{\boldsymbol{k}\sigma} \hat{\phi}^{\dagger}_{m\,\boldsymbol{k}} \hat{\boldsymbol{H}}_{m\,\boldsymbol{k}} \hat{\phi}_{m\boldsymbol{k}} = \sum_{\boldsymbol{k}} \hat{X}^{\dagger}_{m\boldsymbol{k}} \hat{\boldsymbol{H}}^{D}_{m\,\boldsymbol{k}} \hat{X}_{m\boldsymbol{k}}. \tag{3.44}$$

The Bogoliubov quasi particle matrix for this transformation is defined as

$$\hat{X}^{\dagger}_{mk} = \begin{pmatrix} g^{\dagger}_{k\sigma} & c^{\dagger}_{k\sigma} \end{pmatrix}. \tag{3.45}$$

Their relation with old particle operators is

$$\begin{aligned} a^{\dagger}_{k\sigma} &= l_k g^{\dagger}_{k\sigma} + t_k c^{\dagger}_{k\sigma} \\ d^{\dagger}_{k+Q\sigma} &= \sigma\left(t_k g^{\dagger}_{k\sigma} - l_k c^{\dagger}_{k\sigma}\right). \end{aligned} \tag{3.46}$$

The coherency factors satisfy the following relation

$$\begin{aligned} l_k^2, t_k^2 &= \frac{1}{2}\left(1 \pm \frac{\xi_a(k) - \xi_d(k)}{E_g(k) - E_c(k)}\right) \\ l_k t_k &= \frac{\Delta_m(k)}{2E(k)}. \end{aligned} \tag{3.47}$$

Thus the diagonalized Hamiltonian will be

$$H_{mf} \approx \sum_{k\sigma} E_g(k) g^{\dagger}_{k\sigma} g_{k\sigma} + \sum_{k\sigma} E_c(k) c^{\dagger}_{k\sigma} c_{k\sigma} \tag{3.48}$$

where the eigenvalues are

$$E^2_{g/c}(k) = \frac{1}{4}\left[(\xi_a(k) + \xi_d(k)) \pm \sqrt{(\xi_a(k) - \xi_d(k))^2 + 4\Delta_m^2(k)}\right]^2. \tag{3.49}$$

Computing the SDW gap equation: Using the Bogoliubov transformation we defined for SDW state (3.5) we are now able to calculate the expectation value in the SDW gap equation {3.34).

$$\begin{aligned} \langle a^{\dagger}_{k\sigma} d_{k+Q\sigma} \rangle &= \langle (l_k g^{\dagger}_{k\sigma} + t_k c^{\dagger}_{k\sigma}) \sigma (t_k g_{k\sigma} - l_k c_{k\sigma}) \rangle \\ &\approx l_k t_k \left(\langle g^{\dagger}_{k\sigma} g_{k\sigma} \rangle - \langle c^{\dagger}_{k\sigma} c_{k\sigma} \rangle \right) \\ &= l_k t_k \left(f(E_g(k)) - f(E_c(k)) \right) \\ &= \frac{\Delta_m(k)}{2E(k)} \left[\tanh\left(\frac{E_g(k)}{2T}\right) - \tanh\left(\frac{E_c(k)}{2T}\right) \right] \quad . \end{aligned} \tag{3.50}$$

Therefor the SDW gap equation

$$\Delta_m(k) = \sum_{k'} V^m_{kk'} \frac{\Delta_m(k)}{2E(k)} \left[\tanh\left(\frac{E_g(k)}{2T}\right) - \tanh\left(\frac{E_c(k)}{2T}\right) \right]. \tag{3.51}$$

3.3.3 Free Energy in Spin Density Wave State

In magnetic spin density wave state the minimum of the Free energy defined as $\partial \boldsymbol{F}/\partial \Delta_m = 0$, has free energy and SDW order parameter, from which we can compute the equation for SDW order parameter. For pure SDW state the diagonal form of the mean-field Hamiltonian with inclusion of the interaction part could be

$$\boldsymbol{H_{mf}} = \sum_{k\sigma} E_g(\boldsymbol{k}) g^{\dagger}_{k\sigma} g_{k\sigma} + \sum_{k\sigma} E_c(\boldsymbol{k}) c^{\dagger}_{k\sigma} c_{k\sigma} + \frac{\Delta_m^2(\boldsymbol{k})}{2V^m_{kk'}} \tag{3.52}$$

where $E_g(k)$ and $E_c(k)$ are the quasi particles energies. Using the Free energy equations for non interacting particles and minimizing the Free energy we can calculate the SDW gap equation

$$\Delta_m(\boldsymbol{k}) = \sum_{k} V^m_{kk'} \frac{\Delta_m(\boldsymbol{k})}{E_f(\boldsymbol{k}) - E_c(\boldsymbol{k})} \left[\tanh\left(\frac{E_g(\boldsymbol{k})}{2T}\right) - \tanh\left(\frac{E_c(\boldsymbol{k})}{2T}\right) \right]. \tag{3.53}$$

3.4 Spin Density Wave and Superconducting State

In most FebSCs there are clear evidences showing the coexistence of Spin Density Waves with superconductivity in both hole doped and electron doped families. There fore we need to study the coupled system below the superconducting transition temperature. The mean-field Hamiltonian with out the interaction part could be

$$\begin{aligned} \boldsymbol{H_f} \approx & \sum_{k\sigma} \xi_a(\boldsymbol{k}) a^{\dagger}_{k\sigma} a_{k\sigma} + \sum_{k'\sigma} \xi_d(\boldsymbol{k}') d^{\dagger}_{k'\sigma} d_{k'\sigma} \\ & + \sum_{k} \Delta_a(\boldsymbol{k}) \left(a^{\dagger}_{k\uparrow} a^{\dagger}_{-k\downarrow} + h.c \right) + \sum_{k'} \Delta_d(\boldsymbol{k}) \left(d^{\dagger}_{k\uparrow} d^{\dagger}_{k\downarrow} + h.c \right) \\ & + \sum_{k\sigma} \Delta_m(\boldsymbol{k}) \left(a^{\dagger}_{k\sigma} d_{k+Q\sigma} + h.c \right) \end{aligned} \tag{3.54}$$

where the mean-fields are already given in the respective pure states.

3.4.1 Green Function in Spin Density and Superconducting States

In the Nambu notion the Hamiltonian (3.54)could be written as

$$H_f \approx \sum_{k\sigma} \hat{\phi}_k^{\dagger} \hat{H}_k \hat{\phi}_k. \tag{3.55}$$

Here the operators $\hat{\phi}_k^{\dagger}\ and\ \hat{\phi}_k$ are as expressed in (3.12) where the energy matrix is

$$\hat{H}_k = \begin{pmatrix} \hat{H}_{ak} & \hat{\Lambda}_m \\ \hat{\Lambda}_m & \hat{H}_{dk} \end{pmatrix} \tag{3.56}$$

with $\hat{H}_{ak}\ and\ \hat{H}_{dk}$ are as given in superconducting state and the diagonal matrix

$$\hat{\Lambda}_m = \begin{pmatrix} \Delta_m(k) & 0 \\ 0 & \Delta_m(k) \end{pmatrix}. \tag{3.57}$$

We calculate the matrix (3.56) eigenvalue, found that

$$\Omega_{a/d}^2(k) = \frac{1}{2}\left(\xi_a^2(k)+\xi_d^2(k)+\Delta_a^2(k)+\Delta_d^2(k)2\Delta_m^2(k)\right) \pm E(k) \tag{3.58}$$

with

$$E(k) = \sqrt{\left(\Delta_a^2(k)+\Delta_d^2(k)+\xi_a^2(k)+\xi_d^2(k)\right)^2+\Delta_m^2(k)\left((\Delta_a^2(k)+\Delta_d^2(k))^2+(\xi_a(k)+\xi_d(k))^2\right)}. \tag{3.59}$$

The Green function matrix is defined as

$$\hat{G}(k) = \begin{pmatrix} \hat{G}_{ak} & \hat{G}_{ad}(k) \\ \hat{G}_{ad}^{*}(k) & \hat{G}_{dk} \end{pmatrix} \tag{3.60}$$

where the non diagonal matrix are defined previously and the diagonal ones are

$$\hat{G}_{ad}(k) = \begin{pmatrix} G_{ad}^{\uparrow\uparrow}(k) & G_{ad}^{\uparrow\downarrow}(k) \\ G_{ad}^{\downarrow\uparrow}(k) & G_{ad}^{\downarrow\downarrow}(k) \end{pmatrix}. \tag{3.61}$$

The inverse Greens function can be calculated easily using

$$\hat{G}(i\omega,k) = \left(i\omega.\hat{I} - \hat{H}_k\right)^{-1} = \begin{pmatrix} \hat{G}_a(i\omega,k) & \hat{G}_{ad}(i\omega,k) \\ \hat{G}_{ad}^{*}(i\omega,k) & \hat{G}_d(i\omega,k) \end{pmatrix} \tag{3.62}$$

where

$$\hat{G}_{ad}(i\omega,\boldsymbol{k}) = \begin{pmatrix} G_{ad}^{\uparrow\uparrow}(i\omega,\boldsymbol{k}) & G_{ad}^{\uparrow\downarrow}(i\omega,\boldsymbol{k}) \\ G_{ad}^{\downarrow\uparrow}(i\omega,\boldsymbol{k}) & G_{ad}^{\downarrow\downarrow}(i\omega,\boldsymbol{k}) \end{pmatrix}. \tag{3.63}$$

The equations of the components of the matrix (3.63) can easily be found from the inverse matrix.

$$\begin{aligned} G_a^{\uparrow\downarrow}(i\omega,\boldsymbol{k}) &= \langle\langle a_{\boldsymbol{k}\uparrow}^{\dagger}; a_{-\boldsymbol{k}\downarrow}^{\dagger}\rangle\rangle_{\omega} \\ &= \frac{\Delta_a(\boldsymbol{k})\left((i\omega)^2 - E_a^2(\boldsymbol{k})\right) + \Delta_m^2(\boldsymbol{k})\Delta_d(\boldsymbol{k})}{\left(i\omega - \Omega_a(\boldsymbol{k})\right)\left(i\omega + \Omega_a(\boldsymbol{k})\right)\left(i\omega - \Omega_d(\boldsymbol{k})\right)\left(i\omega + \Omega_d(\boldsymbol{k})\right)} \end{aligned} \tag{3.64}$$

and

$$\begin{aligned} G_d^{\uparrow\downarrow}(i\omega,\boldsymbol{k}) &= \langle\langle d_{\boldsymbol{k}+\boldsymbol{Q}\uparrow}^{\dagger}; d_{-\boldsymbol{k}-\boldsymbol{Q}\downarrow}^{\dagger}\rangle\rangle_{\omega} \\ &= \frac{\Delta_d(\boldsymbol{k})\left((i\omega)^2 - E_d^2(\boldsymbol{k})\right) + \Delta_m^2(\boldsymbol{k})\Delta_a(\boldsymbol{k})}{\left(i\omega - \Omega_a(\boldsymbol{k})\right)\left(i\omega + \Omega_a(\boldsymbol{k})\right)\left(i\omega - \Omega_d(\boldsymbol{k})\right)\left(i\omega + \Omega_d(\boldsymbol{k})\right)} \end{aligned} \tag{3.65}$$

where the eigenvalues are calculated in (3.58).

The SC gap equations: The mean value of the right side of the gap equation (3.23) are expressed as a sum over the discrete Matsubara frequencies:

$$\langle a_{\boldsymbol{k}\uparrow}^{\dagger} a_{-\boldsymbol{k}\downarrow}^{\dagger}\rangle = \frac{1}{\beta}\sum_{i\omega} e^{i\omega} G_a^{\uparrow\downarrow}(i\omega,\boldsymbol{k}). \tag{3.66}$$

Substituting the Green function (3.64) to (3.66), summing over Matsubara frequencies results

$$\langle a_{\boldsymbol{k}\uparrow}^{\dagger} a_{-\boldsymbol{k}\downarrow}^{\dagger}\rangle = \frac{1}{\beta}\sum_{i\omega} \frac{\Delta_a(\boldsymbol{k})\left((i\omega)^2 - E_a^2(\boldsymbol{k})\right) + \Delta_m^2(\boldsymbol{k})\Delta_d(\boldsymbol{k})}{\left(i\omega - \Omega_a(\boldsymbol{k})\right)\left(i\omega + \Omega_a(\boldsymbol{k})\right)\left(i\omega - \Omega_d(\boldsymbol{k})\right)\left(i\omega + \Omega_d(\boldsymbol{k})\right)}. \tag{3.67}$$

Summing over Matsubara frequencies and substituting in the mean value gives the following gap equation

$$\begin{aligned} \Delta_d(\boldsymbol{k}) &= \sum_{\boldsymbol{k}} \frac{1}{2\Omega_d(\boldsymbol{k})} \frac{\Delta_a(\boldsymbol{k})\left(\Omega_a^2(\boldsymbol{k}) - E_a^2(\boldsymbol{k})\right) + \Delta_m^2(\boldsymbol{k})\Delta_d(\boldsymbol{k})}{\left(\Omega_a(\boldsymbol{k}) + \Omega_d(\boldsymbol{k})\right)\left(\Delta_a(\boldsymbol{k}) - \Omega_d(\boldsymbol{k})\right)} \left(f(\Omega_d(\boldsymbol{k})) - f(-\Omega_d(\boldsymbol{k}))\right) \\ &+ \sum_{\boldsymbol{k}} \frac{1}{\Omega_a(\boldsymbol{k})} \left[\frac{\Delta_d(\boldsymbol{k})(\Omega_d^2(\boldsymbol{k}) - E_d(\boldsymbol{k})) + \Delta_m^2(\boldsymbol{k})\Delta_a(\boldsymbol{k})}{\left(\Omega_a(\boldsymbol{k}) + \Omega_d(\boldsymbol{k})\right)\left(\Omega_a(\boldsymbol{k}) - \Omega_d(\boldsymbol{k})\right)}\right] \left(f(-\Omega_a(\boldsymbol{k})) - f(\Omega_a(\boldsymbol{k}))\right) \end{aligned} \tag{3.68}$$

and

$$\Delta_a(\boldsymbol{k}) = \sum_{\boldsymbol{k}} \frac{1}{2\Omega_d(\boldsymbol{k})} \frac{\Delta_d(\boldsymbol{k})\left(\Omega_a^2(\boldsymbol{k})-E_a^2(\boldsymbol{k})\right)+\Delta_m^2(\boldsymbol{k})\Delta_a(\boldsymbol{k})}{\left(\Omega_a(\boldsymbol{k})+\Omega_d(\boldsymbol{k})\right)\left(\Delta_a(\boldsymbol{k})-\Omega_d(\boldsymbol{k})\right)}\left(f(\Omega_d(\boldsymbol{k}))-f(-\Omega_d(\boldsymbol{k}))\right) + \sum_{\boldsymbol{k}} \frac{1}{\Omega_a(\boldsymbol{k})}\left[\frac{\Delta_d(\boldsymbol{k})(\Omega_d^2(\boldsymbol{k})-E_d(\boldsymbol{k}))+\Delta_m^2(\boldsymbol{k})\Delta_a(\boldsymbol{k})}{\left(\Omega_a(\boldsymbol{k})+\Omega_d(\boldsymbol{k})\right)\left(\Omega_a(\boldsymbol{k})-\Omega_d(\boldsymbol{k})\right)}\right]\left(f(-\Omega_a(\boldsymbol{k}))-f(\Omega_a(\boldsymbol{k}))\right) \tag{3.69}$$

or

$$\Delta_d(\boldsymbol{k}) = \sum_{\boldsymbol{k}} \frac{1}{2\Omega_d(\boldsymbol{k})} \frac{\Delta_a(\boldsymbol{k})\left(\Omega_a^2(\boldsymbol{k})-E_a^2(\boldsymbol{k})\right)+\Delta_m^2(\boldsymbol{k})\Delta_d(\boldsymbol{k})}{\left(\Omega_a(\boldsymbol{k})+\Omega_d(\boldsymbol{k})\right)\left(\Delta_a(\boldsymbol{k})-\Omega_d(\boldsymbol{k})\right)}\tanh\left(\frac{\Omega_a(\boldsymbol{k})}{2T}\right) + \sum_{\boldsymbol{k}} \frac{1}{\Omega_a(\boldsymbol{k})}\left[\frac{\Delta_a(\boldsymbol{k})(\Omega_d^2(\boldsymbol{k})-E_d(\boldsymbol{k}))+\Delta_m^2(\boldsymbol{k})\Delta_a(\boldsymbol{k})}{\left(\Omega_a(\boldsymbol{k})+\Omega_d(\boldsymbol{k})\right)\left(\Omega_a(\boldsymbol{k})-\Omega_d(\boldsymbol{k})\right)}\right]\tanh\left(\frac{\Omega_d(\boldsymbol{k})}{2T}\right) \tag{3.70}$$

and

$$\Delta_a(\boldsymbol{k}) = \sum_{\boldsymbol{k}} \frac{1}{2\Omega_d(\boldsymbol{k})} \frac{\Delta_d(\boldsymbol{k})\left(\Omega_a^2(\boldsymbol{k})-E_a^2(\boldsymbol{k})\right)+\Delta_m^2(\boldsymbol{k})\Delta_a(\boldsymbol{k})}{\left(\Omega_a(\boldsymbol{k})+\Omega_d(\boldsymbol{k})\right)\left(\Delta_a(\boldsymbol{k})-\Omega_d(\boldsymbol{k})\right)}\tanh\left(\frac{\Omega_d(\boldsymbol{k})}{2T}\right) + \sum_{\boldsymbol{k}} \frac{1}{\Omega_a(\boldsymbol{k})}\left[\frac{\Delta_d(\boldsymbol{k})(\Omega_d^2(\boldsymbol{k})-E_d(\boldsymbol{k}))+\Delta_m^2(\boldsymbol{k})\Delta_d(\boldsymbol{k})}{\left(\Omega_a(\boldsymbol{k})+\Omega_d(\boldsymbol{k})\right)\left(\Omega_a(\boldsymbol{k})-\Omega_d(\boldsymbol{k})\right)}\right]\tanh\left(\frac{\Omega_a(\boldsymbol{k})}{2T}\right). \tag{3.71}$$

The SDW gap equations: The mean value of the right side of the gap equation $\langle a_{\boldsymbol{k}\uparrow}^{\dagger} d_{\boldsymbol{k}+\boldsymbol{Q}\uparrow}\rangle$ is expressed as a sum over the discrete Matsubara frequencies:

$$\langle a_{\boldsymbol{k}\uparrow}^{\dagger} d_{\boldsymbol{k}+\boldsymbol{Q}\uparrow}\rangle = \frac{1}{\beta}\sum_{i\omega} e^{i\omega} G_{ad}^{\uparrow\uparrow}(i\omega,\boldsymbol{k}) \tag{3.72}$$

where the Green function component from the inverse matrix is

$$G_{ad}^{\uparrow\downarrow}(i\omega,\boldsymbol{k}) = \langle\langle a_{\boldsymbol{k}\uparrow}^{\dagger}; d_{\boldsymbol{k}+\boldsymbol{Q}\uparrow}\rangle\rangle_{\omega} = \frac{\Delta_m(\boldsymbol{k})\left((i\omega)^2-\xi_d(\boldsymbol{k})\xi_a(\boldsymbol{k})+\Delta_d(\boldsymbol{k})\Delta_a(\boldsymbol{k})-\Delta_m^2(\boldsymbol{k})\right)}{\left(i\omega-\Omega_a(\boldsymbol{k})\right)\left(i\omega+\Omega_a(\boldsymbol{k})\right)\left(i\omega-\Omega_d(\boldsymbol{k})\right)\left(i\omega+\Omega_d(\boldsymbol{k})\right)}. \tag{3.73}$$

Substituting the Green function (3.73) to (3.72) and summing over Matsubara frequencies results

$$\Delta_m(\boldsymbol{k}) = \sum_{\boldsymbol{k}} \frac{\Delta_m(\boldsymbol{k})}{2\,\Omega_d(\boldsymbol{k})}\left[\frac{\left(\Omega_a^2(\boldsymbol{k})-\xi_a(\boldsymbol{k})\,\xi_d(\boldsymbol{k})+\Delta_d(\boldsymbol{k})\,\Delta_a(\boldsymbol{k})-\Delta_m^2(\boldsymbol{k})\right)}{\left(\Omega_a(\boldsymbol{k})+\Omega_d(\boldsymbol{k})\right)\left(\Delta_a(\boldsymbol{k})-\Omega_d(\boldsymbol{k})\right)}\right]\tanh\left(\frac{\Omega_d(\boldsymbol{k})}{2T}\right)$$
$$+\sum_{\boldsymbol{k}} \frac{\Delta_m(\boldsymbol{k})}{\Omega_a(\boldsymbol{k})}\left[\frac{\left(\Omega_d^2(\boldsymbol{k})+\xi_d(\boldsymbol{k})\,\xi_a(\boldsymbol{k})+\Delta_a(\boldsymbol{k})\,\Delta_d(\boldsymbol{k})-\Delta_m^2(\boldsymbol{k})\right)}{\left(\Omega_a(\boldsymbol{k})+\Omega_d(\boldsymbol{k})\right)\left(\Omega_a(\boldsymbol{k})-\Omega_d(\boldsymbol{k})\right)}\right]\tanh\left(\frac{\Omega_a(\boldsymbol{k})}{2T}\right). \tag{3.74}$$

3.4.2 Bogoliubov Transformation in Spin Density wave and Superconducting State.

The mean-field Hamiltonian (3.6) may be rewritten as

$$\boldsymbol{H}_f \approx \sum_{\boldsymbol{k}\sigma}\xi_a(\boldsymbol{k})\,a^\dagger_{\boldsymbol{k}\sigma}a_{\boldsymbol{k}\sigma}+\sum_{\boldsymbol{k}\sigma}\xi_d(\boldsymbol{k})\,d^\dagger_{\boldsymbol{k}+\boldsymbol{Q}\sigma}d_{\boldsymbol{k}+\boldsymbol{Q}\sigma}+\sum_{\boldsymbol{k}\sigma}\Delta_m(\boldsymbol{k})\left(\sigma\,a^\dagger_{\boldsymbol{k}\sigma}d_{\boldsymbol{k}+\boldsymbol{Q}\sigma}+h.c\right)$$
$$+\sum_{\boldsymbol{k}}\Delta_a(\boldsymbol{k})\left(a^\dagger_{\boldsymbol{k}\uparrow}a^\dagger_{-\boldsymbol{k}\downarrow}+h.c\right)+\sum_{\boldsymbol{k}}\Delta_d(\boldsymbol{k})\left(d^\dagger_{\boldsymbol{k}+\boldsymbol{Q}\uparrow}d^\dagger_{-\boldsymbol{k}-\boldsymbol{Q}\downarrow}+h.c\right). \tag{3.75}$$

Applying the second quasi particle transformation (3.6) to above mean-field Hamiltonian we obtain

$$\boldsymbol{H}_f \approx \sum_{\boldsymbol{k}\sigma}E_g(\boldsymbol{k})\,g^\dagger_{\boldsymbol{k}\sigma}g_{\boldsymbol{k}\sigma}+\sum_{\boldsymbol{k}\sigma}E_c(\boldsymbol{k})\,c^\dagger_{\boldsymbol{k}\sigma}c_{\boldsymbol{k}\sigma}$$
$$+\sum_{\boldsymbol{k}}\Delta_a(\boldsymbol{k})\left(g^\dagger_{\boldsymbol{k}\uparrow}g^\dagger_{-\boldsymbol{k}\downarrow}+h.c\right)+\sum_{\boldsymbol{k}}\Delta_d(\boldsymbol{k})\left(c^\dagger_{\boldsymbol{k}\uparrow}c^\dagger_{-\boldsymbol{k}\downarrow}+h.c\right). \tag{3.76}$$

Using Nambu notion

$$\boldsymbol{H}_f \approx \sum_{\boldsymbol{k}}\hat{\phi}^\dagger_{g\boldsymbol{k}}\hat{\boldsymbol{H}}_{g\boldsymbol{k}}\hat{\phi}_{g\boldsymbol{k}}+\sum_{\boldsymbol{k}}\hat{\phi}^\dagger_{c\boldsymbol{k}}\hat{\boldsymbol{H}}_{c\boldsymbol{k}}\hat{\phi}_{c\boldsymbol{k}} \tag{3.77}$$

where the Nambu spinors are

$$\hat{\phi}^\dagger_{g\boldsymbol{k}} = \begin{pmatrix} g^\dagger_{\boldsymbol{k}\uparrow} & g_{-\boldsymbol{k}\downarrow}\end{pmatrix}$$
$$\hat{\phi}_{c\boldsymbol{k}} = \begin{pmatrix} c^\dagger_{\boldsymbol{k}\uparrow} & c_{-\boldsymbol{k}\downarrow}\end{pmatrix}. \tag{3.78}$$

The energy matrix

$$\hat{\boldsymbol{H}}_{g\boldsymbol{k}} = \begin{pmatrix} E_g(\boldsymbol{k}) & \Delta_a(\boldsymbol{k}) \\ \Delta_a(\boldsymbol{k}) & -E_g(\boldsymbol{k})\end{pmatrix}$$
$$\hat{\boldsymbol{H}}_{c\boldsymbol{k}} = \begin{pmatrix} E_c(\boldsymbol{k}) & \Delta_d(\boldsymbol{k}) \\ \Delta_d(\boldsymbol{k}) & -E_c(\boldsymbol{k})\end{pmatrix}. \tag{3.79}$$

Diagonalizing (3.77) for each band we get

$$\begin{aligned} \boldsymbol{H}_f &\approx \sum_{k\sigma} \hat{\phi}^{\dagger}_{gk} \hat{\boldsymbol{H}}_{gk} \hat{\phi}_{gk} + \sum_{k} \hat{\phi}^{\dagger}_{ck} \hat{\boldsymbol{H}}_{ck} \hat{\phi}_{ck} \\ &= \sum_{k} \hat{X}^{\dagger}_{gk} \hat{\boldsymbol{H}}^{D}_{gk} \hat{X}_{gk} + \sum_{k} \hat{X}^{\dagger}_{ck} \hat{\boldsymbol{H}}^{D}_{ck} \hat{X}_{ck} \end{aligned} \tag{3.80}$$

where $\hat{X}^{\dagger}_{g/ck}$ are the quasi particle matrix with the following transformations

$$\begin{aligned} \hat{X}^{\dagger}_{gk} &= \begin{pmatrix} A^{\dagger}_{k\uparrow} & A_{-k\downarrow} \end{pmatrix} \\ \hat{X}^{\dagger}_{ck} &= \begin{pmatrix} D^{\dagger}_{k\uparrow} & D_{-k\downarrow} \end{pmatrix} \end{aligned} \tag{3.81}$$

with

$$\begin{aligned} g^{\dagger}_{k\uparrow} &= U_k A^{\dagger}_{k\uparrow} + V_k A_{-k\downarrow} \\ c^{\dagger}_{k\uparrow} &= X_k D^{\dagger}_{k} + Y_k D_{-k\downarrow}. \end{aligned} \tag{3.82}$$

The coherence factors satisfy the following relation

$$\begin{aligned} U^2_k, V^2_k &= \frac{1}{2}\left(1 \pm \frac{E_g(\boldsymbol{k})}{\sqrt{E^2_g(\boldsymbol{k}) + \Delta^2_a(\boldsymbol{k})}}\right) \\ U_k V_k &= -\frac{\Delta_a(\boldsymbol{k})}{2E_A(\boldsymbol{k})} \end{aligned} \tag{3.83}$$

and

$$\begin{aligned} X^2_k, Y^2_k &= \frac{1}{2}\left(1 \pm \frac{E_c(\boldsymbol{k})}{\sqrt{E^2_c(\boldsymbol{k}) + \Delta^2_d(\boldsymbol{k})}}\right) \\ X_k Y_k &= -\frac{\Delta_d(\boldsymbol{k})}{2E_D(\boldsymbol{k})} \end{aligned} \tag{3.84}$$

where the eigenvalue

$$E^2_{A/D}(\boldsymbol{k}) = \sqrt{E^2_{g/c}(\boldsymbol{k}) + \Delta^2_{a/d}(\boldsymbol{k})}. \tag{3.85}$$

Applying this transformations diagonalizes the Hamiltonian in the following form

$$\boldsymbol{H}_f \approx \sum_{k\sigma} E_A(\boldsymbol{k}) A^{\dagger}_{k\sigma} A_{k\sigma} + \sum_{k\sigma} E_D(\boldsymbol{k}) D^{\dagger}_{k\sigma} D_{k\sigma}. \tag{3.86}$$

The SC and SDW gap equations: Using the the two Bogoliubov transformations we are now able to calculate the expectation value in the SDW gap equations. We find the

following gap equations:

$$\begin{aligned}\Delta_a(\boldsymbol{k}) &= \sum_{\boldsymbol{k}} V^{m}_{\boldsymbol{k}\boldsymbol{k}'}\frac{\Delta_d(\boldsymbol{k})}{2E_D(\boldsymbol{k})}\tanh\left(\frac{E_D(\boldsymbol{k})}{2T}\right)+\sum_{\boldsymbol{k}} V^{S}_{\boldsymbol{k}\boldsymbol{k}'}\frac{\Delta_a(\boldsymbol{k})}{2E_A(\boldsymbol{k})}\tanh\left(\frac{E_A(\boldsymbol{k})}{2T}\right)\\ \Delta_d(\boldsymbol{k}) &= \sum_{\boldsymbol{k}} V^{S}_{\boldsymbol{k}\boldsymbol{k}'}\frac{\Delta_a(\boldsymbol{k})}{2E_A(\boldsymbol{k})}\tanh\left(\frac{E_A(\boldsymbol{k})}{2T}\right)+\sum_{\boldsymbol{k}} V^{S}_{\boldsymbol{k}\boldsymbol{k}'}\frac{\Delta_d(\boldsymbol{k})}{2E_D(\boldsymbol{k})}\tanh\left(\frac{E_D(\boldsymbol{k})}{2T}\right)\end{aligned} \tag{3.87}$$

and

$$\Delta_m(\boldsymbol{k}) = \sum_{\boldsymbol{k}} V^{m}_{\boldsymbol{k}\boldsymbol{k}'}\frac{\Delta_m(\boldsymbol{k})}{2E(\boldsymbol{k})}\left[\tanh\left(\frac{E_D(\boldsymbol{k})}{2T}\right)-\tanh\left(\frac{E_A(\boldsymbol{k})}{2T}\right)\right] \tag{3.88}$$

where the excitations $E_{A/D}(\boldsymbol{k})$ are given in (3.85).

3.4.3 Free energy in Spin density Wave and Superconducting States

In pure SC and SDW states we defined the condition at which the Free energy minimum. In a thermodynamic system having both magnetic and superconducting order parameters, the minimum of the Free energy defined as $\partial \boldsymbol{F}/\partial \Delta = 0$ and $\partial \boldsymbol{F}/\partial \Delta_m = 0$ has free energy and the two order parameter that is $\Delta_m, \Delta_{a/d} \neq 0.$ From which we can compute the equations for SC as well as SDW order parameter. For our magnetic and superconducting system the diagonal form of the mean-field Hamiltonian with inclusion of the interaction part is

$$\boldsymbol{H}_f = \sum_{\boldsymbol{k}\sigma} E_A(\boldsymbol{k}) A^{\dagger}_{\boldsymbol{k}\sigma} A_{\boldsymbol{k}\sigma} + \sum_{\boldsymbol{k}\sigma} E_D(\boldsymbol{k}) D^{\dagger}_{\boldsymbol{k}\sigma} D_{\boldsymbol{k}\sigma} - 2\frac{\Delta_a(\boldsymbol{k})\Delta_d(\boldsymbol{k})}{V^{S}_{\boldsymbol{k}\boldsymbol{k}'}} + \frac{\Delta^2_m(\boldsymbol{k})}{V^{m}_{\boldsymbol{k}\boldsymbol{k}'}} \tag{3.89}$$

where $E_A(\boldsymbol{k})\ and\ E_D(\boldsymbol{k})$ are the quasi particle energies. From (3.89) the Free energy is calculated to

$$\boldsymbol{F} = -2T\sum_{\boldsymbol{k},\nu=A,D}\ln\left(\cosh\left(\frac{E_\nu(\boldsymbol{k})}{2T}\right)\right) - 2\frac{\Delta_a(\boldsymbol{k})\Delta_d(\boldsymbol{k})}{V^{S}_{\boldsymbol{k}\boldsymbol{k}'}} + 2\frac{\Delta^2_m(\boldsymbol{k})}{V^{m}_{\boldsymbol{k}\boldsymbol{k}'}}. \tag{3.90}$$

Now minimization of the Free energy of the combined system with respect to order parameters and then solving for gap parameters yields the following gap equations.

$$\begin{aligned}\Delta_a(\boldsymbol{k}) &= \sum_{\boldsymbol{k}} V^{m}_{\boldsymbol{k}\boldsymbol{k}'}\frac{\Delta_d(\boldsymbol{k})}{2E_D(\boldsymbol{k})}\tanh\left(\frac{E_D(\boldsymbol{k})}{2T}\right)\\ \Delta_d(\boldsymbol{k}) &= \sum_{\boldsymbol{k}} V^{S}_{\boldsymbol{k}\boldsymbol{k}'}\frac{\Delta_a(\boldsymbol{k})}{2E_A(\boldsymbol{k})}\tanh\left(\frac{E_A(\boldsymbol{k})}{2T}\right)\end{aligned} \tag{3.91}$$

and

$$\begin{aligned}\Delta_m(\boldsymbol{k}) &= \sum_{\boldsymbol{k}}\frac{\Delta_m(\boldsymbol{k})}{2E_D(\boldsymbol{k})}\left[\frac{\left(\xi_a(\boldsymbol{k})+\xi_d(\boldsymbol{k})+\Xi(\boldsymbol{k})\right)}{\Xi(\boldsymbol{k})}\right]\tanh\left(\frac{E_D(\boldsymbol{k})}{2T}\right)\\ &+\sum_{\boldsymbol{k}}\frac{\Delta_m(\boldsymbol{k})}{2E_A(\boldsymbol{k})}\left[\frac{\left(\xi_d(\boldsymbol{k})+\xi_a(\boldsymbol{k})+\Xi(\boldsymbol{k})\right)}{\Xi(\boldsymbol{k})}\right]\tanh\left(\frac{E_A(\boldsymbol{k})}{2T}\right).\end{aligned} \tag{3.92}$$

In general in driving the gap equations we apply the three methods (formalisms) out of which the Green function formalism is the most general one and the most general expressions for the SDW and SC order parameters are

$$\begin{aligned}\Delta_{d/a}(\boldsymbol{k}) &= \sum_{\boldsymbol{k}}\frac{1}{2\Omega_{d/a}(\boldsymbol{k})}\frac{\Delta_{a/d}(\boldsymbol{k})\left(\Omega^2_{a/d}(\boldsymbol{k})-E^2_{a/d}(\boldsymbol{k})\right)+\Delta^2_m(\boldsymbol{k})\Delta_{d/a}(\boldsymbol{k})}{\left(\Omega_a(\boldsymbol{k})+\Omega_d(\boldsymbol{k})\right)\left(\Delta_a(\boldsymbol{k})-\Omega_d(\boldsymbol{k})\right)}\tanh\left(\frac{\Omega_{a/d}(\boldsymbol{k})}{2T}\right)\\ &+\sum_{\boldsymbol{k}}\frac{1}{\Omega_{a/d}(\boldsymbol{k})}\left[\frac{\Delta_{a/d}(\boldsymbol{k})(\Omega^2_{d/a}(\boldsymbol{k})-E_{d/a}(\boldsymbol{k}))+\Delta^2_m(\boldsymbol{k})\Delta_{a/d}(\boldsymbol{k})}{\left(\Omega_a(\boldsymbol{k})+\Omega_d(\boldsymbol{k})\right)\left(\Omega_a(\boldsymbol{k})-\Omega_d(\boldsymbol{k})\right)}\right]\tanh\left(\frac{\Omega_{d/a}(\boldsymbol{k})}{2T}\right)\end{aligned} \tag{3.93}$$

and

$$\begin{aligned}\Delta_m(\boldsymbol{k}) &= \sum_{\boldsymbol{k}}\frac{\Delta_m(\boldsymbol{k})}{2\Omega_d(\boldsymbol{k})}\left[\frac{\left(\Omega^2_a(\boldsymbol{k})-\xi_a(\boldsymbol{k})\xi_d(\boldsymbol{k})+\Delta_d(\boldsymbol{k})\Delta_a(\boldsymbol{k})-\Delta^2_m(\boldsymbol{k})\right)}{\left(\Omega_a(\boldsymbol{k})+\Omega_d(\boldsymbol{k})\right)\left(\Delta_a(\boldsymbol{k})-\Omega_d(\boldsymbol{k})\right)}\right]\tanh\left(\frac{\Omega_d(\boldsymbol{k})}{2T}\right)\\ &+\sum_{\boldsymbol{k}}\frac{\Delta_m(\boldsymbol{k})}{\Omega_a(\boldsymbol{k})}\left[\frac{\left(\Omega^2_d(\boldsymbol{k})+\xi_d(\boldsymbol{k})\xi_a(\boldsymbol{k})+\Delta_a(\boldsymbol{k})\Delta_d(\boldsymbol{k})-\Delta^2_m(\boldsymbol{k})\right)}{\left(\Omega_a(\boldsymbol{k})+\Omega_d(\boldsymbol{k})\right)\left(\Omega_a(\boldsymbol{k})-\Omega_d(\boldsymbol{k})\right)}\right]\tanh\left(\frac{\Omega_a(\boldsymbol{k})}{2T}\right).\end{aligned} \tag{3.94}$$

Depending on the symmetry and structure of the order parameters the three coupled equitations defining the SDW and SC order parameters are solved and utilized for different interplay between the order parameters as the main components of coming two chapters.

1 CHAPTER 4: GAP SYMMETRIES AND ELECTRON STRUCTURE

CHAPTER 4

GAP SYMMETRY AND ELECTRON STRCTURE OF IRON BASED SUPERCONDUCTORS

4.1 Gap symmetry

The interaction between low energy fermions are generally angle dependent in the normal state, before either SDW or SC order sets in, which gives rise to angle dependent SDW and SC gaps even out side the interplay region. In practice we usually refer to the pairing states as s-wave, d-wave, p-wave, and f-wave. Regarding the spin symmetry the s and d waves always correlate to electron paired in spin singlets, where p and f symmetry are in spin triplets. There fore it is interesting to calculate the transition temperatures and the momentum dependence of the gap function for a given band structure and interaction. The symmetry properties and the form of the gap function is uniquely determined by the pairing potential, $V_{kk'}$. If the pairing interaction $V_{kk'}$ in SC gap equation is such that according to BCS theory it can be written as $V_{kk'}=V_0\eta_k\eta_{k'}$ and there fore the momentum dependence of the gap equation $\Delta_k = \Delta_0\eta_k$ where η_k is the factor which describes a certain pairing symmetry as shown in (4.1) for different symmetries.

$$\begin{aligned} \eta_k &= \cos(k_x)-\cos(k_y) && \text{for } d_{x^2-y^2}\ wave \\ &= \cos(k_x)+\cos(k_y) && \text{for extended } s-wave \\ &= \cos(k_x)\cos(k_y) && \text{for } s_{xy}\ wave. \end{aligned} \tag{4.1}$$

In FebSC compounds a theoretical calculation with a $t-J_1-J_2$ model [101] it was found out that the nearest neighbor exchange J_1 induces competing $\cos(k_x)+\cos(k_y)$ and $\cos(k_x)-\cos(k_y)$ (s wave and $\mathbf{d_{x2-y2}}$ wave) pairing

harmonics, while the next nearest neighbor exchange leads to $\cos(k_x)\cos(k_y)$ and $\sin(k_x)\sin(k_y)$ (s wave and d_{xy} wave). In the region of the general phase diagram of FebSC with $J_2 > J_1$, $\cos(k_x)\cos(k_y)$ was the leading instability for the two band Fermi surface, leading to a node less s^{+-} wave state.

For weakly and moderately electron doped FebSCs such Co/Ni-Ba122 and Co/Ni-Ca1111 systems s^{+-} and d_{x2-y2} pairing channels are nearly degenerate. The driving force for the pairing in both channels is inter pocket electron hole interaction, enhanced by spin fluctuations. The probability that the s^{+-} gap has nodes increases with electron doping. For strongly electron doped FebSCs like 11 FebSC family, when only electron pockets remain, the gap has d wave symmetry, which in this situation implies that the angle independent component of the gap changes sign between the two electron pockets. The driving mechanism for the pairing is a direct d wave attraction between electron pockets, again enhanced by spin fluctuations.

For weakly and moderately hole doped Ba122 FebSCs systems s^{+-} pairing is the dominant instability. The driving force is again inter pocket electron hole interaction, enhanced by spin fluctuation. On the other hand for strongly hole doped FebSCs of KFe_2As_2, when only hole Fermi-surfaces remain, the gap symmetry may be d wave, with nodes at on all hole Fermi surfaces. The d-wave pairing mechanism is the combination of a d wave attraction with in the hole pockets.

In Fig. 4.1 we show the momentum dependence of the gap functions of weakly doped iron compounds for both the electron and hole bands in the unfolded BZ are presented respectively. It has the same sign within each Fermi pocket, but the sign changes between the electron and hole pockets. This extended s-wave pairing has now been called as the s^{+-} wave pairing. It can be roughly fitted by the gap function $\Delta_{\boldsymbol{k}} \approx \cos(k_x)\cos(k_y)$.

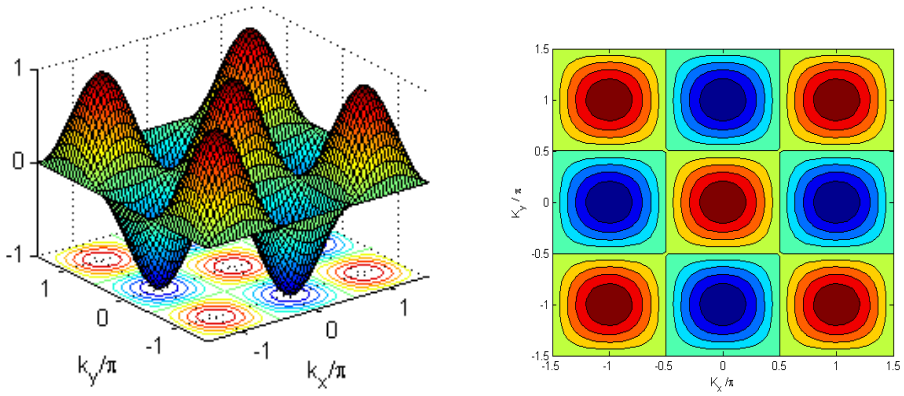

Figure 4.1: The k dependence of the gap functions corresponding to the largest eigenvalue for the (left panel) and the contour of constant gap function (right panel) at zero temperature.

In Fig. 4.1 the the constant gap function contour lines have equal and opposite gap values between electron and hole pockets but the same sign equal values between the same pockets.

4.2 Electronic Structure of Parent compounds

The parent compound of most FebSCs is AFM metal. The Fermi surface in the FebSC parent materials consists of well separated hole pockets at the center of the BZ and electron pockets at the zones of the Brillouin zones. Just from most experimental and the band-structure calculations results reveal three iron 3d orbitals ($\mathbf{d_{xz}}$, $\mathbf{d_{yz}}$, and $\mathbf{d_{xy}}$) give the main contribution to the density of states close to the Fermi level and that these states disperse weakly in the z direction. The resulting Fermi surface consists of hole pockets centered around the center of BZ point and two electron pockets centered around the the corner of BZ. Near optimal doping the the three orbitals $\mathbf{d_{xz}}$, $\mathbf{d_{yz}}$ and $d_{x^2-y^2}$ has nearly the same weight. From two orbital (for $\mathbf{d_{xz}}$ and $\mathbf{d_{yz}}$ orbitals) tight

binding model [37] the dispersion near electron bands for first and second nearest hopping is given by

$$\xi_{a/d}(\boldsymbol{k}) = \frac{1}{2}\left(\xi_{xz}(\boldsymbol{k})+\xi_{yz}(\boldsymbol{k}) \pm \sqrt{\left(\xi_{xz}(\boldsymbol{k})-\xi_{yz}(\boldsymbol{k})\right)^2+\xi_{xy}^2}\right) - \mu \tag{4.2}$$

where

$$\begin{aligned} \xi_{xz}(\boldsymbol{k}) &= -2t_2\cos(k_x)-2t_1\cos(k_y)-4t_3\cos(k_x)\cos(k_y) \\ \xi_{yz}(\boldsymbol{k}) &= -2t_1\cos(k_y)-2t_2\cos(k_x)-4t_3\cos(k_x)\cos(k_y) \\ \xi_{xy}(\boldsymbol{k}) &= -4t_4\sin(k_y)\sin(k_x). \end{aligned} \tag{4.3}$$

Three orbital tight binding model has also been applied to study the band structure of FebSCs. The main difference between the two-orbital model and the three-orbital model exhibits in the orbital contributions to the corresponding Fermi surface. In the two-orbital model [37] the electron Fermi pocket near the (π, 0) point is composed of one orbital $\mathbf{d_{yz}}$ and the hole Fermi pocket around the (0, 0) point is the mix of both the $\mathbf{d_{yz}}$ and the $\mathbf{d_{xz}}$ orbitals. Because that portion of the hole Fermi pocket connected by the nesting wave vector (π, 0) is basically of the $\mathbf{d_{xz}}$ orbital character, the inter-band spin fluctuation coming from this nesting is in fact the inter orbital particle hole scattering between the $\mathbf{d_{xz}}$ and the $\mathbf{d_{yz}}$ orbitals.

In the three orbital model, the orbital composition of the hole Fermi pocket is the same as that in the two-orbital model, and the only difference is that the electron Fermi pocket now is a mix of the $\mathbf{d_{yz}}$ and the $\mathbf{d_{xy}}$ orbitals. Thus, the inter band spin fluctuation with the wave vector (π, 0) involves both the inter orbital scattering between the d_{xz} and the $\mathbf{d_{yz}}$ orbitals, and that between the $\mathbf{d_{xz}}$ and the $\mathbf{d_{xy}}$ orbitals. Though there is such a difference, the inter band spin fluctuation is sensitive to the nesting property of the Fermi surface, which is qualitatively the same in the two cases, so they result in the similar properties of the spin fluctuation. On the other hand, the s^{+-}-wave pairing is mediated by the inter band spin fluctuation and results from the condition $\Delta_a(\boldsymbol{k})\Delta_d(\boldsymbol{k})<0$. There fore, the similar spin fluctuations with the same wave vector

Q will give the same pairing symmetry. In fact, the more complicated five orbital model [37] can also reproduce the same argument.

Even though the three orbitals have more weight in electron and hole pockets at center of BZ and at the corner of the BZ the low temperature physics is more dominant by the $\mathbf{d_{x2-y2}}$ or $\mathbf{d_{xy}}$ orbital and there fore the dispersion

$$\xi_{x^2-y^2}(\boldsymbol{k}) = 2t_1\left(\cos(k_x)+\cos(k_y)\right)+4t_2\cos(k_x)\cos(k_y)-\mu \qquad (4.4)$$

where t_1 and t_2 are the first and second nearest neighbors hopping integral for the $\mathbf{d_{x2-y2}}$ orbital. As most evidences indicate that the undoped material of FebSCs behaves like a semi metal and exhibits itinerant AFM. We use the tight-binding parameters $t_1 = -1.0$, $t_2 = 1.5$, $t_3 = -1.2$, and $t_4 = -0.95$ (in units of $|t_1|$) and show the corresponding energy band structure and Fermi surface for parent compound as shown in Fig. 4.2 to Fig. 4.4. The resulting Fermi surface consists of almost circular hole pockets centered around the centers of the BZs and at the corners of the BZs. When the number of holes doped in to the system is increased the size of the hole pockets increases while the electron pockets size decreases as seen in the Fig. 4.3. Similarly, in Fig. 4.4 in electron doping the size of electron pockets becomes large as compared to that of the hole pockets.

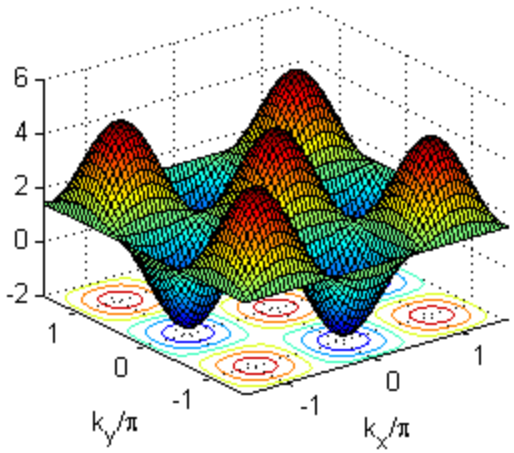

Figure 4.2: The FS of the two-orbital ($\mathbf{d_{xz}}$ and d_{yz}) model of parent compound with $t_1 = -1.0$, $t_2 = 1.5$, $t_3 = -1.2$, $t_4 = -0.95$ and zero chemical potential at zero temperature.

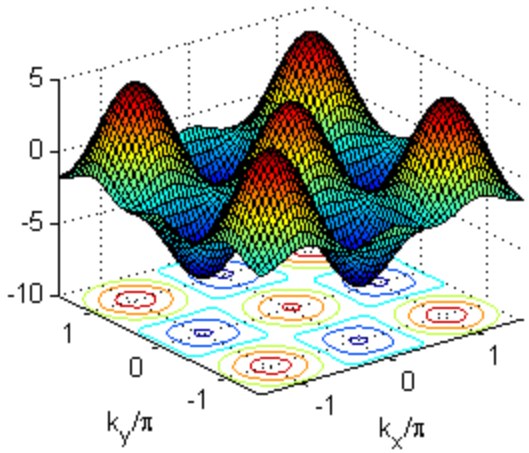

Figure 4.3: The FS of the two-orbital model of normal state with the same hoping parameters given in Fig. 4.2 for hole doped.

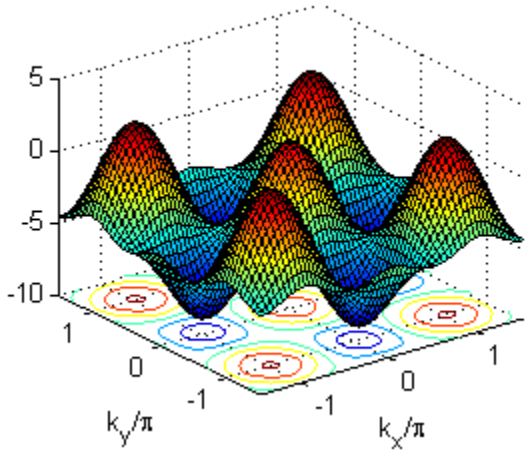

Figure 4.4: The FS of the two-orbital model of normal state with the same hoping parameters given in Fig. 4.2 for electron doped.

4.3 Electronic Structure in Superconducting state

As discussed before most evidences on FebSCs shows that an s^{+-} wave state mediated by spin fluctuations is the favorable superconducting pairing state for moderately doped FebSCs, which shares the same underlying physics as the spin fluctuation mediated $d_{x2\,y2}$ superconducting pairing in cuprates. Though some experimental results which are not consistent with the node-less s^{+-} wave gap. In fact, the FebSCs are complicated because of the multi orbital nature of the energy band and the sensitivity of some physical properties to the compositions of materials. The energy excitation in SC state according to our calculation for single orbital like d_{x2-y2} is

$$\Omega^2_{a/d}(\boldsymbol{k}) = \frac{1}{2}\left(\xi^2_a(\boldsymbol{k})+\xi^2_d(\boldsymbol{k})+\Delta^2_a(\boldsymbol{k})+\Delta^2_d(\boldsymbol{k})2\Delta^2_m(\boldsymbol{k})\right) \pm E(\boldsymbol{k}) \qquad (4.5)$$

We simplify (4.5) to s-wave symmetry and using the tight-binding parameters t_1= 1.0 , t_2=1.5 and $\Delta^0_s=0.1$ the corresponding energy band structure and Fermi surface for electron doped and hole doped at temperature are shown in Fig. 4.5 and Fig. 4.6.

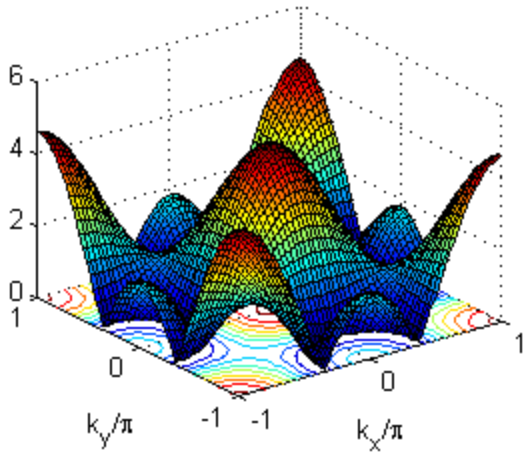

Figure 4.5: The FS in superconducting state and the corresponding energy dispersion for t_1= 1, t_2= 1.5 and $\Delta^0_s=0.1$ for hole doped at zero temperature.

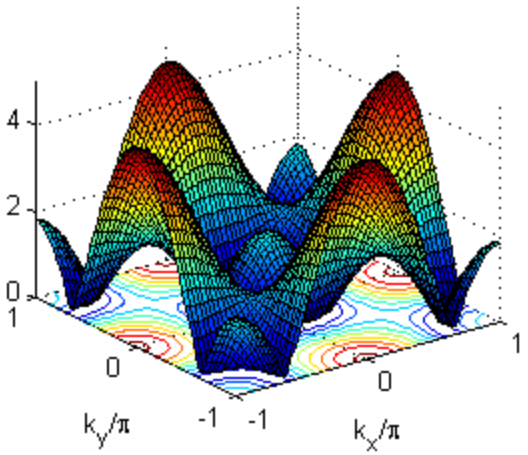

Figure 4.6: The FS in superconducting (SC) state with the corresponding band structure (energy dispersion) for electron electron doped at zero temperature for the parameters in Fig. 4.5 but negative chemical potential.

Here, we consider the effects of electron doping such that $\mu > 0$ and for the case of hole doping the chemical potential $\mu < 0$. From the band structure presented in last two figures, hole doping reduces the size of electron pockets and the vice verse. Furthermore there is an energy gap between the lower and upper energy bands in superconducting state as both figures show.

4.4 Electronic Structure in Spin Density Wave state

The excitation energy of electrons in SDW state for single orbital are described by (4.6). Using the tight-binding parameters used in Fig. 4.4 for $\mathbf{d}_{x2-y2}$ the corresponding energy band structure and Fermi surface at zero temperature are shown in Fig. 4.7 for hole doping and electron doping and Fig. 4.8. In both doping the sizes of the Fss has shown no significant change. Furthermore there is no gap between the upper and lower

bands.

$$\Xi_{d/a}(\boldsymbol{k}) = \frac{1}{2}\left[\xi_a(\boldsymbol{k})+\xi_d(\boldsymbol{k}) \pm\sqrt{\left(\xi_a(\boldsymbol{k})-\xi_d(\boldsymbol{k})\right)^2+4\Delta_m^2(\boldsymbol{k})}\right]. \tag{4.6}$$

In the figures we show in SDW state no Fermi level, fully gaped one.

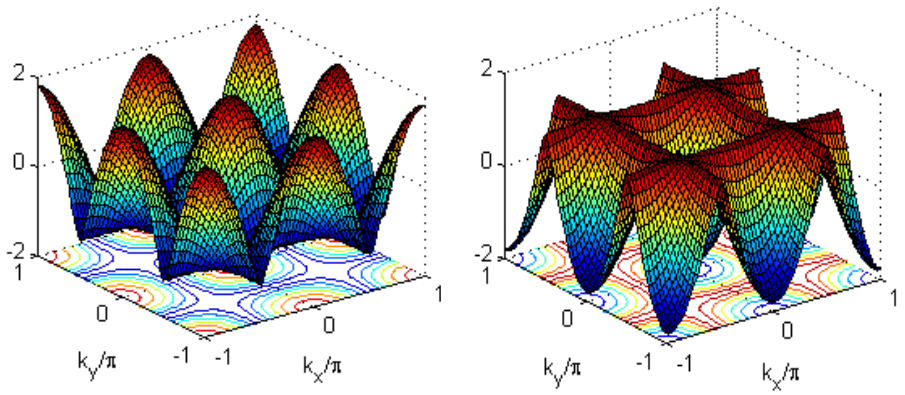

Figure 4.7: The FS in spin density wave (SDW) state and energy excitations for hole doped the dispersion of upper band (left panel) the lower band (right panel) at zero temperature and $\Delta_m^0=0.2$

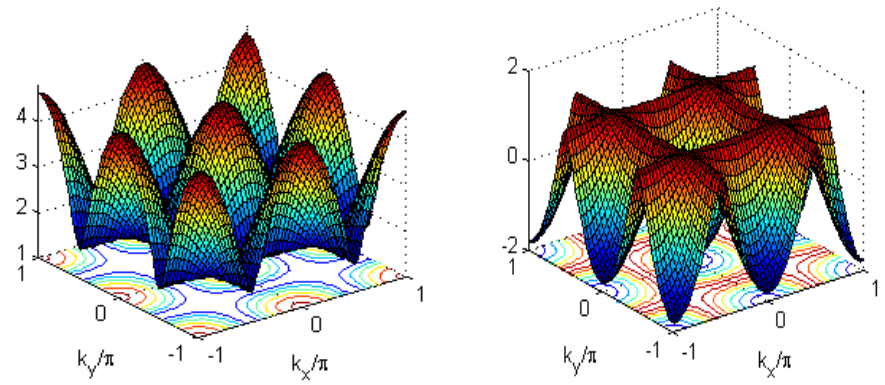

Figure 4.8: The FS and corresponding band structure in SDW for electron doped the dispersion of upper band (left panel) the lower band (right panel).

4.5 Summery

In this chapter we tried to see the most convenient gap symmetry and electron structure to study the low temperature interplay between magnetic SDW order and superconductivity of FebSCs. The isotopic gap function resulted from inter pocket hopping by the same orbital (like $\mathbf{d}_{xz}$, $\mathbf{d}_{yz}$ and $\mathbf{d}_{x2\text{-}y2}$) is chosen to be best preference for our problem. Furthermore, the s^{+-} wave symmetry mediated by spin fluctuations is the favorable superconducting pairing state, which shares the same underlying physics as the spin fluctuation mediated $\mathbf{d}_{x2\ y2}$ superconducting pairing in high T_c cuprates. Using the three orbitals and single orbital the effect of electron/hole doping on the the size of respective pockets for normal state, SC state and SDW state at zero temperature are also presented based on our calculation. The two bands (the upper and lower bands) cross the Fermi-level in SDW state and gaped in SC state.

1 CHAPTER 5: SPIN DENSITY WAVE AND SC INTERPLAY

CHAPTER 5

SPIN DENSITY WAVE AND SUPERCONDUCTIVITY IN INTERPLAY

5.1 Commensurate SDW and Superconductivity

The nature of magnetism in under doped region in FebSCs is an intensively studied topic, due to its comp with superconductivity and the possible relation with the pairing mechanism. In the early time of discovery of FebSCs the nature of magnetic order had been in debate. Most recent studies have indicated the commensurate SDW order in several systems including the parent compounds and doped compounds [36]. The reports support the idea that superconductivity in iron based materials can be induced via electron or hole doping or pressure. Experiments on doped Ba122 FebSCs [38,39] confirm that the commensurate SDW order appears below the structural transition temperature and SC coexists with SDW order in under doped region. Although these results indicate that the static SDW order competes with SC, it remains unclear during the discovery whether the SDW order truly coexists microscopically with superconducting regions. Near optimal superconductivity, it has been shown that the commensurate SDW order changes into transversely incommensurate SDW order that coexists and competes with superconductivity [36]. Other studies in underdoped on other doped 122 FebSCs compounds like $BaFe_2(As_{1-x}P_x)_2$, $Ba(Fe_{1-x}Ru_x)_2As_2$ and K-Ba122 [150-152] reveal the microscopic coexistence between SDW and superconductivity.

Homogeneous coexistence of the SDW and SC states has also been suggested for electron-doped oxygen free 1111 family Co-Ca1111 [40]. An overlap between the AFM and SC domes decreases with increasing inter layer distance of FeAs planes; therefore, the doped Ba122 series has a large overlap region, the Ca1111 series has a

smaller one. To sum up the homogeneous coexistence between SDW and- SC orders is becoming common to doped Ba122 and electron doped Ca111 compounds of FebSCs.

Numerical Results: Now with the help of the recent evidences supporting the microscopic coexistence between commensurate SDW and SC in underdoped region and phase separations we tried to show how the interplay results using the coupled gap equations derived in chapter three. From the common fermilogy of most FebSCs, the two band dispersions near Fermi-surfaces are $\xi_a(\boldsymbol{k})=-\xi_k+C$ and $\xi_d(\boldsymbol{k})=\xi_{\boldsymbol{k}}+C$ where C describes the deviation from a perfect nesting and independent of $\xi_{\boldsymbol{k}}$. There fore the coupled equations are solved and explicitly integrated over $\xi_{\boldsymbol{k}}$ with constant density of states at the Fermi level and coupling constants $\lambda_s \, and \, \lambda_m$. A unit upper energy cut offs is taken. In our calculation the pure magnetic SDW and SC transition temperatures are doping dependent as shown in figure 5.1 and 5.3. To simplify our calculation we first define T_c^0 and T_m^0 which are the SC and SDW transition temperatures at perfect nesting (at zero doping) respectively. This will help us to map out the phase boundary between the two states. And zero temperature and zero doping SDW and SC order parameters Δ_m^0 and Δ_s^0 are also calculated to normalize the doping parameter defined by $\bar{C}=C/2\Delta_m^0$. Then the interplay between the two orders result in the form of phase diagrams are studied by normalizing SDW and SC transition temperatures and respective order parameters for different magnetic and SC interactions defined by T_c^0/T_m^0. The calculated results are presented in the following sections, first for pure states and then for mixed systems.

5.1.1 Spin Density Wave state

In the absence of superconducting cooper pairs doping is the only variable that affects magnetic critical temperature T_m which is doping dependent. Here in our calculation we assume that the superconducting state has an extended $\mathbf{s}^{+-}$ wave symmetry and is characterized by an equal in magnitude, but opposite in sign isotropic SC order parameter on the Fermi surfaces as discussed in section 4.1. There fore taking a momentum independent interaction that usually gives rise to a momentum independent sign reversal s wave gap, we can approximate the interactions by V^S and V^m as constants for SC and SDW respectively. Hence the SDW state gap equation with this assumption becomes

$$\Delta_m = \frac{V^m}{2}\sum_{\boldsymbol{k}} \frac{\Delta_m}{E(\boldsymbol{k})}\left[\tanh\left(\frac{\Xi_d(\boldsymbol{k})}{2T}\right) - \tanh\left(\frac{\Xi_a(\boldsymbol{k})}{2T}\right)\right] \qquad (5.1)$$

where $\Xi_{d/a}(\boldsymbol{k}) = C \pm \sqrt{\xi_{\boldsymbol{k}}^2 + \Delta_m^2}$ and $E(\boldsymbol{k}) = \sqrt{\xi_{\boldsymbol{k}}^2 + \Delta_m^2}$. We know that at perfect nesting, the band dispersions satisfy $\xi_a(\boldsymbol{k}) = -\xi_d(\boldsymbol{k})$ where **k** is measured from the center of the corresponding band and the two Fermi surfaces are circular with equal sizes at the beginning. A deviation from a perfect nesting may be tuned by doping or pressure and is parametrized by the small detuning parameter C where $2C = \xi_a(\boldsymbol{k}) + \xi_d(\boldsymbol{k})$.

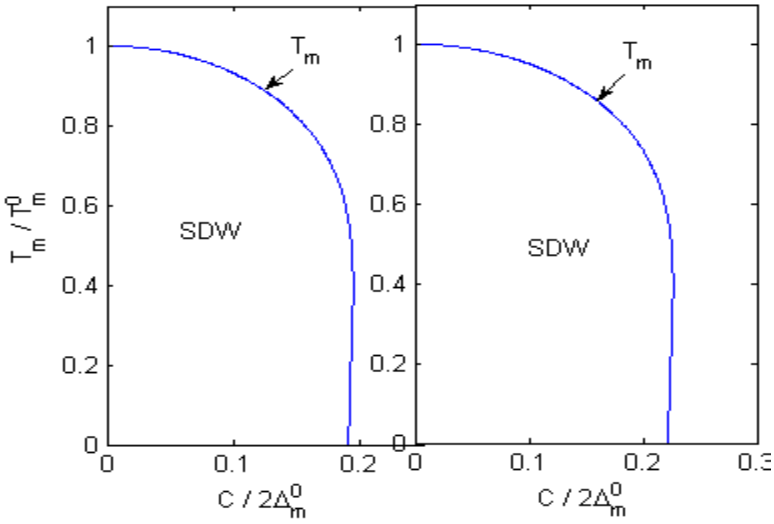

Figure 5.1: The phase diagram, the normalized SDW transition temperature $\bar{T}_m = T_m / T_m^0$ as a function of normalized doping $\bar{C} = C / 2\Delta_m^0$ of pure SDW state for electron doped (left panel) and hole doped (right panel).

In Fig. 5.1 we present the phase diagram for commensurate SDW state for electron-doped (left panel) and hole doped (right panel). The normalized transition temperatures show reentrant behavior at about $T = 0.4 T_m^0$ at different doing levels. The reentrant temperature is independent of magnetic coupling interactions. The reentrant is supported by observations in Co-Ba122 families [65]. In our calculation this could be the maximum temperature below which superconductivity and magnetic order coexist. The zero temperature phase septation point between SDW and SC is usually defined as Quantum critical point (QCP), separate ordered to disordered state. As seen in Fig. 5.2 $\bar{C} = 0.1914 \; and \; 0.2225$ are the QCP for electron doped and hole doped respectively. Therefore below these critical points the magnetic phase is expected to be ordered. From the reentrant line presented in Fig. 5.2 we understand

magnetic instability about and above the critical points for each doping as pure SDW state is considered. As for the effect of doping on the magnetic transition temperature, as the range of doing increases magnetism will be suppered, presented in the model phase diagram.

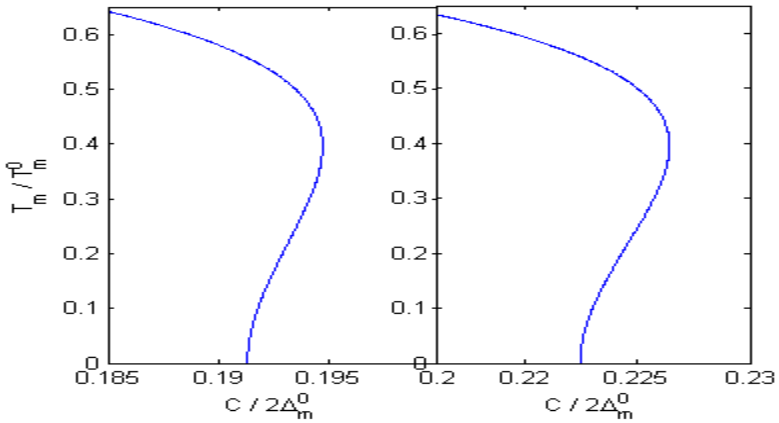

Figure 5.2: The phase diagram, the normalized SDW $\bar{T}_m = T_m / T_m^0$ as a function of normalized doping $\bar{C} = C / 2\Delta_m^0$ of pure SDW state for hole doped (left panel) and electron doped (right panel) near the boundary showing the reentrant below $T = 0.4\, T_m^0$.

At the end the parent FebSC families ordered AFM metal behavior defined by zero doping (C=0) is gradually changed to disordered magnetic system as doping increases to the QCP. The effect of doping is suppression of the long range AFM order and leave the space to superconductivity. These and the reentrant behavior are the results we underline from the pure SDW state. This reveals the presences of magnetic instability near the respective QCP.

5.1.2 Superconducting State

In FebSCs, superconductivity appears at finite doping when magnetic transition is suppressed, this can be achieved when there is competition between magnetism and superconductivity. In the absence of magnetic interaction our numerical calculation on the respective pure states for both s^{+-} and s^{++}-wave symmetries have been shown in Fig. 5.3. Here, for the gap is required to change sign under shift by $Q=(\pi,0)$. To find the gap function it is instructive to simplify the gap equation for the momentum independent interaction:

Near the edge of the two Fermi-surfaces there is homogeneity and the two order parameters can be taken as equal and opposite, with this assumption we can take $\Delta_a(\boldsymbol{k})=-\Delta_d(\boldsymbol{k})=\Delta_s$ for that reason. With this in mind the two SC gap equations of section 3.2 are simplified to

$$\Delta_S = \frac{V^S}{2}\sum_{\boldsymbol{k}} \frac{\Delta_S}{2E_d(\boldsymbol{k})}\tanh\left(\frac{E_d(\boldsymbol{k})}{2T}\right)+\frac{V^S}{2}\sum_{\boldsymbol{k}} \frac{\Delta_S}{2E_a(\boldsymbol{k})}\tanh\left(\frac{E_a(\boldsymbol{k})}{2T}\right) \qquad (5.2)$$

with the energy excitations $E_{d/a}(\boldsymbol{k})=\sqrt{\xi_{\boldsymbol{k}}^2+C^2+\Delta_S^2\pm 2C\,\xi_{\boldsymbol{k}}}$. For T_c calculation we neglect Δ_s^2 from the dispersion.

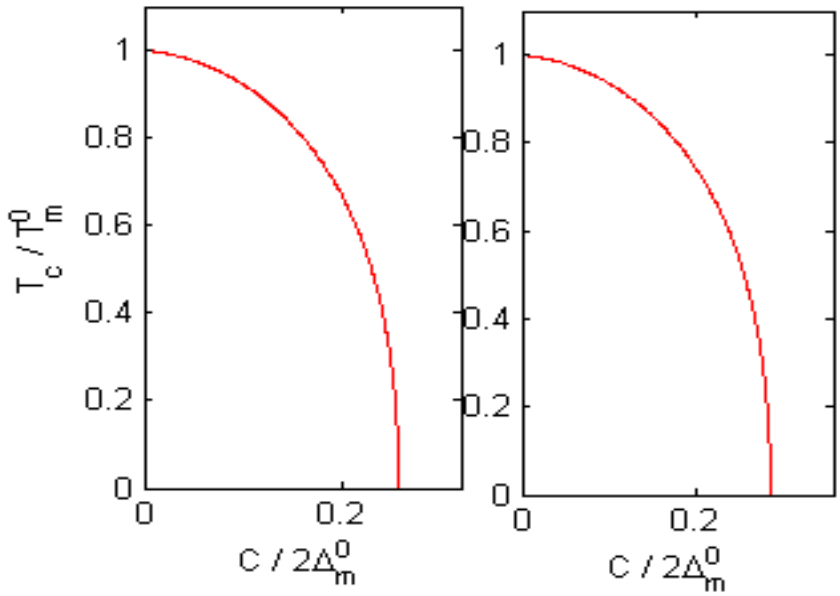

Figure 5.3: The phase diagram of pure SC state for hole doped (left panel) and electron doped (right panel).

The competition between SDW and SC may result in suppression of the superconducting state in the under doped region of the phase diagram. In the over doped region, where there is no magnetically ordered state, yet superconductivity can also be suppressed and eventually disappears. The size of the Fermi surface in over doped region of the phase diagram also changes significantly: for electron (hole) doped samples, it is characterized by increasingly large electron (hole) pockets and decreasing small hole (electron) pockets as seen in session 4.2, which eventually disappear at a certain doping level. In Fig. 5.3 we present effect of doping (C) on SC transition temperatures T_c of the pure SC state for both hole and electron doped FebSCs materials.

5.1.3 Commensurate SDW and s^{+-} wave Superconductivity

In previous two sessions we presented the effect of doping on both **SDW** and **SC** states critical temperatures. The coexistence state will be studied by considering the effects of the interplay between the two orders and doping. Now we have several experimental investigations showing the homogeneous coexistence between commensurate magnetism and sign changing s wave superconductivity in hole and electron doped FebSCs. The phase diagram of the model is quite rich due to the various couplings interactions as we define by T_c^0/T_m^0. In this session we focus on regimes where SDW and superconductivity coexist or compete. For homogeneous system near the Fermi-surfaces the SC and SDW gap equations (3.93) and (3.94) are simplified to

$$\Delta_S = \frac{V^s}{2}\sum_{\boldsymbol{k}} \frac{\Delta_S}{2\,\Omega_a(\boldsymbol{k})}\tanh\left(\frac{\Omega_a(\boldsymbol{k})}{2T}\right) + \frac{V^S}{2}\sum_{\boldsymbol{k}} \frac{\Delta_S}{\Omega_d(\boldsymbol{k})}\tanh\left(\frac{\Omega_d(\boldsymbol{k})}{2T}\right) \qquad (5.3)$$

and

$$\Delta_m = \frac{V^m}{2}\sum_{\boldsymbol{k}} \frac{\Delta_m}{\Xi_{\boldsymbol{k}}}\left[\frac{\Xi_a(\boldsymbol{k})}{2\,\Omega_a(\boldsymbol{k})}\tanh\left(\frac{\Omega_a(\boldsymbol{k})}{2T}\right) - \frac{\Xi_d(\boldsymbol{k})}{\Omega_d(\boldsymbol{k})}\tanh\left(\frac{\Omega_d(\boldsymbol{k})}{2T}\right)\right] \qquad (5.4)$$

where $\Omega_{d/a}(\boldsymbol{k}) = \sqrt{\xi_{\boldsymbol{k}}^2 + C^2 + \Delta_S^2 + \Delta_m^2 \pm 2C\sqrt{\xi_{\boldsymbol{k}}^2 + \Delta_m^2}}$. Now the coexistence phase of SDW and SC orders for homogeneous system reduced to the coupled equations (5.3) and (5.4). Following the same arguments stated at the beginning and solving the coupled equations for different magnetic and SC coupling interactions defined by T_c^0/T_m^0 the interplay between commensurate SDW_c and SC_{+-} is presented in the form of phase diagrams from Fig. 5.4 to Fig. 5.10.

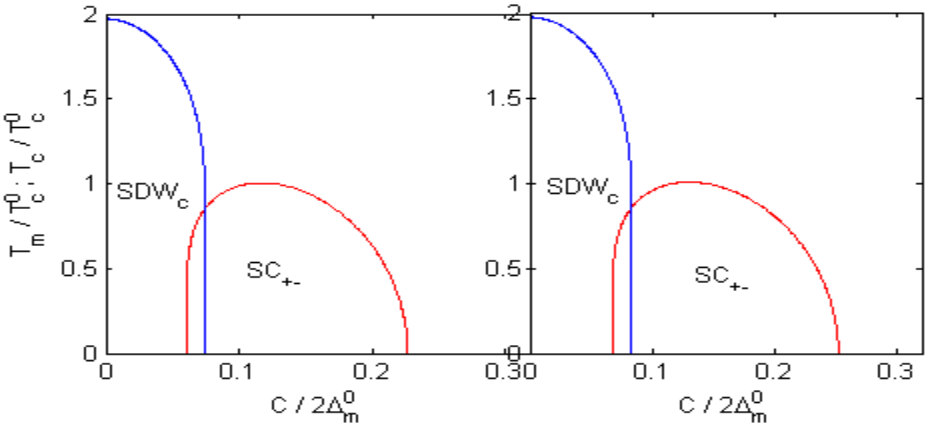

Figure 5.4: Normalized SDW transition temperature $\bar{T}_m = T_m/T_c^0$ and normalized s^{+-} -wave SC transition temperature $\bar{T}_c = T_c/T_c^0$ as a function of doping parameter $\bar{C} = C/2\Delta_m^0$ for $T_c^0/T_m^0 = 0.5$ for electron doped (left panel) and hole doped (right panel).

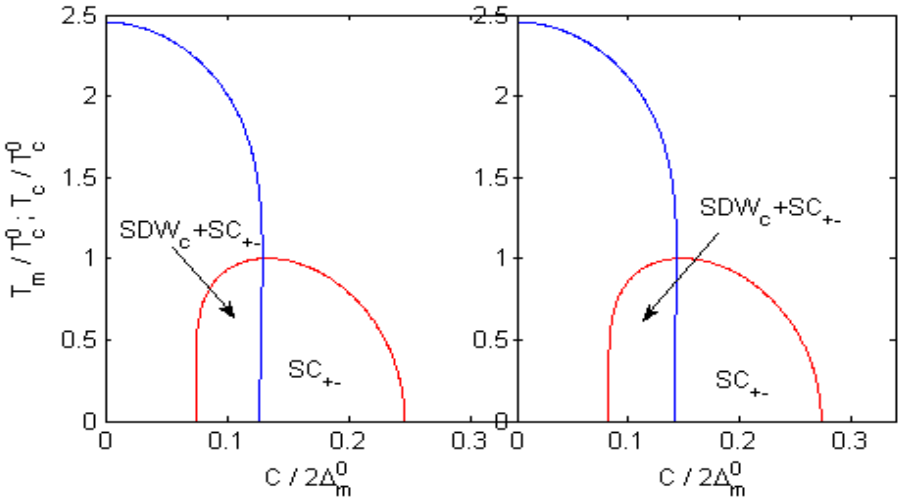

Figure 5.5: Normalized SDW $\bar{T}_m$ and normalized s^{+-} -wave SC $\bar{T}_c$ as a function of doping parameter $\bar{C}$ for $T_c^0/T_m^0 = 0.40$ for electron doped (left panel) and hole doped (right panel).

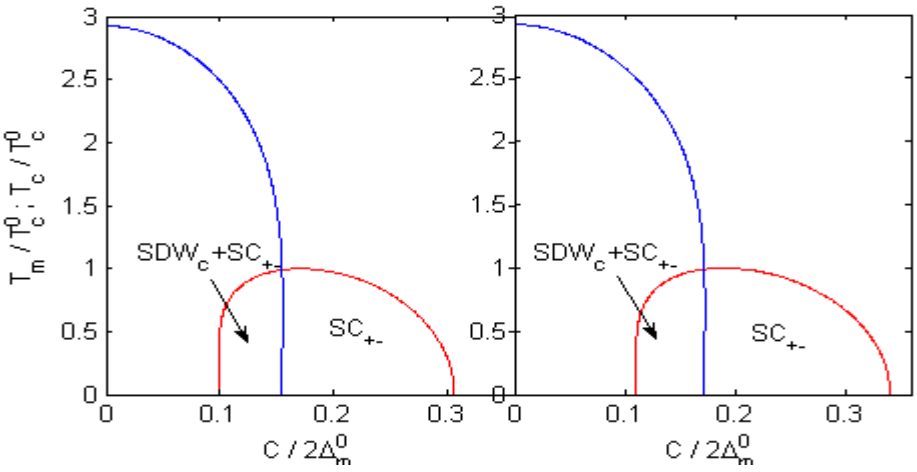

Figure 5.6: Normalized SDW $\bar{T}_m$ and normalized s^{+-} -wave SC $\bar{T}_c$ as a function of doping parameter $\bar{C}$ for $T_c^0/T_m^0=0.3333$ for electron doped (left panel) and hole doped (right panel).

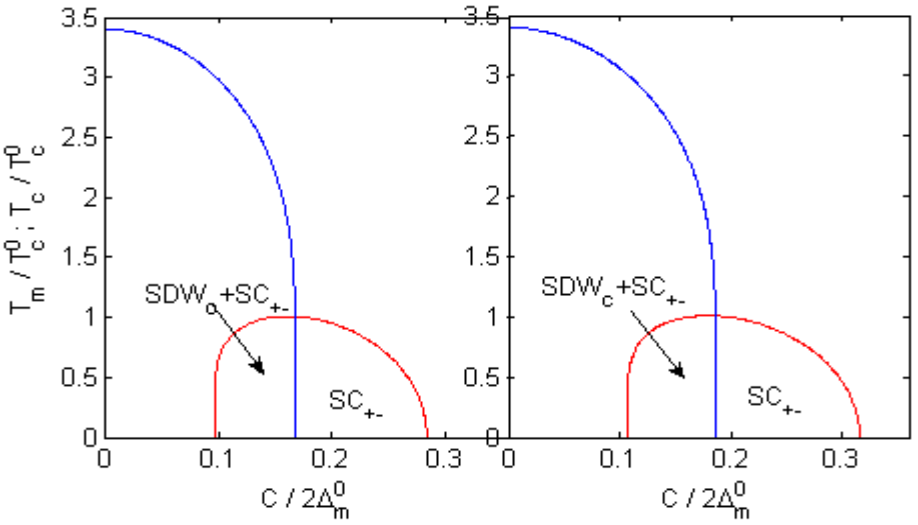

Figure 5.7: Normalized SDW $\bar{T}_m$ and normalized s^{+-} -wave SC $\bar{T}_c$ as a function of doping parameter $\bar{C}$ for ratio $T_c^0/T_m^0=0.285$ for electron doped (left panel) and hole doped (right panel).

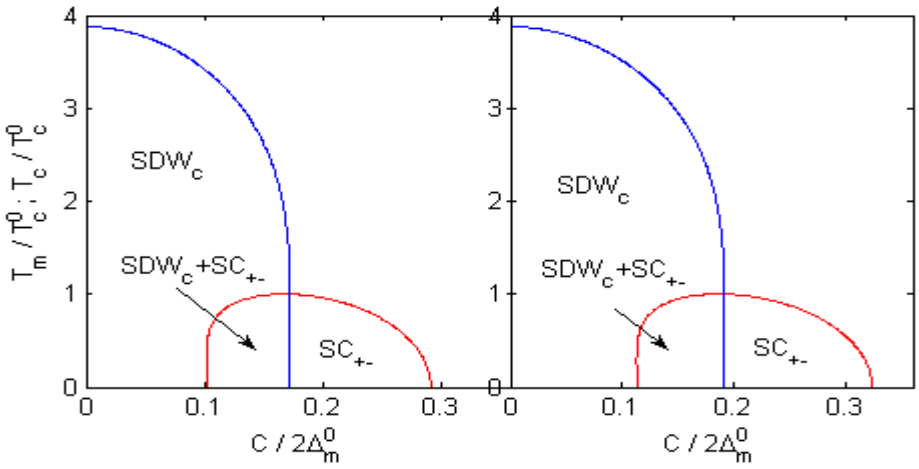

Figure 5.8: Normalized SDW $\bar{T}_m$ and normalized s^{+-} -wave SC $\bar{T}_c$ as a function of doping parameter $\bar{C}$ for $T_c^0/T_m^0 = 0.25$ for electron doped (left panel) and hole doped (right panel).

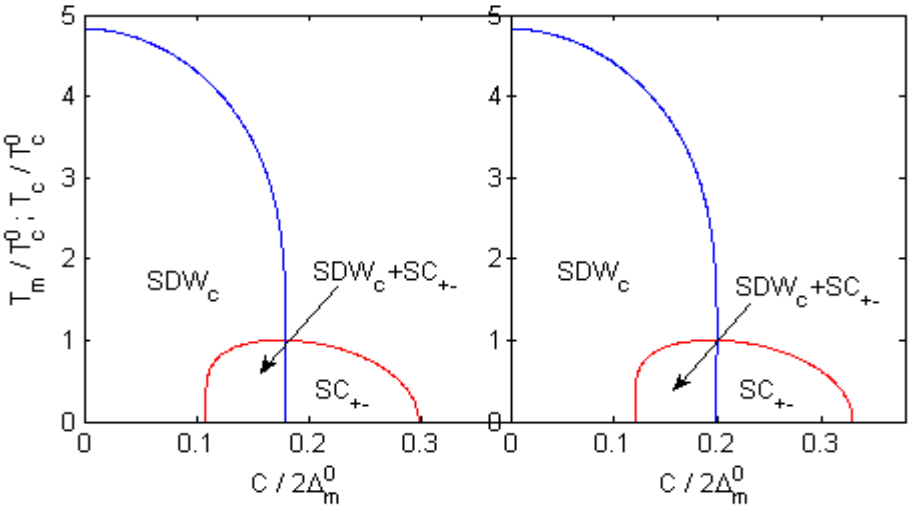

Figure 5.9: Normalized SDW $\bar{T}_m$ and normalized s^{+-} -wave SC $\bar{T}_c$ as a function of doping parameter $\bar{C}$ for $T_c^0/T_m^0 = 0.20$ for electron doped (left panel) and hole doped (right panel).

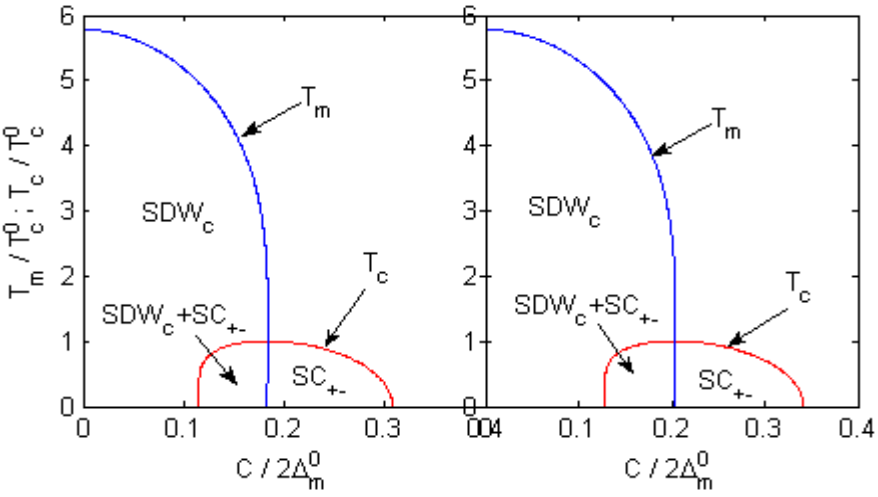

Figure 5.10: Normalized SDW $\bar{T}_m$ and normalized s^{+-} -wave SC $\bar{T}_c$ as a function of doping parameter $\bar{C}$ for $T_c^0/T_m^0=0.18$ for electron doped (left panel) and hole doped (right panel).

The transition temperatures: In Fig. 5.4 to Fig. 5.10, we present the interplay region of the normalized SDW transition temperature $\bar{T}_m$ and SC transition temperature $\bar{T}_m$ as a function of normalized doping parameter $\bar{C}$ for four different coupling interaction cases. We can see that the two order parameters coexist microscopically in underdoped region for all interactions considered. The coexistence region is extended to zero temperature from the crossing point. In the first case where $T_c^0/T_m^0=0.50$ SDW_c and SC_{+-} coexist below $T=0.8T_c^0$ as shown in Fig. 5.4, however in all other interaction presented from Fig. 5.5 to Fig. 5.10 homogeneous coexistence between commensurate SDW and s^{+-} superconductivity is possible for all temperatures below $T=T_c^0$. It is found that the width of the coexistence increases as the ratio T_c^0/T_m^0 gets smaller

and smaller. In other words for strong magnetic interaction the width of coexistence region increase and moves to the larger doping region. For a particular T_c^0/T_m^0 the $SDW_c + SC_{+-}$ region is larger for hole doped than electron doped one.

The result presented in Fig. 5.7 (right panel) can be compared with the experimental reports for hole doped such as K-Ba122 and Fig. 5.9 with electron doped $Ba(Fe_{1-x}ACo_x)_2As_2$ where A = Co and Fig. 5.10 is for A= Ni compounds of FebSCs. Furthermore in all cases coexistence is possible when the SDW couplings strength relative to the SC interaction is larger $(T_m^0 > T_c^0)$. From Fig. 5.11 one of the interesting result of our calculation reveals the reentrant of the non magnetically ordered phase at low temperatures which is observed in some both hole/electron doped Ba122 FebSCs.

To sum up the results presented in normalized critical temperatures and normalized imperfect nesting parameter C plane come up with the the expected interplay result showing the microscopic coexistence of commensurate SDW order and s^{+-} wave SC order in the underdoped region at low temperature limit.

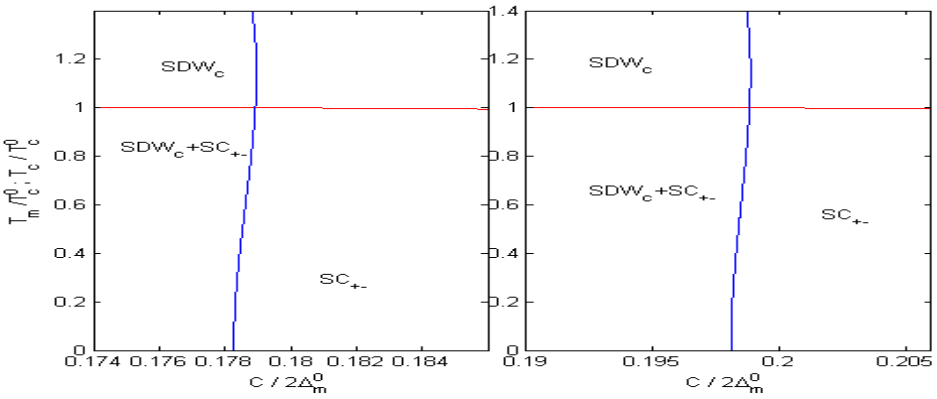

Figure 5.11: Normalized SDW $\bar{T}_m$ and normalized s^{+-} -wave SC $\bar{T}_c$ as a function of doping parameter $\bar{C}$ for ratio $T_c^0/T_m^0=0.20$ for electron doped (left panel) and hole doped (right panel) near the boundary between SDW and SC phases, reentrant of T_m .

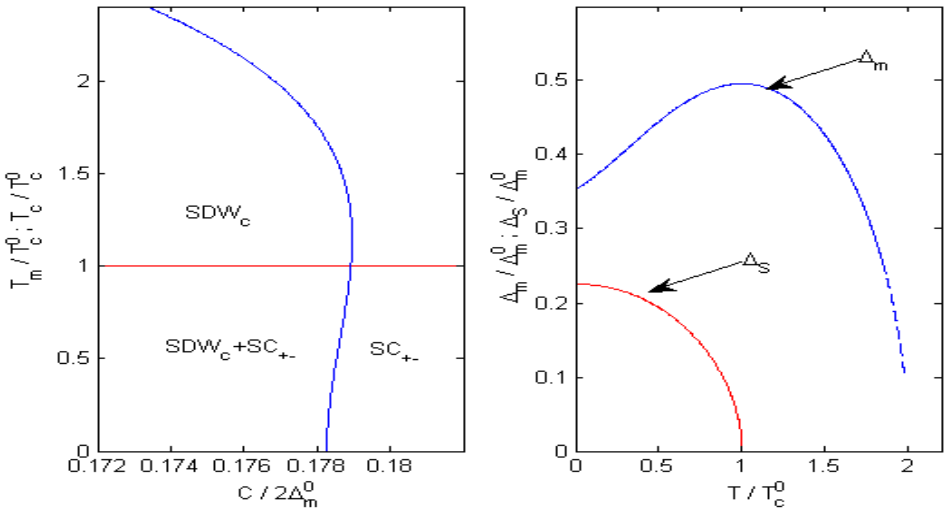

Figure 5.12: The Normalized transition temperatures (left panel): The normalized SDW order parameter $\bar{\Delta}_m=\Delta_m/\Delta_m^0$ and SC order parameter $\bar{\Delta}_s=\Delta_s/\Delta_m^0$ as a function of temperature in the mixed phases for $C/2\Delta_m^0=0.1750$ for electron doped (right panel) .The SDW order parameter is suppressed inside the SC state.

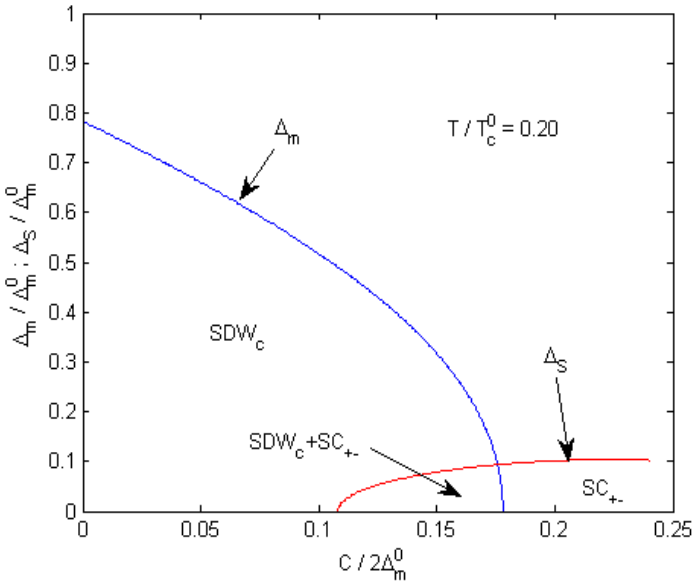

Figure 5.13: The normalized SC order parameter $\bar{\Delta}_s$ and SDW order parameter $\bar{\Delta}_m$ as a function of doping $\bar{C}$ for $\bar{T}=0.20$ for electron doped of Fig. 5.12.

Coexistence of the Order Parameters: The phase diagram in the temperature and doping evaluation of the normalized two states energy gap parameters, $\Delta_m \, and \, \Delta_S$ in the mixed states is presented in Fig. 5.12 and Fig. 5.13. In Fig. 5.12 (left panel) the temperature region of $0 \le T \le T_c^0$ and the doping $0.24 \le C \le 0.356\,\Delta_m^0$ represents the parameter space where SDW and SC coexist microscopically. Fig. 5.12 (right panel) plots the normalized SDW and normalized SC order parameters as function of temperature for $C/2\,\Delta_m^0 = 0.1750$ is presented. Due to the competition between the two orders in coexistence region (in SC state), the magnetic Δ_m decreases below T_c. The reentrant behavior is presented in the left panel of Fig. 5.12.

Once electrons or holes are doped into the parent compound, the magnetic order is gradually suppressed to zero, and superconducting order appears. The parent compound of FebSC is a poor metal with out superconductivity. As electrons are doped into the material, the superconducting order appears at a certain doping concentration. As the doping concentration becomes larger, it will disappear again. Similar behavior also occurs in the hole doping region. One of the most interesting observations is that, in both electron and hole doping regions, both the SDW and SC orders do not vanish at a small region. There fore, the magnetism and superconductivity are not exclusive with each other when SDW_c and SC_{+-} orders interplay is considered. .

It is clear that in the coexisting region the SDW order parameter decreases as temperature is lowered below T_c because superconductivity begins to partially gap out the Fermi surface. The plots of Fig. 5.13 shows the order parameters Δ_m and Δ_S as functions of doping parameter C at a fixed low temperature $T = 0.20\, T_{c.}^{0}$ showing the commensurate SDW and SC order coexist in the underdoped region at low temperature limit. The two most interesting results of Fig. 5.12 and Fig.5.13, are the strong suppression of the SDW order parameter in the SC phases and the suppression of SC order parameter in magnetic state which are observed behavior of the order parameters in the coexistence region.

5.1.3.1 Summery

In the study of interplay between commensurate SDW_c orders and SC_{+-} order using the gap equations derived. The normalized evolution of the critical temperatures and order parameters were presented after calculating the T_c^0 and T_m^0. We have obtained the phase diagram in the plane of the normalized SDW and SC transition temperatures T_m and T_c and normalized doping parameter C. By calculating different magnetic and SC couplings interactions defined by T_c^0/T_m^0 we presented possible cases of microscopic phase coexistence of the commensurate SDW_c and SC_{+-} phases. In other words we employed a systematic way of determining the homogeneous, microscopic coexistence between commensurate SDW order and s^{+-} wave symmetry SC states at low temperatures. Our results are experimentally confirmed ones on both doped Ca-111 and 122 families of FebSC systems. Even more interestingly, the result of our study showed the strong suppression of the SDW_c order parameter in the SC_{+-} phases and the suppression of SC state in under and over doped regions are some of the interesting result of the last section.

5.1.4 Commensurate Spin-density wave and s^{++} wave Superconductivity

The nematic and orbital fluctuations are being observed at the phase boundary between the magnetic and SC phases in some FebSCs [147, 153]. This may reveal the presence of the same sign s-wave wave symmetry superconductivity in the region. Therefore in this session we consider the case when the superconducting order parameter in a conventional s^{++} wave (the same sign in both electron on hole and electron Fermi surfaces) and investigate the interplay with commensurate SDW order. Here the only difference is on the interaction and on the dispersion are $\Delta_a(\boldsymbol{k})=\Delta_d(\boldsymbol{k})=\Delta_S$ and

$$\Omega_{d/a}(\boldsymbol{k})=\sqrt{\xi_{\boldsymbol{k}}^2+C^2+\Delta_S^2+\Delta_m^2\pm 2\sqrt{C^2(\xi_{\boldsymbol{k}}^2+\Delta_m^2)+\Delta_m\Delta_S}}. \tag{5.5}$$

In the absence of magnetism most properties of s^{+-} wave and s^{++} wave superconductivity are the same. The pure s^{++} wave SC state can also be represented by Fig. 5.3. The interplay may result first transition from commensurate SDW to s^{++} wave SC state as observed. This case has been considered experimentally and the conclusion was that the transition from the SDW to SC phase is always of first order, regardless of shapes of the Fermi pockets or the shift of chemical potentials. This result implies that the very coexistence between SDW and **SC** in FebSCs is an implication that the pairing state is not a conventional s^{++} state. In our calculations in Fig. 5.14 to Fig. 5.17 we have presented the transition from commensurate SDW to pure s^{++} wave SC state is first order as supported experimentally.

We analyzed as to what happens when SC is s^{++} wave symmetry and magnetic order is commensurate for four different interaction cases $T_c^0/T_m^0=0.18\,,0.20\,,0.25\,,0.285$. When magnetic order is commensurate, the transition between SDW_c and SC_{++} phases remains of first order, shown in the the

same Figs. and the mixed state does not occur. In contrast, for an s^{+-} SC, once the SDW order becomes commensurate, the transformation from commensurate SDW to SC involves the coexistence phase even though the transition from commensurate SDW to SC phase would be of first order. Furthermore the evolution of order parameters Δ_m and Δ_S with doping at $T=0.2T_c^0$ in Fig. 5.18 shows the absence of overlapped region.

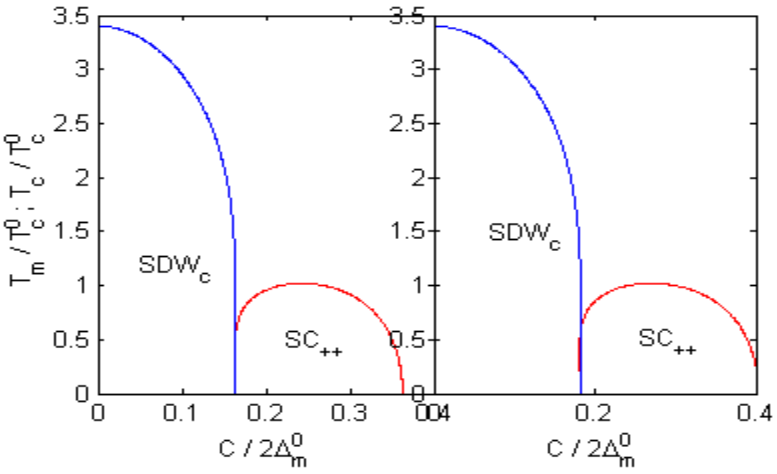

Figure 5.14: Normalized SDW $\bar{T}_m$ and normalized s^{++} -wave SC $\bar{T}_c$ as a function of doping parameter $\bar{C}$ for $T_c^0/T_m^0=0.2850$ for electron doped (left panel) and hole doped (right panel)**.**

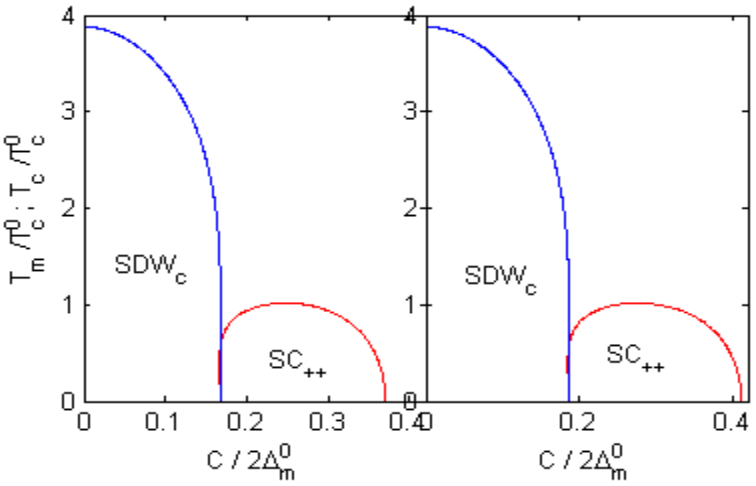

Figure 5.15: Normalized SDW $\bar{T}_m$ and normalized s^{++} -wave SC $\bar{T}_c$ as a function of doping parameter $\bar{C}$ for $T_c^0/T_m^0=0.25$ for electron doped (left panel) and hole doped (right panel)**.**

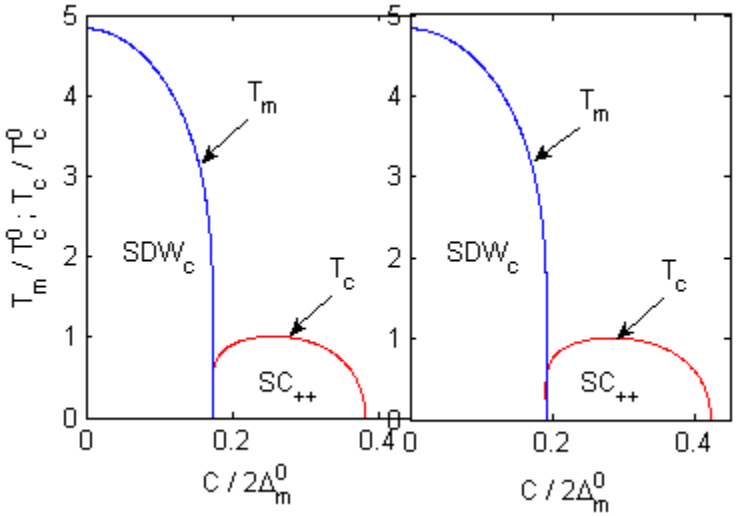

Figure 5.16: Normalized SDW $\bar{T}_m$ and normalized s^{++} -wave SC $\bar{T}_c$ as a function of doping parameter $\bar{C}$ for $T_c^0/T_m^0=0.20$ for electron doped (left panel) and hole doped (right panel)**.**

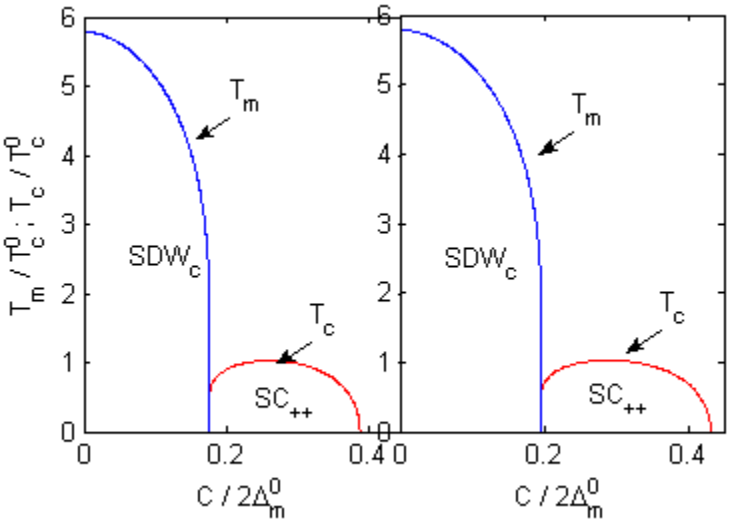

Figure 5.17:Normalized SDW $\bar{T}_m$ and normalized s^{++} -wave SC $\bar{T}_c$ as a function of doping parameter $\bar{C}$ for $T_c^0/T_m^0=0.18$ for electron doped (left panel) and hole doped (right panel).

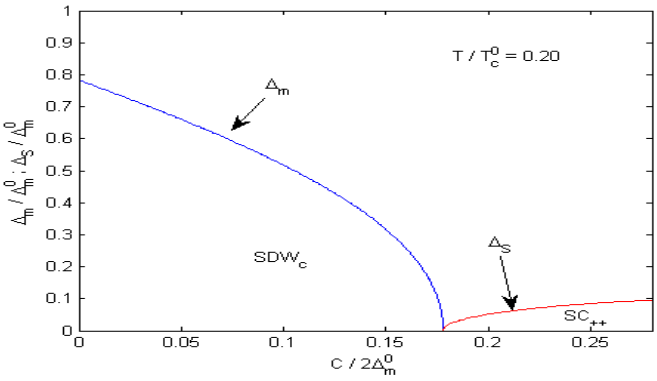

Figure 5.18: The normalized **SC**$_{++}$ order parameter $\bar{\Delta}_s$ and normalized SDW order parameter $\bar{\Delta}_m$ as a function of doping $\bar{C}$ for electron doped for at $T=0.20\,T_c^0$ of Fig. 5.17.

In this section the interplay between SDW_c and SC_{++} orders result shows the phase separation between the two phases. The transition between commensurate SDW and SC phases is always of first order, and the mixed phase does not appear for both hole and electron doped FebSCs compounds for the considered interactions. The result will be different when the SDW order becomes incommensurate as it will be demonstrated in section 5.2.

5.1.5 Summery

The microscopic coexistence between commensurate antiferromagneic spin density wave and s -wave (both s^{+-} and s^{++} waves) superconductivity in electron/hole doped FebSCs has been investigated theoretically. In following itinerant nature of magnetism produced by Fermi surface nesting between hole and electron Fermi pockets, we investigate in detail the competition between the of these two phase order parameters. We demonstrate microscopic coexistence between SC_{+-} and SDW_c states in hole and electron doped FebSCs compounds. Solving for gap equation from mean-field Hamiltonian for the competition between SDW and SC and applying numerically techniques we show that a conventional SC_{++} state does not allow a coexistence regime. Mean while, the unconventional SC_{+-} state, whose gap function changes sign from one Fermi surface sheet to the other, coexist with commensurate SDW_c, depending on the strength of coupling interactions. Our results are consistent with most acceptable investigations on electron/hole doped Ba122 and Ca111 FebSCs families. We find different result with inclusion incommensurability as revealed in coming session. On the other hand the first order transition from SDW_c to SC_{++} presented in Fig. 5.14 to Fig. 5.18 is consistent with the phase separated compounds in doped Li111 and La1111 compounds of FebSCs.

5.2 Incommensurate Spin Density Wave and Superconductivity

Magnetic incommensurability in most FebSCs systems are observed phenomenon near the optimal doping and overdoped region. The results presented in the last section, if we keep an SDW order commensurate, an overladed region of SDW and s^{+-} wave SC phase appears in under doped region and phase separation for SDW_c and SC_{++}. For both electron and hole doped system incommensurability is common at optimal doping, therefore we include the incommensurate parameter in both band energies. That is dispersion near electron band $\xi_d(\boldsymbol{k})=\xi_k+C+\delta$ and the other hole band $\xi_a(\boldsymbol{k})=-\xi_k+C+\delta$ where δ is incommensurate parameter defined by $\delta=V_F(\boldsymbol{Q}_\delta-\boldsymbol{Q}_0)$. In Fig. 5.19 the phase diagram of pure SDW state for non zero $C\ and\ \delta$ is shown.

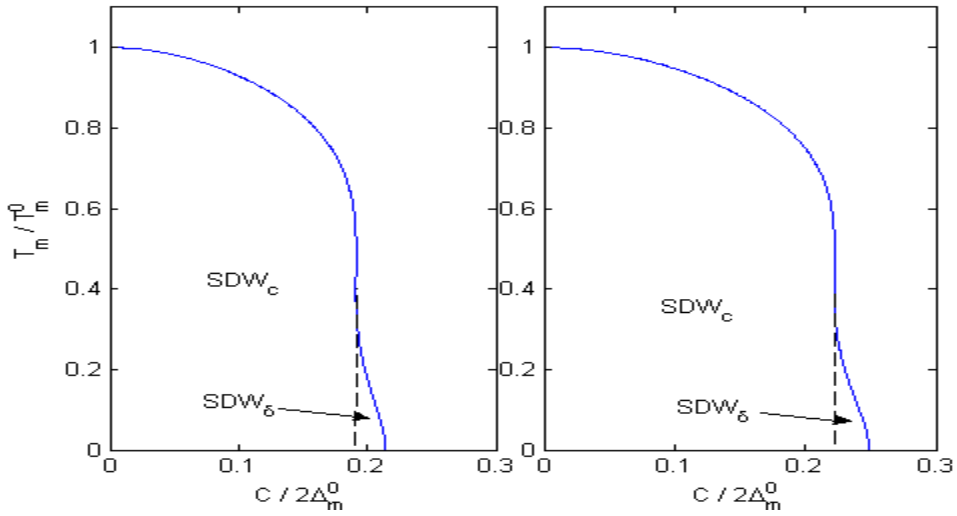

Figure 5.19: The normalized SDW transition temperature for pure magnetic state which is the same as Fig. 5.1 for electron doped (left panel) and hole doped (right panel) for non zero incommunsurability.

For non zero δ incommensuration occurs before the commensurate transition becomes first order and it is calculated at $T=0.54\,T_m^0$. In the Fig. 5.19 solid lines are second order transition lines into a state with a SDW order, dashed lines are first order transition lines into an SDW state with an incommensurate SDW order.

5.2.1 Incommensurate spin-density wave and s^{+-} wave superconductivity

The report of most experimental probes on doped Ba122 FebSCs [36] reveals the transition from long range AFM to short range order is first order. The competition between SDW and s^{+-} SC orders for non zero δ are presented in this section. For three cases considered, $T_c^0/T_m^0=0.18,\,0.20,\,0.285$ a non zero incommensurate δ emerges below a particular temperature defined as the maximum temperature below which the transition from commensurate SDW to incommensurate SDW is first order T_δ^0 that depends on considered ratio. As a result of non zero δ the coexistence regions moves to larger doping region for both doped systems. Therefore, this broadens the coexistence region of the the two phases by $SDW_\delta+SC_{+-}$ region. It is calculated for larger T_c^0/T_m^0 incommunsurability developed at higher temperature as can be seen as will be seen latter. For $T_c^0/T_m^0=0.18$ the commensurate to incommensurate transition temperature $T_\delta^0=2.4\,T_c^0$ and similarly for $T_c^0/T_m^0=0.20$ it is found thet $T_\delta^0=1.8\,T_c^0$. The width of the coexistence between incommensurate SDW and s^{+-} wave SC state (SDW_δ +SC_{+-}) increases as the interaction parameter T_c^0/T_m^0 gets smaller.

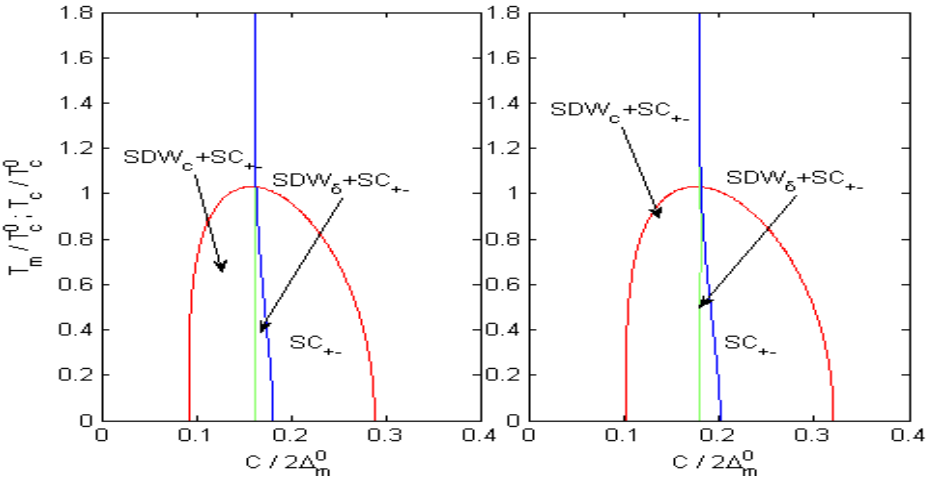

Figure 5.20: The normalized SDW and SC transition temperatures for $T_c^0/T_m^0=0.285$ but here we include incommunsurebility parameter δ different from zero for electron doped (left panel) and hole doped (right panel).

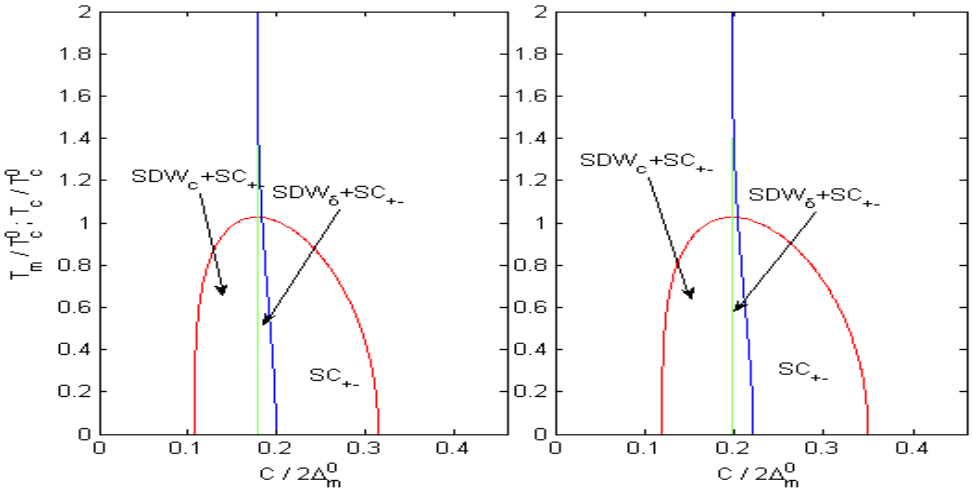

Figure 5.21: The normalized SDW and SC transition temperatures which for $T_c^0/T_m^0=0.20$ but here we include incommunsurebility parameter $\boldsymbol{\delta}$ different from zero for electron doped (left panel) and hole doped (right panel).

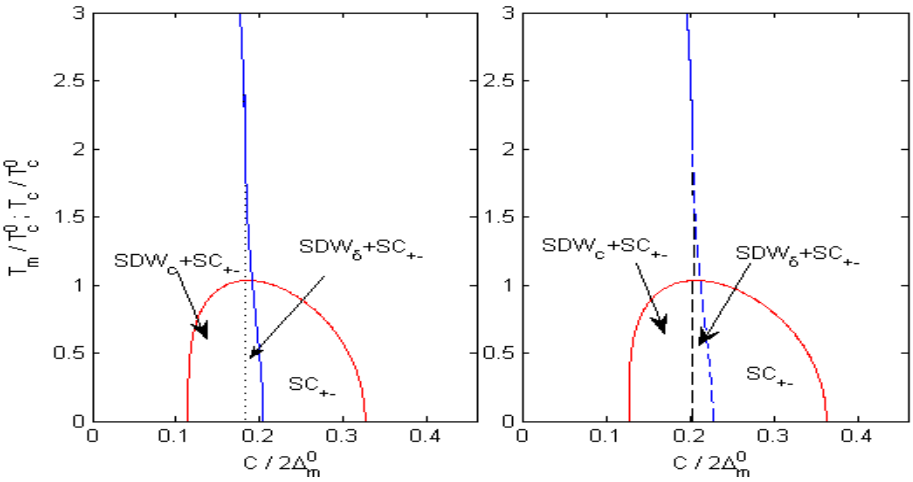

Figure 5.22: The normalized SDW and SC transition temperatures for a unconventional s^{+-} SC order parameter, at non zero δ for $T_c^0/T_m^0=0.18$ for electron doped (left panel) and hole doped (right panel). The coexistence of SDW+SC state appear, when SDW order becomes incommensurate unlike to when SDW is commensurate.

The competition between commensurate SDW and SC_{+-} order parameters with non zero incommensurate parameter δ. it is found out that there will be further overlap region developed (SDW_δ + SC_{+-} region). Furthermore the first order phase transition from commensurate SDW_c to incommensurate order SDW_δ is also another investigation. This had been in equation at early stage of the discovery of FebSCs but recent evidences have been confirmed in Co/Ni/K-Ba122 FebSC compounds.

5.2.2 Incommensurate Spin-density wave and s^{++} wave Superconductivity

As interplay between commensurate magnetism and s^{++} wave superconductivity showed the result of the interaction produces first order transition from magnetic to pure SC state. This is not repeated when the magnetic order changed to incommensurate as presented in Fig. 5.23 to Fig.5.24. From the Figs. we see that $SDW_{\delta}+SC_{++}$ region is below a finite temperature that increases when T_c^0/T_m^0 is smaller above which there is first order transition from SDW_{δ} to SC_{++} orders. showing that coexistence region does not cover the whole under doped region.

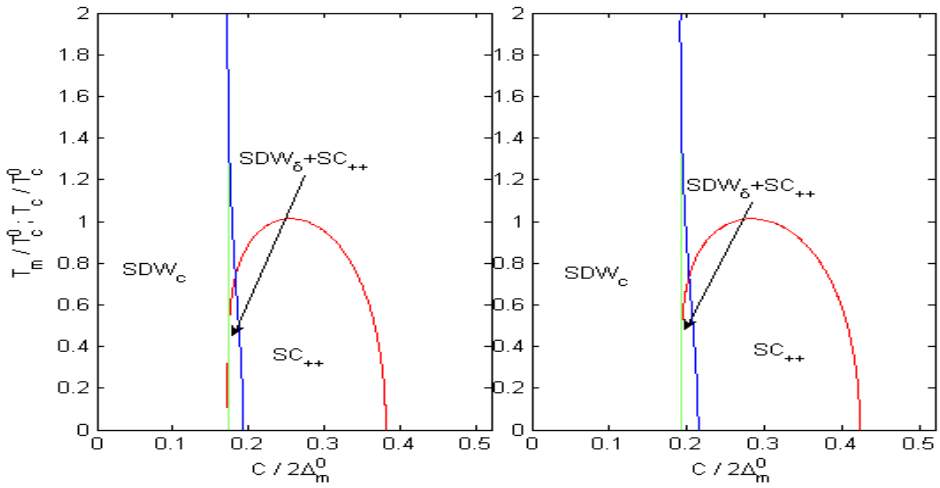

Figure 5.23: The normalized SDW and SC transition temperatures for a conventional s^{++} SC order parameter, at non zero δ, $T_c^0/T_m^0=0.20$. The coexistence region, $SDW_{\delta}+SC_{++}$ appear, when SDW order becomes incommensurate unlike to when SDW is commensurate.

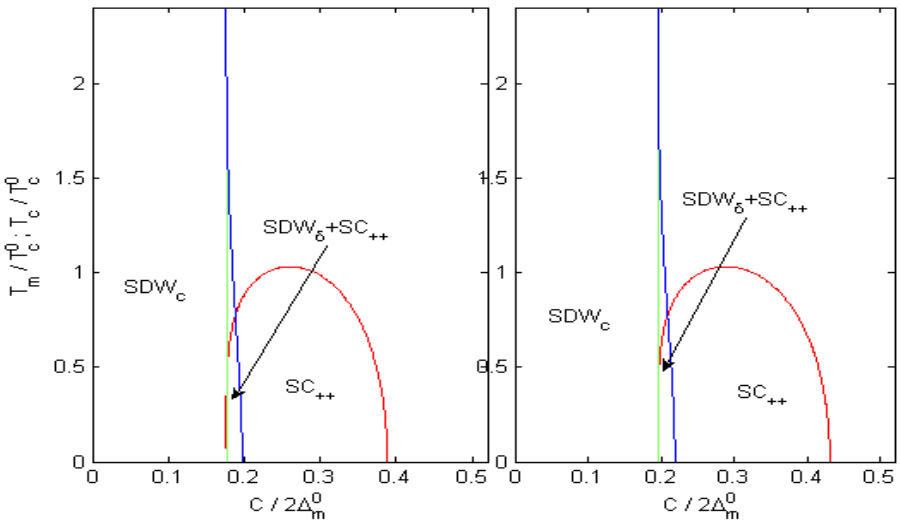

Figure 5.24: The normalized SDW and SC transition temperatures for a conventional s^{++} SC order parameter, at non zero δ, for $T_c^0/T_m^0 = 0.18$. The coexistence region, $SDW_\delta+SC_{++}$ appear, when SDW order becomes incommensurate unlike to when SDW is commensurate.

Here with systematic inclusion of incommunsurability brings the second order phase transition from SDW to s^{++} SC states below some temperature that increases as T_c^0/T_m^0 gets smaller as shown in this session figures. This may support the most accepted experimental reports on the overlap between the magnetic and s^{++} superconductivity at quantum critical point on 1111 FebSCs like electron doped 1111 FebSC family. Furthermore the result support the observed orbital fluctuations near optimal doping that will be responsible for SC_{++} superconductivity..

5.3 Summery

To sum up our model calculations have come up with two basic results: first the unconventional sign reversal s-wave superconductivity and spin-density wave phases coexist microscopically in under doped region for all coupling interactions considered, however the width of the coexistence region depends on the ratio between $T_c^0 \, and \, T_m^0$, that is the width of the coexistence region gets larger when the SC interaction is weaker as presented in the respective phase diagram figures. The second result the interplay between s^{++} wave SC order and commensurate SDW reveals the first order transition from magnetic SDW to SC states. The second order transition from SDW to SC_{++} states is possible when the SDW is incommensurate for all coupling interactions considered. Like the interplay between SDW_c and SC_{+-} orders the width of SDW_δ+SC_{++} region increases when SC interaction is weaker. In both cases for particular interaction the overlaped region of hole doped is slightly greater than that of electron doped one. The two results are consistent with most recent experimental and theoretical investigations on most doped 111, 1111 and 122 families of FebSCs compounds.

CHAPTER 6: SUMMERY AND CONCLUSION

CHAPTER 6

CHAPTER 6

SUMMERY AND CONCLUSION

The interplay between magnetism and superconductivity had attracted immence interest and effort following the discovery of magnetic superconductors like heavy fermion, cuprate and recent iron based superconductors. The study of their interplay between has also been fascinating area of study due to complex magnetic interactions in the systems. Basic experimental evidences are the magnetic order in most FebSCs is the result of nesting between the fermions pockets and most FebSCs families have distinct Fermi-surfaces pockets, hole type and electron type at the the center and corners of the unfolded Briuilion zones. The interaction between fermions forming the pockets is important to study the low temperature physics of FebSCs.

Starting from the model Hamiltonian consisting of itinerant electrons responsible for magnetic and superconducting pairing interactions as discussed in chapter 3. Using either Green function or Bogoligiv transformation gap equations for SDW and SC order parameters have been established for pure systems and for interacting ones. The gap equations have been studied in detail as physically accepted choice of parameters. We have established the homogeneous coexistence of antiferromagnetic SDW and s-wave superconductivity state and also the phase separation. Some of the important findings are as follows which are in excellent agreement with experiment.

First from pure state gap equations, we defined $T_c^0(\Delta_S^0)$ and $T_m^0(\Delta_m^0)$ as the pure SC and SDW transition temperatures at perfect nesting (zero doping) and the respective zero temperature order parameters. The interplay between SDW and SC order parameters are presented in form of phase diagram on the normalized critical

temperatures $T_{c/m}/T^0_{c/m}(\Delta^0_m)$ and normalized doping parameter $C/2\Delta^0_{m.}$ for different magnetic and SC coupling interactions relations are defined by T^0_c/T^0_m as presented in chapter 5. This will help us for experiment result comparison of different FebSCs compounds.

First in pure SDW state (in the absence of superconducting interaction) we presented the transition from commensurate SDW and incommensurate SDW state for both electron and hole doped FebSCs is at $T=0.54T^0_m$ and commensurate SDW reenter at $T=0.40T^0_m$ for all magnetic coupling interaction. Showing that SDW_δ order developed before SDW_c order reenter at $0.40T^0_m$ and the first order transition from SDW_c state to SDW_δ state below $0.54T^0_m$ are the result of the first part even though the effect of SC interaction on T_m was not considered

The results of the competition between the commensurate SDW_c order and SC_{+-} order for different interactions are presented, reveal the microscopic coexistence of SDW_c and SC_{+-} phases however the width of coexistence depends on the interactions. Further more relatively large width of overlapped region, $SDW_c + SC_{+-}$ moves to higher doping region when the superconducting interaction becomes weaker.

Recent experimental probes are reporting the orbital fluctuations existence near the phase boundary between SDW and SC state and small electro-phonon coupling in FebSCs compounds, showing that the sign preserving s-wve superconductivity (SC_{++}). The interplay between SDW_c and SC_{++} orders calculations come up with the first order phase transition from **SDW_c** to **SC_{++}** state for all interactions considered which can be compared with phase separated doped 1111 and 111 FebSCs families.

Commensurate SDW and SC_{+-} orders competition revealed the homogeneous overlap between the two phases. For non zero incommensurate parameter δ. It is

found out that there will be further overlap region developed (SDW_δ + SC_{+-} region). Furthermore the first order phase transition from commensurate SDW_c to incommensurate order SDW_δ is investigated with the inclusion of SC interaction below T_m^δ. This had been in equation at early time of discovery of FebSCs but recent evidences has been confirming on doped Ba122 FebSCs compounds.

In the first part of competition between SDW_c to SC_{++} orders, the first order phase transition from SDW_c to SC_{++} states. For non zero $C \; and \; \delta$ the result be different. So with systematically the inclusion of incommunsurability brings the microscopic phase coexistence between SDW to SC_{++} states in-small temperature and doping ranges near quantum critical point as explained in section 5.2. This may support the most recent experimental reports on the overlap between the magnetic and s^{++} wave superconductivity at quantum critical point in doped Ca1111 FebSCs. Furthermore the result may answer the question of the orbital fluctuations observed recently near optimal doping.

Even more interestingly, the result of our study showed the zero temperature phase separation or coexistence between the two states. The strong suppression of the SDW order parameter in the SC phases and the suppression of SC order parameters in magnetic underdoped region (due to interplay) and nonmagnetic overdosed region (due to increasing miss match between Fermi pockets)are some of the interesting result.

Finally calculations of numerical estimates have been made in a mean-field approximation where fluctuations and other interactions like intra-pocket have been ignored, this inclusion may affect the findings some what but not substantial. The results can also be applicable to all antiferromagnetic superconductors with similar pairing symmetry and electronic structures.

1 **BIBLIOGRAPHY**

BIBLIOGRAPHY

BIBLIOGRAPHY

[1] H. Kamerlingh Onnes, Comm. Phys. Lab. Univ. Leiden, Nos. ***119***, *120, 122 (1911).*

[2] J. R. Schrieffer, Theory of Superconductivity, Westview Press, Boulder, 1999; M. Tinkham, Introduction to Superconductivity, *Dover Books on Physics, New York, 2004*

[3] A. A. Abrikosov, *Rev. Mod. Phys.* ***76***, *975 (2004).*

[4] M. Kugler et al., *Rev. Mod. Phys.* ***79***, *353 (2007).*

[5] A. P. Schnyder et al., *Phys. Rev. B* ***70***, *214511 (2004)*

[6] G. E. Devlin and E. Corenzwit, *Phys. Rev.* ***120***, *1964 (1960).*

[7] H. Fröhlich, *Phys. Rev.* ***79***, *845 (1950).*

[8] J. Bardeen, *Phys. Rev.* ***106***, *162 (1957)*; , *Phys. Rev.*, ***108***, *1175 (1957).*

[9] B. T. Matthias et al . ,*Phys. Rev. Lett. 1, 92 (1958).*

[10] A. A. Abrikosov, and L. P. Gor'kov, Zh. Eksp. *Teor. Fiz.* ***39***, *1781 (1960).*

[11] V. L. Ginzburg, Zh. Eksp. *Teor. Fiz.* ***31***, *202 (1956).*

[12] N. F. Berk, and J. R. Schrieffer, *Phys. Rev. Lett.* ***17***, *433 (1966).*

[13] B. T. Matthias et al. , *Proc. Nat. Acad. Sci. USA* ***74***, *1334 (1977).*

[14] O. Fisher et al. , *Solid State Commun.* ***17***, *721 (1975).*

[15] A. K. Cheetham, and P. Day, Solid State Chemistry: Compounds, Oxford University Press, New York (2001).

[16] Z. Fisk et al., *Science* ***239***, *33 (1988).*

[17] F. Steglich et al. ,*Phys. Rev. Lett.* ***43***, *1892 (1979).*

[18] P. Chandra et al., *Nature* ***417***, *381 (2002).*

[19] N. K. Sato et al., *Nature* ***410***, *340 (2001).*

[20] C. Geibel, et al., *Phys. B: Cond. Mat.* ***83***, *305 (1991).*

[21] H. v. L¨hneysen, *Physica B **197**, 551 (1994).*

[22] M. B. Maple, P*hysica B **215**, 110 (1995).*

[23] N. D. Mathur et al ., *Nature **394**, 39 (1998).*

[24] A. W. Sleight, *Phys. Today 24 (June 1991).*

[25] J. D. Jorgensen, *Phys. Today 34 (June 1991).*

[26] N. F. Mott, The basis of the electron theory of metals, with special reference to the transition metals. *Proceedings of the Physical Society of London Series A 62, 416 (1949).*

[27] R. J. Cava et al., *Phys. Rev. Lett. **58**, 408 (1987).*

[28**]** A. Partrick et al., *Rev. Mod. Phys. **78**, 1 (2006).*

[29] H. H. Wen et al., *Euro. Phys. Lett. **82**, 17009 (2008).*

[30] H. Luetkens et al. , *Nature Mat. **8**, 305 (2009).*

[31] A. J. Drew et al., *Nature Mat. O **8**, 310 (2009).*

[32] J. Zhao et al., *Nature Mat. **7,** 953 (2008).*

[33] I. Mazin and J. Schmalian, *Physica C, **469,** 614 (2009).*

[34] H. Mazin., *Nature **464**, 183 (2010).*

[35] Z. p. Yin, et al., *Nature physics, **1083**, 51923 (2011).*

[36] D. Pengcheng et al., *Nature physics, **1083**, 52483 (2012).*

[37] R. Prozorov et al., *J. Phys **449**, 012020 (2013).*

[38] Z. Hou et al., *Chin. Phys. B **22**, 087413, (2013).*

[39] G. R. Stewart, *Rev. Mod. Phys. **83**, 1589 (2011).*

[40] Yu Shun-Li and Li Jian-Xin ., *Chin. Phys. B **22**, 087411 (2013).*

[41] Y. Kamihara et al., *J. Am. Chem. Soc. **128**, 1001 (2006).*

[42] H. Eschrig et al., *Phys. Rev. B **81**, 155447 (2010).*

[43] C. Liu et al., *Phys. Rev. B **82**, 075135 (2010).*

[44] K. Kuroki et al., *Phys. Rev. Lett. **101**, 087004 (2008).*

[45] T. Miyake et al., J. *Phys. Soc. Jpn. **79**, 044705 (2010).*

[46] X. Dai et al., *Phys. Rev. Lett.* ***101****, 057008 (2008).*

[47] L. Boeri et al., *Phys. Rev. Lett.* ***101****, 026403 (2008).*

[48] H.J. Grafe et al., *Phys. Rev. Lett.* ***101****, 047003 (2008).*

[49] K. Matano et al., *Eur. Phys. Lett.* ***83****, 57001 (2008).*

[50] P, Shen et al., *Europhys. Lett.* ***85*** *67003 (2009)*

[51] A. Drew et al., Nature Mater. 8, 310 (2009).

[52] H.H. Wen and S. Li, *Annu. Rev. Cond. Matt. Phys.* ***2****, 121 (2011).*

[53] M. Rotter et al., *Phys. Rev. Lett.* ***101****, 107006 (2008).*

[54] A. S. Sefat et al., *Phys. Rev. Lett.* ***101****, 117004 (2008).*

[55] N. Ni et al., *Phys. Rev. B* ***78****, 214515 (2008).*

[56] V. Brouet et al., *Phys. Rev. B* ***80****, 165115 (2009).*

[57] T. Kondo et al., *Phys. Rev. B* ***81****, 060507 (2010).*

[58] M. Rotter et al., *Phys. Rev. B* ***78****, 020503 (2008).*

[59] T. Sato et al., *Phys. Rev. Lett.* ***103****, 047002 (2009).*

[60] R. Cortes-Gil et al., *Chem. Mater.* ***22****, 4304 (2010).*

[61] S. Aswartham et al., arXiv:1203.0143 (2012).

[62] G. Wu et al., *J. Phys.: Condens. Matter* ***20****, 422201 (2008).*

[63] T. Park et al., *J. Phys.: Condens. Matter* ***20****, 322204 (2008).*

[64] Z. Ren et al., *Phys. Rev. Lett.* ***102****, 137002 (2009).*

[65] P. Richard et al., *Rep. Prog. Phys.* ***74****, 124512 (2011).*

[66] C. Liu et al., *Phys. Rev. Lett.* ***101****, 177005 (2008).*

[67] H. Ding et al., *Europ. Phys. Lett.* ***83****, 47001 (2008).*

[68] V. B. Zabolotnyy et al., *Nature* ***457****, 569 (2009).*

[69] D. V. Evtushinsky et al., *Phys. Rev. B* ***79****, 054517 (2009).*

[70] P. Richard et al., *Phys. Rev. Lett.* ***102****, 047003 (2009).*

[71] D. V. Evtushinsky et al., *New J. Phys.* ***11****, 055069 (2009).*

[72] D. V. Evtushinsky et al., *J. Phys. Soc. Jpn.* ***80****, 023710 (2011).*

[73] S. Thirupathaiah et al., *Phys. Rev. B **81**, 104512 (2010).*

[74] C. Liu et al., *Nat Phys **6**, 419 (2010).*

[75] C. Liu et al., *Phys. Rev. B **84**, 020509 (2011).*

[76] M. Yi et al., PNAS **108**, 6878 (2011).

[77] E. van Heumen et al., *Phys. Rev. Lett. **106**, 027002 (2011).*

[78] M. Yi et al., *Phys. Rev. B **80**, 024515 (2009).*

[79] J. Fink et al., *Phys. Rev. B **79**, 155118 (2009).*

[80] P. Richard et al., *Phys. Rev. Lett. **104**, 137001 (2010).*

[81] Y. Kim et al., *Phys. Rev. B **83**, 064509 (2011).*

[82] T. Yoshida et al., *J. Phys. Chem. Solids **72**, 465 (2011).*

[83] C. Liu et al., *Phys. Rev. Lett. **102**, 167004 (2009).*

[78] J. G. Analytis et al., *Phys. Rev. B **80**, 024515 (2009).*

[84] S. E. Sebastian et al., *J. Phys. Condens. Matter **20**, 422203 (2008)*

[72] D. V. Evtushinsky et al., *J. Phys. **11**, 055069 (2009).*

[85] T. Sato et al., *Phys. Rev. Lett. **103**, 047002 (2009).*

[86] N. Ni,. et al., *Phys. Rev. B **78**, 214515 (2008).*

[87] J. H Chu et al., *Phys. Rev. B **79**, 014506 (2009).*

[88] C. Lester et al., *Phys. Rev. B **79**, 144523 (2009).*

[89] D. K. Pratt et al., *Phys. Rev. Lett. **103**, 087001 (2009).*

[90] A.D Christianson et al., *Phys. Rev. Lett. **103**, 087002 (2009).*

[91] M. Y Wang et al., *Phys. Rev. B **81**, 174524 (2010*).

[92] M. Y Wang et al., *Phys. Rev. B **83**, 094516 (2011).*

[93] D. K Pratt et al., *Phys. Rev. Lett. **106**, 257001 (2011).*

[94] H. Q Luo et al., *Phys. Rev. Lett. **108**, 247002 (2012).*

[95] S. Nandi et al., *Phys. Rev. Lett. **104**, 057006 (2010).*

[96] H. Chen et al., *Europhys. Lett. **85**, 17006 (2009).*

[97] J. T Park et al., *Phys. Rev. Lett. **102**, 117006 (2009).*

[98] S. Avci et al., *Phys. Rev. B **83**, 172503 (2011).*

[99] H. Ding et al., *Eur. Phys. Lett. **83**, 47001 (2008).*

[100] X. P. Wang et al., *Phys. Rev. B **85**, 214518 (2012).*

[101] A. Carrington, *Rep. Prog. Phys. **74**, 124507 (2011).*

[102] R.M. Fernandes et al., *Phys. Rev. B **85**, 024534 (2012).*

[103] M.S. Torikachvili et al., *Phys. Rev. Lett. **101**, 057006 (2008).*

[104] H. Kontani and S. Onari, *Phys. Rev. Lett. **104**, 157001 (2010).*

[105] P. A. Lee and X.G. *Phys. Rev. B **78** ,144517 (2008).*

[106] D. S. Inosov et al., *Nature Physics **6**, 178 (2010).*

[107] A. D. Christianson et al., *Nature Physics **456**, 930 (2008).*

[108] X. Zhang, et al., Phys. Rev. Lett. 102, 147002 (2009).

[109] E. Wiesenmayer et al., *Phys. Rev. Lett. **107**, 237001 (2011)*

[110] X. Wang et al., *Solid State Commun. **148**, 538 (2008).*

[111] J. H. Tapp et al., *Phys. Rev. B **78**, 060505 (2008).*

[112] S. V. Borisenko et al., *Phys. Rev. Lett. **105**, 067002 (2010).*

[113] A. A. Kordyuk et al., *Phys. Rev. B **83**, 134513 (2011).*

[114] G. F. Chen et al., *Phys. Rev. Lett. **102**, 227004 (2009).*

[115] S. Li et al., *Phys. Rev. B **80**, 020504 (2009).*

[116] M. A. Tanatar et al., *Phys. Rev. B **85**, 014510 (2012).*

[117] D. R. Parker et al., *Phys. Rev. Lett. **104**, 057007 (2010).*

[118] C. He et al., *Phys. Rev. Lett. **105**, 117002 (2010).*

[119] C. He et al., *J. Phys. Chem. Solids **72**, 479 (2011).*

[120] C. Putzke et al., *Phys. Rev. Lett. **108**, 047002 (2012).*

[121] T. M. McQueen et al., *Phys. Rev. B **78**, 024521 (2008).*

[122] X. C. Wang et al., *Solid State Commun. **148**, 538 (2008).*

[123] Z. Deng et al., *Euro Phys. Letters, **87**, 37004 (2009).*

[124] K. Segawa and Y. Ando, *J. Phys. Soc. Jpn. **78**, 104720 (2009).*

[125] B. C. Sales et al., *Phys. Rev. B* ***79****, 094521 (2009).*

[126] F. C. Hsu et al., *PNAS* ***105****, 14262 (2008).*

[127] T. Imai et al., *Phys. Rev. Lett.* ***102****, 177005 (2009).*

[128] A. V. Fedorchenko et al., *Low Temp. Phys.* ***37****, 83 (2011).*

[129] Y. Xia et al., *Phys. Rev. Lett.* ***103****, 037002 (2009).*

[130] A. Tamai et al., *Phys. Rev. Lett.* ***104****, 097002 (2010).*

[131] K. Nakayama et al., *Phys. Rev. Lett.* ***105****, 197001 (2010).*

[132] H. Miao et al., *Phys. Rev. B* ***85****, 094506 (2012).*

[133] N. Katayama et al., *J. Phys. Soc. Jpn.* ***79****, 113702 (2010).*

[134] S. Graser et al., *Phys. Rev. B* ***81****, 214503 (2010).*

[135] M. Y. Wang, M. Y. et al., *Nature Commun.* ***2****, 580 (2011).*

[136] W. Bao et al., *Phys. Rev. Lett.* ***102*** *.247001 (2009).*

[137] S. Li et al., *Phys. Rev. B* ***79****, 054503 (2009).*

[138] T. Hanaguri et al., *Science* ***328****, 474 (2010).*

[139] J. Guo et al., *Phys. Rev. B* ***82****, 180520 (2010).*

[140] M. Wang et al., *Nat. Commun.* ***2,*** *580 (2011).*

[141] C. H. Li et al., *Phys. Rev. B* ***83****, 184521 (2011).*

[142] Y. J. Yan et al., *Sci. Rep.* ***2,*** *212 (2012).*

[143] T. Qian et al., *Phys. Rev. Lett.* ***106****, 187001 (2011).*

[144] D. Mou et al., P*hys. Rev. Lett.* ***106****, 107001 (2011).*

[145] Y. Zhang et al., *Nat. Mater.* ***10****, 273 (2011).*

[146] F. Chen et al., *Phys. Rev. B 1, 021020 (2011).*

[147] A. Chubukov, *Ann, Rev. Cond. Matt. Phys.* ***3****, 57 (2012).*

[148] T. Nakano et al.,*Phys. Rev. B* ***83****, 180508(R) (2011)*

[149] N. Fujiwara et al., *Phys. Rev. B* **85**, *094501 (2012).*

[150] S. Matti et al., *Phys. Rev. B* ***85****, 144527 (2012)*

[151] Y. Nakai et al., *J. Phys. Soc. Jpn.* ***81*** *033701 (2012)*

BIBLIOGRAPHY

[152] A. Thaler et al., *Phys. Rev. B* ***82,*** *014534 (2010)*

[153] R. Zhou et al., *Phys. Rev. B* ***86*** *180501 (2012)*

[154] *G. D.* Mahan, Many-Particle Physics, Kluver Academic/Plenum *Publishers (New York), 3rd edition (2000)*

APPENDIX

APPENDIX

APPENDIX

I. Matsubara Green function

Let us define the following matrix of Matsubara (or 'imaginary-time') Green functions

$$\begin{aligned}\hat{G}_{ij}(\boldsymbol{k},\tau) &= -\langle T_\tau \psi_{\boldsymbol{k}}(\tau)\oplus\psi^\dagger_{\boldsymbol{k}}(0)\rangle_{ij}\\ &= -\langle T_\tau \psi_{\boldsymbol{k}}(\tau)\psi^\dagger_{\boldsymbol{k}}(0)\rangle.\end{aligned} \tag{I-1}$$

The time-ordering operator T_τ rearranges all the following operators so that the value of the time argument increases from the right to the left and a factor of (-1) is associated with each transposition during the thought process. The expectation value is evaluated as a grand canonical statistical average.

In the Matsubara formalism we work with a discrete frequency Fourier-transform. The The relations between the Green functions in time and frequency are

$$\begin{aligned}\hat{G}(\boldsymbol{k},i\omega_n) &= \int_0^\beta d\tau e^{i\omega_n\tau}\hat{G}(\boldsymbol{k},\tau)\\ \hat{G}(\boldsymbol{k},\tau) &= \frac{1}{\beta}\sum_{\boldsymbol{n}} e^{-i\omega_n\tau}\hat{G}(\boldsymbol{k},i\omega_n).\end{aligned} \tag{I--2}$$

The Matsubara frequencies ω_n in the case of fermions take the values $\omega_n=(2n+1)\pi T$ and $\omega_n=2n\pi T$ for bosons where $n\in Z$. The Green function defined above can be written using the Heaviside (theta) step function:

$$\hat{G}(\boldsymbol{k},\tau)=-\theta(\tau)\langle\hat{\psi}_{\boldsymbol{k}}(\tau)\oplus\hat{\psi}^\dagger_{\boldsymbol{k}}(0)\rangle+\theta(-\tau)\langle\hat{\psi}^\dagger_{\boldsymbol{k}}(0)\oplus\hat{\psi}_{\boldsymbol{k}}(\tau)\rangle. \tag{I-3}$$

Taking the time derivative of this equation we obtain

$$\begin{aligned}\partial_\tau\hat{G}(\boldsymbol{k},\tau) &= -\delta(\tau)\langle\hat{\psi}_{\boldsymbol{k}}(\tau)\oplus\hat{\psi^\dagger_{\boldsymbol{k}}}(0)\rangle-\delta(\tau)\langle\psi^\dagger_{\boldsymbol{k}}(\tau)\oplus\hat{\psi}_{\boldsymbol{k}}(0)\rangle-\langle T_\tau\partial_\tau\hat{\psi}(\tau)\oplus\hat{\psi^\dagger}(0)\rangle\\ &=-\delta(\tau)1+\langle T_\tau\hat{\boldsymbol{H}}\hat{\psi}(\tau)\oplus\hat{\psi}^\dagger(0)\rangle\\ &=-\delta(\tau)1+\boldsymbol{H}\langle T_\tau\hat{\psi}(\tau)\oplus\psi^\dagger(0)\rangle \;=\; -\delta(\tau)1-\hat{H}_{\boldsymbol{k}}\cdot\hat{G}.\end{aligned}$$

(I-4)-

APPENDIX

The delta function arose from the derivative of $\theta(\tau)$ and $\theta(-\tau)$ and the anti-commutation relations. Performing the Fourier transform we obtain the frequency dependent version of this identity. Here we write both on one line:

$$\left(-\partial_\tau - \hat{\boldsymbol{H}}_{\boldsymbol{k}}\right)\hat{G}(\boldsymbol{k},\tau) \;=\; \delta(\tau)1\left(i\omega_n - \hat{\boldsymbol{H}}_{\boldsymbol{k}}\right)\cdot\hat{\boldsymbol{G}}\left(\boldsymbol{k}, i\omega_n\right) \;=\; 1. \tag{I-5}$$

According to the last identity, we can obtain $\hat{G}(\boldsymbol{k}, i\omega_n)$ by inversion of the matrix $(i\omega_n - \hat{H}_{\boldsymbol{k}})$.

$$\hat{G}(\boldsymbol{k}, i\omega_n) \;=\; \left(i\omega_n.\hat{I} \;-\; \hat{\boldsymbol{H}}_{\boldsymbol{k}}\right)^{-1}. \tag{I-6}$$

where I is a unit matrix. As an example for 2X2 matrix $\hat{R}$

$$\hat{R} \;=\; \begin{pmatrix} A & B \\ C & D \end{pmatrix}, \quad (\hat{R})^{-1} \;=\; \frac{adj\,\hat{R}}{det\,\hat{R}} \tag{I-7}$$

where $det\,\hat{R}$ is the determinant and $adj\,\hat{R}$ stands for the adjoint matrix to matrix $\hat{R}$ A. To explain construction of this object let us first define the (i, j) minor of $\hat{R}$, denoted M_{ij}, as the determinant of the $(n-1)X(n-1)$ matrix that results from deleting row i and column j of $\hat{R}$. Next we define the (i,j) cofactor of $\hat{R}$ as $C_{ij}=(-1)i+jM_{ij}$. The adjoint matrix is the transpose of the cofactor matrix: $adj\,\hat{R}=C^T$. An example which can be written compactly in one line is the inverse of a general 2X2 matrix.

$$(\hat{R})^{-1} \;=\; \begin{pmatrix} A & B \\ C & D \end{pmatrix}^{-1} \;=\; \frac{1}{AD-BC}\begin{pmatrix} D & -C \\ -B & A \end{pmatrix}. \tag{I-8}$$

For $n\,X\,n$ matrix with $n>3$ competition method is easier to find its inverse.

II. Summation of the Matsubara frequencies

In order to calculate the spin density wave and superconducting gap functions one needs to evaluate the sum over ω_n in expressions of the form

$$R = -T \sum_{\mathbf{k}, i\omega_n} \frac{1}{(E^i_{\mathbf{k}} - i\omega_n)(E^j_{\mathbf{k}} - i\omega_n - i\omega_m)} \tag{II-1}$$

with the Matsubara frequencies $i\omega_n$. Here, one is only considering fermionic systems. Therefore the sum runs over the fermionic frequencies $i\omega_n = T(2n+1)\pi i$

There are several ways to evaluate this sum. One way [148] is to inspect the following integral

$$I = -\lim_{R\to\infty} \oint \frac{dZ}{2\pi i} \frac{1}{(E^i_{\mathbf{k}} - Z)(E^j_{\mathbf{k}} - Z - i\omega_m)} f(Z) \tag{II-2}$$

with the Fermi function f (z) given by:

$$f(Z) = \frac{1}{e^{\beta Z} + 1}. \tag{II-3}$$

The poles and the corresponding residues of the integrand are:

$$\begin{aligned} Z_n &= \frac{(2n+1)\pi i}{\beta} \\ R_n &= \frac{1}{\beta\left(E^i_{\mathbf{k}} - \frac{(2n+1)\pi i}{\beta}\right)\left(E^j_{\mathbf{k}} - \frac{(2n+1)\pi i}{\beta} - E^j_{\mathbf{k}}\right)}. \end{aligned} \tag{II-4}$$

$$Z_1 = E^i_{\mathbf{k}} \qquad R_1 = \frac{f(E^i_{\mathbf{K}})}{\beta(E^i_{\mathbf{k}} - E^j_{\mathbf{k}} - i\omega_n)}. \tag{II-5}$$

$$Z_2 = E^i_{\mathbf{k}} - i\omega_m \qquad R_2 = \frac{f(E^j_{\mathbf{K}} - i\omega_m)}{\beta(E^i_{\mathbf{k}} - E^j_{\mathbf{k}} + i\omega_m)}. \tag{II-6}$$

According to the residue theorem the integral is given by the sum of all residues:

$$I = -T\sum_{\mathbf{k},i\omega_n}\frac{1}{(E^i_{\mathbf{k}}-i\omega_n)(E^j_{\mathbf{k}}-i\omega_n-i\omega_m)} - \frac{f(E^i_{\mathbf{k}})}{(E^j_{\mathbf{k}}-E^i_{\mathbf{k}}-i\omega_m)} - \frac{f(E^j_{\mathbf{k}}-i\omega_m)}{(E^i_{\mathbf{k}}-E^j_{\mathbf{k}}+i\omega_m)}. \quad \text{(II-7)}$$

If ω_m is a bosonic frequency $\omega_m=2\pi m k_B T$ with $m\in Z$, one can write

$$f(E^j_{\mathbf{k}}+i\omega_m) = \frac{1}{e^{\frac{E^j_{\mathbf{k}}}{T}}e^{\frac{i\omega_m}{T}}+1} = \frac{1}{e^{\frac{E^j_{\mathbf{k}}}{T}}.1+1} = f(E^j_{\mathbf{k}}). \quad \text{(II-8)}$$

In the limit $R\to\infty$ the integral vanishes. Hence one has:

$$-T\sum_{i\omega_n}\frac{1}{(E^i_{\mathbf{k}}-i\omega_n)(E^j_{\mathbf{k}}-i\omega_n-i\omega_m)} = \frac{f(E^j_{\mathbf{k}})-f(E^i_{\mathbf{k}})}{i\omega-(E^j_{\mathbf{k}}-E^i_{\mathbf{k}})}. \quad \text{(II-9)}$$

Finally one has:

$$R = -T\sum_{\mathbf{k},i\omega_n}\frac{1}{(E^i_{\mathbf{k}}-i\omega_n)(E^j_{\mathbf{k}}-i\omega_n-i\omega_m)} = \sum_{\mathbf{k}}\frac{f(E^i_{\mathbf{k}})-f(E^j_{\mathbf{k}})}{i\omega_m-(E^i_{\mathbf{k}}-E^j_{\mathbf{k}})}. \quad \text{(II-10)}$$

We note that the Fermi function obeys $f(-x)=1-f(x)$. Using this one finds immediately

$$-T\sum_{\mathbf{k},i\omega_n}\frac{1}{(E^i_{\mathbf{k}}-i\omega_n)(E^j_{\mathbf{k}}-i\omega_n-i\omega_m)} = \frac{f(E^j_{\mathbf{k}})-f(E^i_{\mathbf{k}})}{i\omega-(E^j_{\mathbf{k}}-E^i_{\mathbf{k}})}. \quad \text{(II-11)}$$

$$-T\sum_{\mathbf{k},i\omega_n}\frac{1}{(-E^i_{\mathbf{k}}-i\omega_n)(E^j_{\mathbf{k}}-i\omega_n-i\omega_m)} = \frac{f(E^j_{\mathbf{k}})+f(E^i_{\mathbf{k}})-1}{i\omega-(E^j_{\mathbf{k}}+E^i_{\mathbf{k}})}. \quad \text{(II-12)}$$

$$-T\sum_{\mathbf{k},i\omega_n}\frac{1}{(E^i_{\mathbf{k}}-i\omega_n)(-E^j_{\mathbf{k}}-i\omega_n-i\omega_m)} = \frac{1-f(E^j_{\mathbf{k}})-f(E^i_{\mathbf{k}})}{i\omega-(E^j_{\mathbf{k}}-E^i_{\mathbf{k}})}. \quad \text{(II-13)}$$

$$-T\sum_{\mathbf{k},i\omega_n}\frac{1}{(-E^i_{\mathbf{k}}-i\omega_n)(-E^j_{\mathbf{k}}-i\omega_n-i\omega_m)} = \frac{f(E^i_{\mathbf{k}})-f(E^j_{\mathbf{k}})}{i\omega-(E^j_{\mathbf{k}}+E^i_{\mathbf{k}})}. \quad \text{(II-14)}$$

III. Green function in single band Superconductivity

The single band superconducting state that the mean field Hamiltonian is written as

$$\begin{aligned} \boldsymbol{H} &\approx \sum_{k\sigma} a^{\dagger}_{k\sigma} a_{k\sigma} \\ &+ \sum_{k'} \Delta_a(\boldsymbol{k}) \left(a^{\dagger}_{k\uparrow} a^{\dagger}_{k\downarrow} + h.c \right) \end{aligned} \tag{III-1}$$

where the mean fields are

$$\Delta_a(\boldsymbol{k}) = \sum_{k\sigma} V^{s}_{kk'} \langle a^{\dagger}_{k\uparrow} a^{\dagger}_{-k\downarrow} \rangle. \tag{III-2}$$

The essential tool which we use is the Nambu Matsubara Green function which is defined via dyadic product of vectors $\hat{\Phi}_{k}$ and $\hat{\Phi}^{\dagger}_{k}$ introduced as follows

$$\boldsymbol{H} \approx \sum_{k\sigma} \hat{\phi}^{\dagger}_{k} \hat{H}_{k} \hat{\phi}_{k} \tag{III-3}$$

where the Nambu spinors are

$$\hat{\phi}^{\dagger}_{k} = \begin{pmatrix} a^{\dagger}_{k\uparrow} & a_{-k\downarrow} \end{pmatrix}. \tag{III-4}$$

The energy matrix

$$\hat{\boldsymbol{G}}_{k} = \begin{pmatrix} \xi_a(\boldsymbol{k}) & \Delta \\ \Delta & -\xi_a(\boldsymbol{k}) \end{pmatrix}. \tag{III-5}$$

The causal (or time-ordered) version is defined as the expectation value of the time-order dyadic product:

$$\begin{aligned} \hat{\boldsymbol{G}}(\boldsymbol{k},\tau) &= \langle T_{\tau} \hat{\Phi}_{\boldsymbol{k}}(\tau) \hat{\Phi}_{\boldsymbol{k}^{\dagger}}(0) T_{\tau} \rangle = \begin{pmatrix} G_{\uparrow}(\boldsymbol{k},\tau) & G_{\uparrow\downarrow}(\boldsymbol{k},\tau) \\ G^{*}_{\uparrow\downarrow}(\boldsymbol{k},\tau) & G_{\downarrow}(\boldsymbol{k},\tau) \end{pmatrix} \\ &= -\begin{pmatrix} \langle T_{\tau} a_{k\uparrow}(\tau) a^{\dagger}_{k\uparrow}(0) \rangle & \langle T_{\tau} a_{k\uparrow}(\tau) a_{-k\downarrow}(0) \rangle \\ \langle T_{\tau} a^{\dagger}_{-k\downarrow}(\tau) a^{\dagger}_{k\uparrow}(0) \rangle & \langle T_{\tau} a^{\dagger}_{-k\downarrow}(\tau) a_{-k\downarrow}(0) \rangle \end{pmatrix} \end{aligned} \tag{III-6}$$

in which the diagonal components are called the normal Green functions (or normal

propagators) and the off-diagonal are refereed to as anomalous. Their explicit definitions

The Fourier transform of $\hat{G}(\boldsymbol{k},\tau)$ defined in (I) can be evaluated as

$$\hat{\boldsymbol{G}}(\boldsymbol{k},i\omega_n) = (i\omega_n.\hat{I}_2-\hat{\boldsymbol{H}}_{\boldsymbol{k}})^{-1} = \begin{pmatrix} G_{\uparrow}(\boldsymbol{k},i\omega_n) & G_{\uparrow\downarrow}(\boldsymbol{k},i\omega_n) \\ G^{*}_{\uparrow\downarrow}(\boldsymbol{k},i\omega_n) & G_{\downarrow}(\boldsymbol{k},i\omega_n) \end{pmatrix}. \quad \text{(III-7)}$$

We can apply (I-4) then the

$$\hat{\boldsymbol{G}}(\boldsymbol{k},i\omega_n) = \frac{1}{(i\omega_n)^2-\xi_a^2(\boldsymbol{k})-\Delta^2}\begin{pmatrix} i\omega_n+\xi_a(\boldsymbol{k}) & \Delta^{*} \\ \Delta & i\omega_n-\xi_a(\boldsymbol{k}) \end{pmatrix}. \quad \text{(III-8)}$$

It can also be expressed $\hat{G}(\boldsymbol{k},i\omega_n)$ in terms of the Pauli matrices

$$\hat{\boldsymbol{G}}(\boldsymbol{k},i\omega_n) = \frac{i\omega_n\hat{\tau}_0+\xi_a(\boldsymbol{k})\hat{\tau}_3+\Delta_k\hat{\tau}_1}{(i\omega_n)^2-\xi_a^2(\boldsymbol{k})-\Delta^2}. \quad \text{(III-9)}$$

From which the components of the inverse Green function are

$$\hat{G}_{\uparrow}(\boldsymbol{k},i\omega_n) = \frac{i\omega_n+\xi_a(\boldsymbol{k})}{(i\omega_n)^2-\xi_a^2(\boldsymbol{k})-\Delta^2}. \quad \text{(III-10)}$$

$$\hat{G_{\uparrow\downarrow}}(\boldsymbol{k},i\omega_n) = \frac{\Delta}{(i\omega_n)^2-\xi_a^2(\boldsymbol{k})-\Delta^2}. \quad \text{(III-11)}$$

IV. Green Function in Hybridized two band Superconductivity

The two band hybridized super-conductors which the pairing occurred by conduction band electrons and other band electrons. The interplay of SC and magnetism is one of the most interacting phenomenon of superconductors. The nesting properties of Fermi surface in low dimensional systems arise the SDW state and charge density wave state in the interplay of superconductivity and magnetic system. Some times two band are involved for superconductivity like cuprate, heavy fermion and iron iron pnictide superconductors. For example the Hamiltonian of heavy fermion systems composed of conduction electron, f-electron band, the hybridization of conduction electron and f-electron band. Here the hybridization of the two band is important.

Consider two band systems, band a and band d, the hybridized mean-field Hamiltonian is

$$\begin{aligned} \boldsymbol{H}_f \approx & \sum_{k\sigma} \xi_a(\boldsymbol{k}) a^\dagger_{k\sigma} a_{k\sigma} + \sum_{k\sigma} \xi_d(\boldsymbol{k}) d^\dagger_{k\sigma} d_{k\sigma} + \sum_{k\sigma} \eta_k \left(a^\dagger_{k\sigma} d_{k\sigma} + h.c \right) \\ & + \sum_{k} \Delta_k \left(a^\dagger_{k\uparrow} a^\dagger_{-k\downarrow} + h.c \right) + \sum_{k} \Delta_k \left(d^\dagger_{k\uparrow} d^\dagger_{-k\downarrow} + h.c \right). \end{aligned} \tag{IV-1}$$

With Nambu notion

$$\boldsymbol{H} \approx \sum_{k\sigma} \hat{\psi}^\dagger_k \hat{\boldsymbol{H}}_k \hat{\psi}_k \tag{IV-2}$$

where the Nambu spinors are $\hat{\psi}^\dagger_k = \left(a^\dagger_{k\uparrow} \quad a_{-k\downarrow} \quad d^\dagger_{k\uparrow} \quad d_{-k\downarrow} \right)$ and its conjugate. The energy matrix

$$\hat{\boldsymbol{H}}_k = \begin{pmatrix} \hat{\xi}_a & \hat{\eta} \\ \hat{\eta} & \hat{\xi}_d \end{pmatrix} \tag{IV-3}$$

with

$$\hat{\xi}_{a/d} = \begin{pmatrix} \xi_{a/d}(\boldsymbol{k}) & \Delta \\ \Delta & -\xi_{a/d}(\boldsymbol{k}) \end{pmatrix} \qquad and \quad \hat{\eta} = \eta \hat{\tau}_0. \tag{IV-4}$$

The eigenvalues of matrix (II-3) $\pm E_{\boldsymbol{k}}^{+}, \pm E_{\boldsymbol{k}}^{-}$ are given by

$$(E_{\boldsymbol{k}}^{\pm})^2 = \left(\frac{\xi_a(\boldsymbol{k}) - \xi_d(\boldsymbol{k})}{2}\right) + \left(\frac{\xi_a(\boldsymbol{k}) + \xi_d(\boldsymbol{k})}{2}\right) + \Delta^2 + \eta^2 \pm \sqrt{\left(\frac{\xi_a(\boldsymbol{k}) - \xi_d(\boldsymbol{k})}{2}\right)^2 + \eta^2}. \tag{IV-5}$$

Introducing the finite temperature Green function

$$\begin{aligned} \hat{\boldsymbol{G}}(\boldsymbol{k}, \tau) &= \langle T_\tau \hat{\psi}_{\boldsymbol{k}}(\tau) \hat{\psi}_{\boldsymbol{k}}^{\dagger}(0) \rangle \\ &= \begin{pmatrix} G_{\uparrow}^{a}(\boldsymbol{k}\tau) & G_{\uparrow\downarrow}^{a}(\boldsymbol{k}\tau) & \hat{G_{\uparrow\uparrow}^{ad}}(\boldsymbol{k}\tau) & G_{\uparrow\downarrow}^{ad}(\boldsymbol{k}\tau) \\ G_{\downarrow\uparrow}^{a}(\boldsymbol{k}\tau) & \hat{G_{\downarrow}^{a}}(\boldsymbol{k}\tau) & G_{\downarrow\uparrow}^{ad}(\boldsymbol{k}\tau) & G_{\downarrow\downarrow}^{ad}(\boldsymbol{k}\tau) \\ G_{\uparrow\uparrow}^{da}(\boldsymbol{k}\tau) & G_{\uparrow\downarrow}^{da}(\boldsymbol{k}\tau) & \hat{G_{\uparrow}^{d}}(\boldsymbol{k}\tau) & G_{\uparrow\downarrow}^{d}(\boldsymbol{k}\tau) \\ G_{\downarrow\uparrow}^{da}(\boldsymbol{k}\tau) & G_{\downarrow\downarrow}^{da}(\boldsymbol{k}\tau) & G_{\downarrow\uparrow}^{d}(\boldsymbol{k}\tau) & G^{d}\downarrow(\boldsymbol{k}\tau) \end{pmatrix}. \end{aligned} \tag{IV-6}$$

The Fourier transform of $\hat{G}(\boldsymbol{k}, \tau)$ can be evaluated as

$$\begin{aligned} \hat{\boldsymbol{G}}(\boldsymbol{k}, i\omega) &= (i\omega . \hat{I}_4 - \hat{\boldsymbol{H}}_{\boldsymbol{k}})^{-1} \\ &= \begin{pmatrix} G_{\uparrow}^{a}(\boldsymbol{k}i\omega) & G_{\uparrow\downarrow}^{a}(\boldsymbol{k}i\omega) & \hat{G_{\uparrow\uparrow}^{ad}}(\boldsymbol{k}i\omega) & G_{\uparrow\downarrow}^{ad}(\boldsymbol{k}i\omega) \\ G_{\downarrow\uparrow}^{a}(\boldsymbol{k}i\omega) & \hat{G_{\downarrow}^{a}}(\boldsymbol{k}i\omega) & G_{\downarrow\uparrow}^{ad}(\boldsymbol{k}i\omega) & G_{\downarrow\downarrow}^{ad}(\boldsymbol{k}i\omega) \\ G_{\uparrow\uparrow}^{da}(\boldsymbol{k}i\omega) & G_{\uparrow\downarrow}^{da}(\boldsymbol{k}i\omega) & \hat{G_{\uparrow}^{d}}(\boldsymbol{k}i\omega) & G_{\uparrow\downarrow}^{d}(\boldsymbol{k}i\omega) \\ G_{\downarrow\uparrow}^{da}(\boldsymbol{k}i\omega) & G_{\downarrow\downarrow}^{da}(\boldsymbol{k}i\omega) & G_{\downarrow\uparrow}^{d}(\boldsymbol{k}i\omega) & G^{d}\downarrow(\boldsymbol{k}i\omega) \end{pmatrix}. \end{aligned} \tag{IV-7}$$

Or

$$\hat{\boldsymbol{G}}_{\uparrow}(\boldsymbol{k}, i\omega_n) = \left(i\omega_n - \frac{\xi_a(\boldsymbol{k}) - \xi_d(\boldsymbol{k})}{2}\hat{\rho}_3\hat{\sigma}_3 - \frac{\xi_a(\boldsymbol{k}) + \xi_d(\boldsymbol{k})}{2}\hat{\rho}_0\hat{\sigma}_3 + \Delta\hat{\rho}_0\hat{\sigma}_1 - \eta\hat{\rho}_1\hat{\sigma}_3\right)^{-1}. \tag{IV-8}$$

Analytical work may take long steps to calculate the inverse of the matrix and see the components however computational techniques simplifies the work. Some of the components of the inverse Green function (IV-7) are therefore

$$G_a^{\uparrow\downarrow}(i\omega,\boldsymbol{k}) = \frac{\Delta_a(\boldsymbol{k})\left((i\omega)^2-E_a^2(\boldsymbol{k})\right)+\Delta_m^2(\boldsymbol{k})\Delta_d(\boldsymbol{k})}{\left(i\omega-\Omega_a(\boldsymbol{k})\right)\left(i\omega+\Omega_a(\boldsymbol{k})\right)\left(i\omega-\Omega_d(\boldsymbol{k})\right)\left(i\omega+\Omega_d(\boldsymbol{k})\right)}. \quad \text{(IV-9)}$$

$$G_d^{\uparrow\downarrow}(i\omega,\boldsymbol{k}) = \frac{\Delta_d(\boldsymbol{k})\left((i\omega)^2-E_d^2(\boldsymbol{k})\right)+\Delta_m^2(\boldsymbol{k})\Delta_a(\boldsymbol{k})}{\left(i\omega-\Omega_a(\boldsymbol{k})\right)\left(i\omega+\Omega_a(\boldsymbol{k})\right)\left(i\omega-\Omega_d(\boldsymbol{k})\right)\left(i\omega+\Omega_d(\boldsymbol{k})\right)}. \quad \text{(IV-10)}$$

$$G_{ad}^{\uparrow\downarrow}(i\omega,\boldsymbol{k}) = \frac{\Delta_m(\boldsymbol{k})\left((i\omega)^2-\xi_d(\boldsymbol{k})\xi_a(\boldsymbol{k})+\Delta_d(\boldsymbol{k})\Delta_a(\boldsymbol{k})-\Delta_m^2(\boldsymbol{k})\right)}{\left(i\omega-\Omega_a(\boldsymbol{k})\right)\left(i\omega+\Omega_a(\boldsymbol{k})\right)\left(i\omega-\Omega_d(\boldsymbol{k})\right)\left(i\omega+\Omega_d(\boldsymbol{k})\right)}. \quad \text{(IV-11)}$$

PUBLICATION

1. Commensurate spin density wave and superconductivity in hole doped and electron doped Wjcmp (accepted Paper ID: 4700288, 2014)

CONFERENCE

1. Interrelationship of Superconductivity and Spin Density Wave in Ferropnictides ISCM 2012 (Abstract ID: 606)
2. Magnetism and Superconductivity in hole doped and electron doped superconductors. ISCM 2014 (Abstract ID: 2724)